Graphene-based drug delivery platforms

Master's Thesis

University of Jyväskylä

Department of Chemistry

29.7.2021

Ia-Beate Liljedahl

Abstract

The literature part of this Master's thesis will focus on graphene-based nanomaterials as drug delivery platforms. The chemical properties and functionalization of pristine graphene and its oxygen-containing derivatives, graphene oxide and reduced graphene oxide, will be discussed. The biological behaviour of the graphene-based nanomaterials is introduced, including behaviour in biological fluids, bioaccumulation, administration routes, immune and inflammatory reply, cell targeting, cellular toxicity and behaviour with the blood components. The attachment of multiple anticancer drugs to the graphene-based platforms and the release of the drugs from them is described.

The miniproject was an introductory project for the experimental part. Graphene oxide and reduced graphene oxide-based constructs with phenylalanine *tert*-butyl ester were synthesized and characterized at the University of Jyväskylä. In the experimental part, conducted at Orion Corporation, the aim was to synthesize graphene oxide-based conjugates having covalently bound linker for strain promoted alkyne-azide cycloaddition (SPAAC). In the SPAAC reactions, bicyclononyne (BCN) containing conjugate and an azide group of the synthesized small molecule were used to form 1,2,3-triazole. The rGO-amine-BCN-PEG conjugate was successfully synthesized and characterized with FT-IR.

Tiivistelmä

Tämän pro gradu -tutkielman kirjallisuuskatsaus käsittelee grafeenipohjaisia lääkekuljettimia. Tutkielmassa perehdytään grafeenin ja sen johdannaisten, grafeenioksidin ja pelkistetyn grafeenioksidin, kemiallisiin ominaisuuksiin ja funktionalisointiin sekä grafeeniin pohjautuvien materiaalien biologiseen käyttäymiseen, mukaan lukien käyttäytyminen biologisissa nesteissä, biokertyminen, annostelureitit, immuunivasteet ja tulehdukselliset vasteet, solutargetointi, solumyrkyllisyys ja käyttäytyminen veren komponenttien kanssa. Lisäksi esitellään syöpälääkeaineiden liittäminen grafeenipohjaisiin lääkeainekuljettimiin ja lääkeaineiden vapauttaminen alustoista.

Kokeellista osiota alustavassa miniprojektissa valmistettiin grafeenioksidiin ja pelkistettyyn grafeenioksiin pohjautuvat yhdisteet, GO-PheO*t*Bu ja rGO-PheO*t*Bu Jyväskylän yliopistossa. Tutkielman kokeellinen osio suoritettiin Orionilla, ja työn tavoite oli valmistaa grafeenioksidiin pohjautuvia konjugaatteja, joihin liitettyjä linkkereitä voidaan hyödyntää SPAAC-reaktioissa. SPAAC-reaktioissa tavoite oli muodostaa 1,2,3-triatsoli bisyklononyynin sisältämän konjugaatin ja syntetisoidun pienmolekyylin atsidiryhmän avulla. Projektissa valmistettiin rGO-amiini-BCN-PEG konjugaatti, jonka rakenne vahvistettiin FT-IR karakterisoinnilla.

Table of contents

Preface

This Master's thesis was conducted between August 2020 and June 2021. The experimental part was performed at Orion Corporation from November 2020 until March 2021.

I am grateful to the Orion Corporation for the possibility to accomplish the experimental project at their facilities, and I want to thank Senior Scientist Mikko Myllymäki for supervising me during the project. I am very grateful to my supervisor, Professor Maija Nissinen, for her useful advice throughout this Master's thesis project. I also want to thank Dr Efstratios Sitsanidis and M.Sc. Romain Chevigny for their support to perform the measurements at the University of Jyväskylä.

Thank you all my friends in Jyväskylä for the unforgettable times during my studies. Special thanks I want to introduce to my biggest supporters – my family – you are incredible.

Abbreviations

ADR	Adriamycin
AFM	Atomic force microscopy
BCN	Bicyclononyne
BCNU	1,3-bis(2-chloroethyl)-1-nitrosourea
BSA	Bovine serum albumin
CCK-8	Cell Counting Kit-8
CF	Ciprofloxacin
CNT	Carbon nanotube
CPT	Camptothecin
CVD	Chemical vapour deposition
DA	Dopamine
DBCO	Dibenzocyclooctyne
DCs	Immature dendritic cells
DDS	Drug delivery systems
DIPEA	*N,N*-Diisopropylethylamine
DOX	Doxorubicin
DTT	Dithiothreitol
DXR	Doxorubicin
EDC	1-ethyl-3-(3-dimethylaminopropyl)carbodiimide hydrochloride
EPR	Enhanced permeability and retention
FA	Folic acid
FBS	Fetal bovine serum
FLG	Few-layer graphene

FMA	Fluorescein o-methacrylate
FR	Folate receptor
FTIR	Fourier Transform Infrared Spectroscopy
GBN	Graphene based nanomaterial
GFN	Graphene family nanomaterial
GSH	Glulathione
GO	Graphene oxide
HL-7702	Human liver cell line
HRP	Horseradish peroxidase
in vivo	In a living organism
in vitro	Outside a living organism
LC	Loading capacity
LE	Loading efficiency
MCF-7	Breast cancer cell line
MFG	Multi-functional graphene
Mpeg-ISC	Hetero-bifunctional methoxy-PEG-isocyanate
MRC-5	Human lung fibroblast line
MTT	3-(4,5-dimethylthiazol-2-yl)-2,5-diphenyltetrazolium bromide
MTX	Methotrexate
nGO	Nanosized graphene oxide
NHS	*N*-hydroxysuccinimide
NLS	Nuclear localisation signal
NOTA	1,4,7-triazacyclononane-1,4,7-triacetic acid
OVA	Ovalbumin antigen
PAA	Polyallylamine

PAA	Polyacryclic acid
PBS	Phosphate-buffered saline
PEG	Polyethylene glycol
PEI	Polyethyleneimine
PheO*t*Bu	Phenylalanine *tert*-butyl ester
PLA	Poly(lactide)
PLL	Poly-L-lysine
PPG	Polypropylene glycol
PSS	Poly(sodium 4-styrenesulfonates)
PTX	Paclitaxel
PVA	Poly(vinyl alcohol)
PVP	Polyvinylpyrrolidone
rGO	Reduced graphene oxide
RES	Reticuloendothelial system
ROS	Reactive oxygen species
SEM	Scanning electron microscope
siRNA	Small-interfering RNA
SPAAC	Strain promoted azide-alkyne cycloaddition
TEM	Transmission Electron Microscopy
TME	Tumour microenvironment
U937	Human macrophage line
UPNP	Upconversion nanoparticle
VEGF	Vascular endothelial growth factor
VPF	Vascular permeability factor
XPS	X-ray photoelectron spectroscopy

Literature part

1. Introduction

1.1 Pristine graphene

Graphene, a two-dimensional carbon layer (Figure 1), was isolated in 2004 using mechanical exfoliation, called a scotch-tape method.[1] The structure of pristine graphene consists of hexagonally arranged sp^2 hybridized carbon atoms attached to three other carbon atoms. Graphene has a large surface area, high mechanical flexibility, and it can be functionalized in multiple ways.[2] Due to the hexagonal structure of graphene, different aromatic compounds can bind to pristine graphene. Graphene is a promising platform for drug delivery in humans. Most commonly, drugs bind to pristine graphene through noncovalent interactions or hydrophobic interactions.[1]

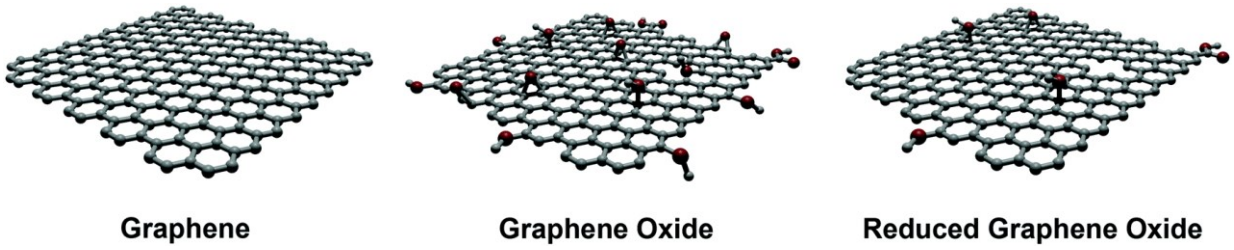

Figure 1. Graphene is a carbon layer. GO and rGO are graphene derivatives bearing carboxyl, hydroxyl and epoxy functional groups in their structures. Chem. Soc. Rev., **2017**, *46*, 4400-4416 – Published by The Royal Society of Chemistry.

Without any oxygen-containing functional groups, pristine graphene is a hydrophobic material. This means that graphene must be made hydrophilic before it can be utilized in biological environments.[1] Covalent or noncovalent functionalization is used when graphene is made water-soluble.[2] The solubilization of pristine graphene in a biological environment can be achieved by modifying the graphene surface with surfactants or using non-polar solvents.[1]

Graphene can be synthesized by using top-down and bottom-up methods.[3] The top-down method isolates graphite layers to obtain graphene layers, whereas, in the bottom-up method, graphene is made by combining carbon molecules.[3] Mechanical exfoliation, chemical exfoliation and chemical synthesis belong to the top-down methods. The bottom-up methods are divided into pyrolysis, epitaxial growth, chemical vapour deposition (CVD) and other methods.[4]

1.2 Graphene oxide

Graphene oxide (GO; Figure 1) is a graphene derivative, which can be made using different oxidation methods, such as the Hummers' method[5] where chemical oxidation of graphene is achieved by using oxidizing agents or acids.[6] In Hummers' method, a mixture of graphene, potassium permanganate, and sulfuric acid is sonicated. As a result, graphite salts, which can be used as a precursor for graphene oxide, are formed. GO is a hydrophilic material due to the oxygen-containing functional groups. The GO layer can be further functionalized hydrophobically, covalently, electrostatically, or by using π bonds.[1]

Two models demonstrate the structure of GO.[1] The Lerf-Klinowski model[7] visualizes that the edges of GO have carboxyl groups, whereas the planar part has epoxy and hydroxyl groups.[8] Based on the second model, GO edges have carboxyl groups, whereas the planar structure has oxidative debris.[9]

The solubility of graphene-based materials affects the biological behavior of the materials significantly.[8] The solubility properties of GO are better than pristine graphene, as pristine graphene consists only of sp^2 hybridized carbon atoms causing its hydrophobicity. Conversely, GO's oxygen-containing groups make it hydrophilic and biocompatible.

1.3 Reduced graphene oxide

Reduced graphene oxide (rGO; Figure 1) is a graphene derivative with oxygen-containing functional groups in its structure.[6] It is an intermediate form of graphene and GO, and it is formed by thermal or chemical reduction of GO. The amount of oxygen-containing functional groups in rGO's structure is less than in GO. During the reduction of GO, reducing agents, such as hydrazine or hydrogen, are utilized.[6]

2. Functionalization of graphene-based nanomaterials

This chapter introduces compounds that have been used for the functionalization of graphene-based nanomaterials. Most commonly, graphene oxide is utilized to attach different molecules noncovalently or covalently, as GO has suitable functional groups at the edges and on its basal plane (Figure 2). Graphene-based drug carriers for targeted drug delivery can be achieved with the help of the functionalization of graphene-based structures.

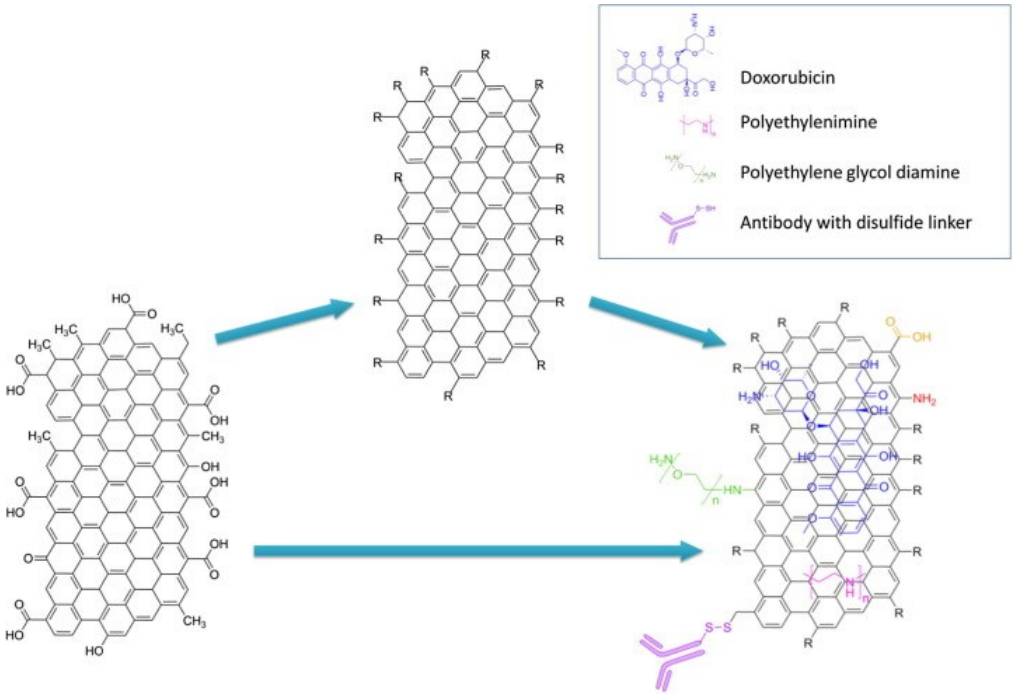

Figure 2. An example of the functionalization of graphene-based materials. Graphene-based materials can be functionalized covalently, with polyethylene glycol diamine and antibody bearing a linker. Noncovalent attachment is conducted, for instance, with polyethyleneimine and anticancer drug doxorubicin. Published in European Journal of Pharmaceutics and Biopharmaceutics, *104*, McCallion, C.; Burthem, J.; Rees-Unwin, K.; Golovanov, A., and Pluen, A., Graphene in therapeutics delivery: Problems, solutions and future opportunities, 235-250, Copyright Elsevier 2016.

2.1 Polyethylene glycol and bovine serum albumin

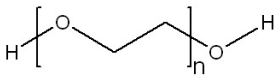

Figure 3. The chemical structure of polyethylene glycol.

The functionalization of graphene-based structures with polyethylene glycol (PEG; Figure 3) and bovine serum albumin (BSA) increases biocompatibility and physiological stability and decreases cytotoxicity.[10] Previous studies showed that the amount of serum proteins adsorbed onto the PEGylated nanosized graphene oxide (nGO) was reduced compared with the unfunctionalized GO.[10] The selectivity towards the proteins was also improved in nGO-PEG, as it bound to six different serum proteins.[11] Additionally, nGO-PEG dispersed successfully in serum after robust centrifugation. PEGylated and BSA functionalized GO and rGO probably have high stability in water, PBS and culture medium, while pristine GO is prone to aggregate and precipitate in PBS.[10]

To be utilized in a biological environment, nanomaterials need to be biodegradable.[10] GO has been shown to degrade in the presence of horseradish peroxidase (HRP). Instead, HRP does not degrade PEGylated or BSA functionalized GO or rGO, probably because the PEG and BSA molecules block the HRP from attaching to GO's surface.[10] Conversely, GO-PEG with a disulfide linkage (GO-SS-PEG) has been observed to be an appropriate construct for biomedical applications since the disulfide linkage is biodegradable and can be cut easily.[10] The disulfide bond can be cut by dithiothreitol (DTT), which leads to the release of PEG. The cytotoxicity effect of GO-SS-PEG was noted to be equal to GO-PEG, as either of the constructs did not affect cytotoxicity significantly.

As observed by by Liu *et al.*,[12] PEG increases the water solubility of GO-based drug complexes, such as camptothecin-based nGO-PEG-SN38. In addition to water, the PEG-nGO complex was very stable in PBS, cell medium and serum. The water solubility of nGO-PEG-SN38 was reached at SN38 concentrations above 1 mg/ml, while free SN38 was observed to be water-insoluble.

2.2 Dextran

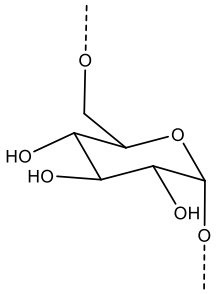

Figure 4. The chemical structure of Dextran.

Dextran polymer (Figure 4) can be utilized for the noncovalent functionalization of graphene.[13] GO-based constructs can form contact with blood cells, response system, blood vessels and immune system, causing various adverse effects, such as coagulation of blood cells and hemolysis. Due to this, the ability of the Dextran functionalized graphene nanoplatelets (GNP-Dex) to affect these phenomena has been evaluated. GNP-Dex with a maximum concentration of 100 mg/ml were shown to be water-soluble and stable. Additionally, they were not observed to induce activation of platelets, blood cell hemolysis or proinflammatory effects. The platelet activation was tested using the GNP-Dex concentrations of 1 mg/ml, 7 mg/ml and 10 mg/ml. The study showed that none of these concentrations affected platelet activation or aggregation.

The activation of platelets can be observed from the release of a platelet factor PF_4, a protein capable of causing aggregation of platelets and blood clots.[13] GNP-Dex constructs have been shown to induce the release of PF_4 from two separate blood samples with different GNP-Dex concentrations. No significant difference was observed between the different GNP-Dex concentrations or the blood samples.

Red and white blood cells have been treated with GNP-Dex constructs to study blood cell hemolysis.[13] No hemolysis was observed after the treatment with three different concentrations, 1 mg/ml, 7 mg/ml and 10 mg/ml. Instead, the cells exposed to polyethyleneimine (PEI) were observed to change their morphology compared to the unexposed cells, due to hemolysis. These PEI-treated cells were also observed to aggregate.

2.3 Amine

Amine-functionalized graphene (G-NH_2) has been observed to be more biocompatible than other graphene derivatives, GO and rGO, as the amine-functionalized form did not cause hemolysis or thrombosis in studies on mice.[14] In contrast, GO and rGO had a thrombogenic effect.[14] Hence, based on the study, amine-functionalized graphene could be safely used *in vivo*.

The thrombogenicity of graphene oxide and amine-functionalized graphene was investigated by administrating 250 µg of GO and G-NH_2 intravenously per one kilogram of the mice's weight.[14] No thrombosis was observed after the administration of G-NH_2 but GO had caused thrombosis in the lungs.

The release of Ca^{2+} ions from platelets was measured after exposure to GO and amine-functionalized graphene. After Ca^{2+} is released from the platelets, the platelets are activated, leading to platelet aggregation. Ca^{2+} release from the platelets exposed to GO was observed, while platelets exposed to amine-functionalized graphene did not release Ca^{2+}. Therefore, the platelets treated with amine functionalized graphene were not activated. The reason for this is the surface charge of the graphene-based construct.[14] If the surface of the graphene construct has a negative charge, the charge is capable of shifting onto the platelet, and graphene interacts with platelets, further releasing Ca^{2+}. Instead of that, a positive surface of amine-functionalized graphene did not shift the charge onto the platelet.

2.4 Polylysine

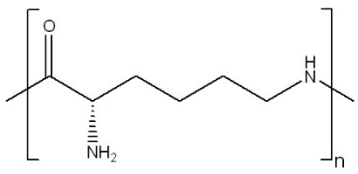

Figure 5. The chemical structure of polylysine.

The addition of poly-L-lysine (PLL; Figure 5) on the GO sheets enhances GO material's biocompatibility and makes the sheets soluble in water.[15] The epoxy groups of GO and amino groups

of PLL have been bound to form amide bonds with the help of KOH and $NaBH_4$. These complexes, further synthesized with HRP, formed graphene-PLL/HRP composites (Figure 6).

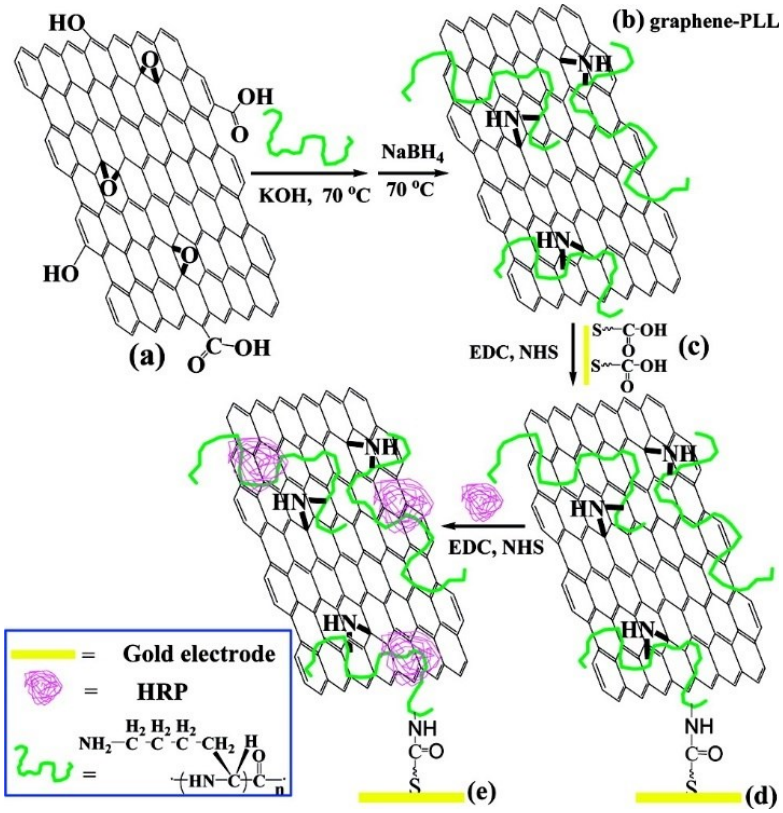

Figure 6. PLL functionalization of graphene-based construct achieved with $NaBH_4$ and KOH. The graphene-PLL platform enabled the further attachment of HRP on the structure. Published in *Langmuir*, *25(20)*, Shan, C.; Yang, H.; Han, D.; Zhang, Q.; Ivaska, A., and Niu L., Water-Soluble Graphene Covalently Functionalized by Biocompatible Poly-L-lysine, **2009**, 12030-12033.

2.5 Polyallylamine

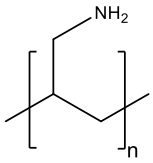

Figure 7. The chemical structure of polyallylamine.

Polyallylamine (PAA; Figure 7), bearing plenty of amine groups, can be used to functionalize GO. This kind of functionalization has been conducted by adding PAA to the suspension of GO sheets,

followed by sonication and filtration.[16] The study showed that the epoxy groups form linkages with PAA followed by the formation of particles. The sonication of the particles produced a homogeneous suspension of PAA-GO, *i.e.*, a colloidal suspension of the PAA-linked GO sheets formed. The filtration and washing of the complex led to the formation of paper material.[16]

2.6 Poly(vinyl alcohol)

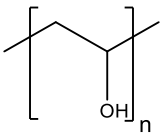

Figure 8. The chemical structure of poly(vinyl alcohol).

The advantages of using poly(vinyl alcohol) (PVA, Figure 8) for the functionalizing of GO are PVA's ability to change the crystallinity and thermal stability of the formed materials.[17] When graphene oxide sheets were covalently functionalized with PVA (Figure 9), the conjugates were observed to dissolve in DMSO when heated. The study showed that a tiny amount of graphene oxide can significantly enhance the thermal stability of the formed nanocomposites, as the prepared materials degraded at 100°C higher temperature than PVA.

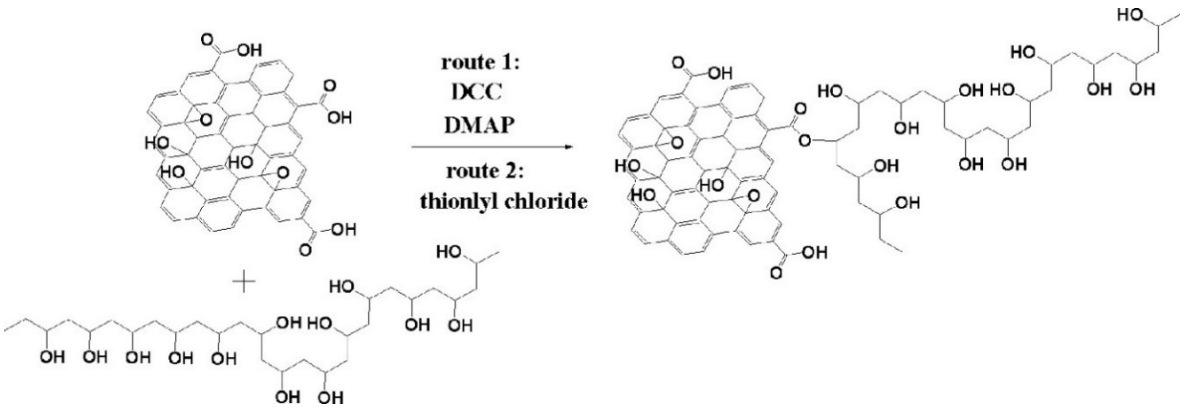

Figure 9. PVA functionalization of graphene oxide made in two different ways, using DCC and DMAP or thionyl chloride. Published in *Macromolecules*, *42*, Salavagione, H.J.; Gómez, M.A., and Martínez G., Polymeric Modification of Graphene through Esterification of Graphite Oxide and Poly(vinyl alcohol), **2009**, 6331-6334.

2.7 Polyethylenimine

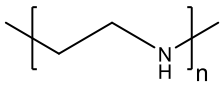

Figure 10. The chemical structure of polyethylenimine.

Polyethylenimine (PEI; Figure 10) functionalized GO may be used as a drug platform for ciprofloxacin (CF)[18] and doxorubicin (DOX)[19]. PEI may attach either electrostatically or covalently on GO.[18] The covalent binding can be utilized in making GO-based drug delivery films with PEI molecules as crosslinkers. Following the crosslinking of PEI, which enhances the stability of the film in water compared to pristine GO, ciprofloxacin (CF) drug can bound to the construct. CF released faster in a PBS solution of pH 5.5 compared to PBS buffer of pH 7.4.[18] In a more acidic environment, electrostatic interactions are weaker between CF and PEI, as they both are positively charged, and PEI chains have repulsive electrostatic interaction. These factors reduce the releasing speed of CF in a more acidic environment. Therefore, PEI enhances the drug loading capacity of CF onto the GO surface, as PEI reduces GO to some extent, enhances the stability of the prepared film due to a crosslinker feature, and gives more space for drug loading.

Additionally, PEI can be used for attaching nanocrystals to the GO-PEI surface (Figure 11).[19] The oleic acid-coated nanocrystals belong to the group of upconversion nanoparticles (UCNPs) and can be dispersed in water via binding to the PEI-functionalized GO. As Yan *et al*.[19] showed, doxorubicin (DOX), an aromatic anticancer drug, can be bound noncovalently on the surface of the PEI-GO-UCNP composites, leading to effective destruction of cancer cells, as *in vitro* experiments revealed.

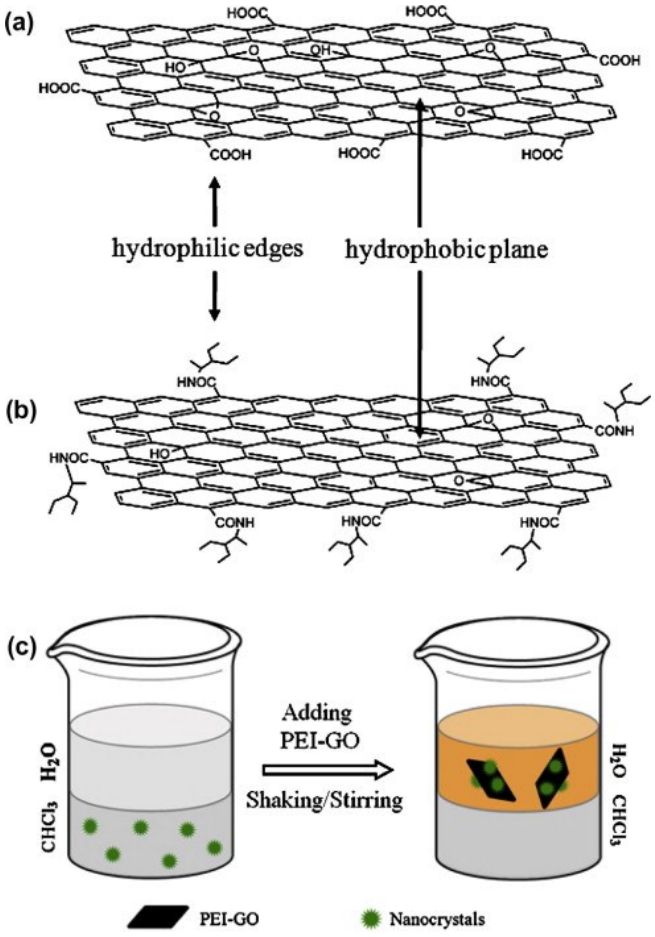

Figure 11. (a) GO has hydrophobicity and hydrophilicity on its structure. (b) Due to its hydrophilicity, PEI was bound on GO. (c) The nanocrystals were attached to the PEI-GO sheets. Reprinted from Carbon, *516*, Yan, L.; Chang, Y., Zhao, L.; Gu, Z.; Liu, X.; Tian, G.; Zhou, L.; Ren, W.; Jin, S.; Yin, W.; Chang, H.; Xing, G.; Gao, X, and Zhao, Y.., The use of polyethylenimine-modified graphene oxide as a nanocarrier for transferring hydrophobic nanocrystals into water-dispersible hybrids for use in drug delivery, 120-129, Copyright 2013, with permission from Elsevier.

2.8 Polyacrylic acid

Polyacrylic acid (PAA; Figure 12) can enhance graphene-based nanocarrier's solubility and entry to a cell.[20] A covalent attachment of 1,3-bis(2-chloroethyl)-1-nitrosourea (BCNU) onto the PAA-GO complex can increase the uptake of the drug complex in cancer cells. As there are carboxyl groups in the PAA structure, it can form an amide bond with BCNU, enhancing the loading of drugs onto the nanocarrier's surface. PAA conjugated GO was observed to raise the half-life of BCNU by more than half, and it also prevented the hydrolysis of BCNU.[20]

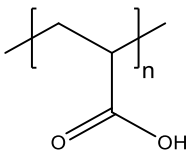

Figure 12. The chemical structure of polyacrylic acid.

PAA functionalized multifunctional graphene (MFG) construct has been developed (Figure 13).[21] PAA was covalently bound to magnetic graphene, which then enabled the covalent binding of fluorescein o-methacrylate (FMA) to the structure. Magnetic graphene (MG) was prepared by removing oxygen-containing functional groups from the surface of GO and breaking down ferrocene to form iron nanoparticles. However, as the oxygen groups were removed, the magnetic graphene lacked biocompatibility, but PAA and FMA were found to re-introduce the dispersibility in water. Because of the considerable magnetic properties of MG, it may be used in drug transport with the possibility to utilize magnetic field in drug release and controlled transport.[21]

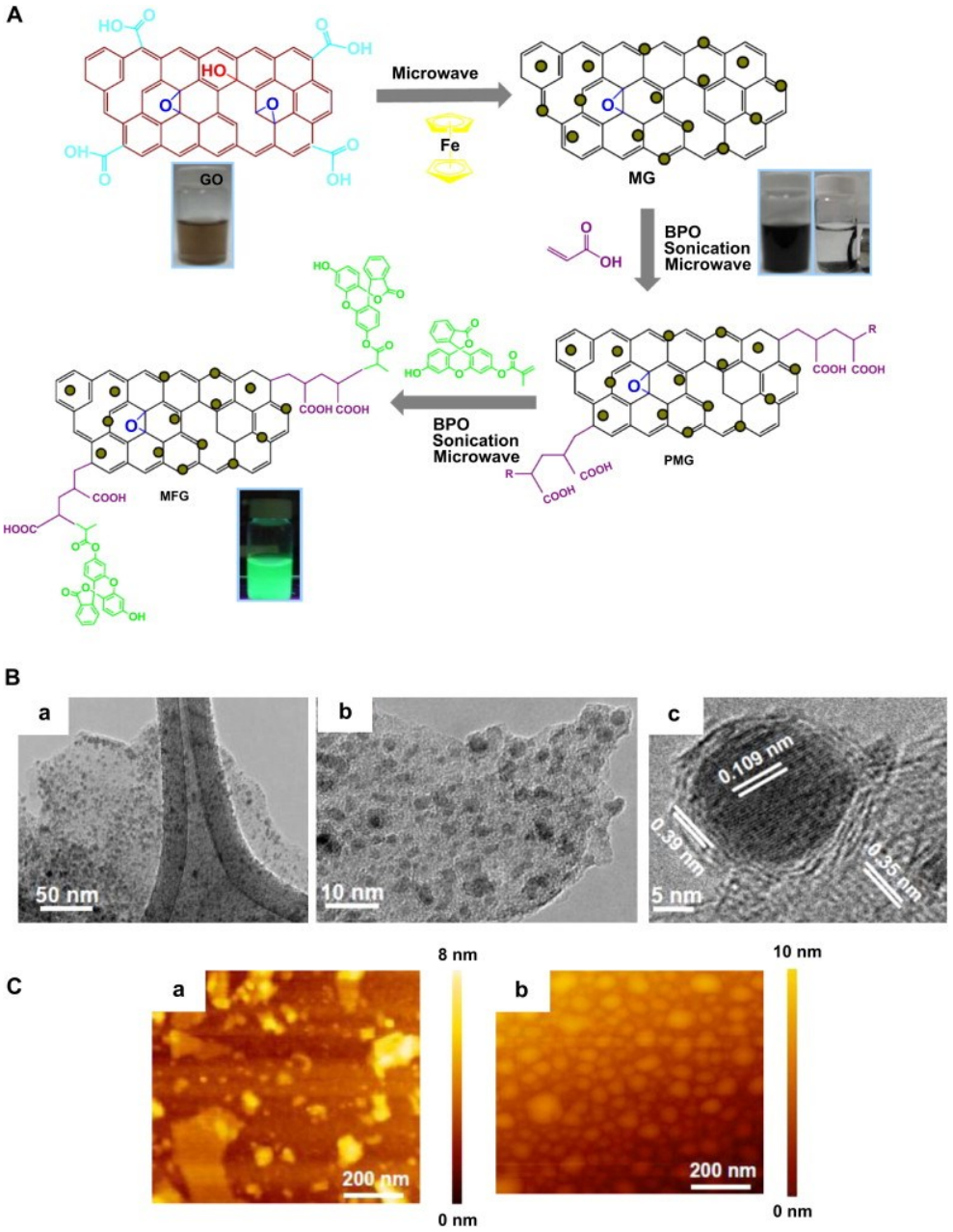

Figure 13. A) Preparation of multifunctional graphene. B) TEM images of magnetic graphene. C) AFM image of (a) GO and (b) multifunctional graphene. Reprinted from Biomaterials, *33*, Gollavelli, G. and Ling, Y., Multi-functional graphene as an *in vitro* and *in vivo* imaging probe, 2532-2545, Copyright 2012, with permission from Elsevier.

2.9 Chitosan

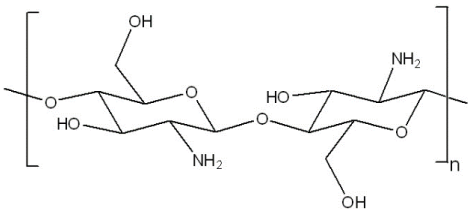

Figure 14. The chemical structure of chitosan.

Chitosan (Figure 14) can enhance the nanocarrier's biocompatibility and stability.[22] Because of this, galactosylated chitosan functionalized GO platform can be utilized for loading of DOX. The GO-chitosan material can bind a large amount of drug, and it is cytotoxic towards tumors. The GO-chitosan construct was successfully synthesized by the solution-mixing method following evaporation through ultrasonication when the amide bonds between GO and chitosan were formed.[23] Chitosan may enhance the degradation properties of complexes and make them more stable, which was shown by the remarkable increase of the degradation temperature of the construct.[23]

2.10 Folic acid

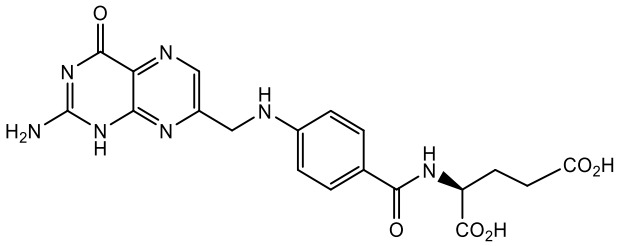

Figure 15. The chemical structure of folic acid.

Folic acid (FA; Figure 15) has the capacity of targeting specific folate receptors of the target cells.[24] Folic acid can bind on the graphene oxide by forming amide bonds (Figure 16). Following the FA functionalization, doxorubicin (DOX) and camptothecin (CPT) can be attached on the FA functionalized GO.[24]

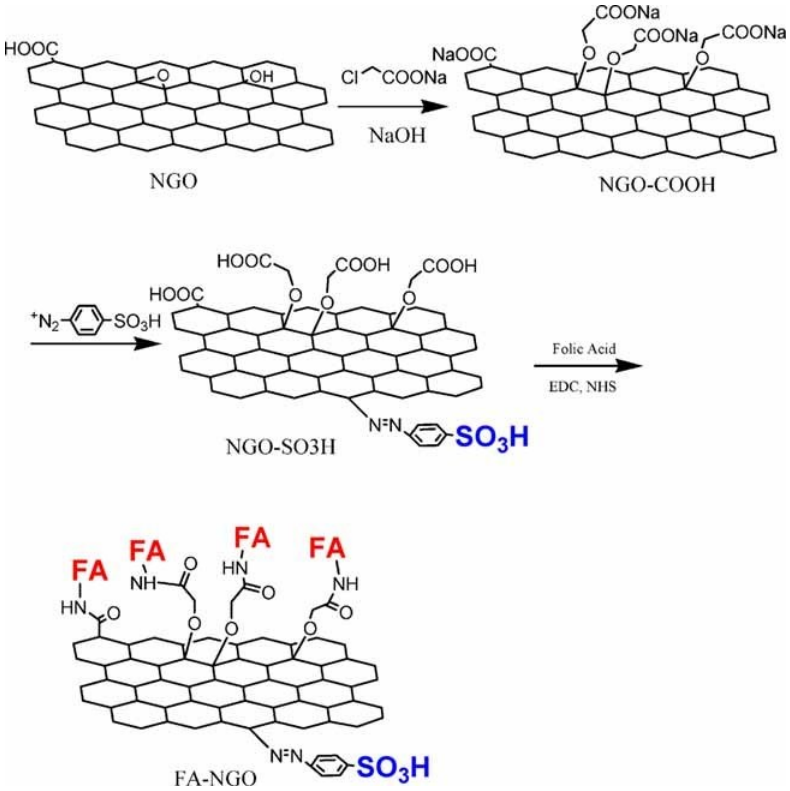

Figure 16. Folic acid functionalization of GO sheets by using EDC and NHS as activators. Copyright 2010 Wiley. Used with permission from Zhang, L.; Xia, J.; Zhao, Q.; Liu, L., and Zhang, Z., Functional Graphene Oxide as a Nanocarrier for Controlled Loading and Targeted Delivery of Mixed Anticancer Drugs, Small, John Wiley and Sons.

The fluorescence properties and cellular uptake of the FA-nGO materials can be enhanced by attaching rhodamine (Rho B).[24] The cellular uptake has been investigated by attaching doxorubicin (DOX) to the conjugates and using MCF-7 cells and A549 to which the conjugates have been targeted. The MCF-7 cells have FA receptors on their structure, whereas A549 cells do not have, enabling FA-nGO materials to target more effectively the MCF-7 cells than A549 cells. In this case, the receptor-mediated endocytosis can be utilized for targeting the FA containing conjugates to the target cells. In the colloidal stability tests, the produced FA-nGO conjugates had better balance in the buffer. The precipitates of nGO were observed in the buffer, but FA-nGO did not cause precipitation.[24]

2.11 Tween 80

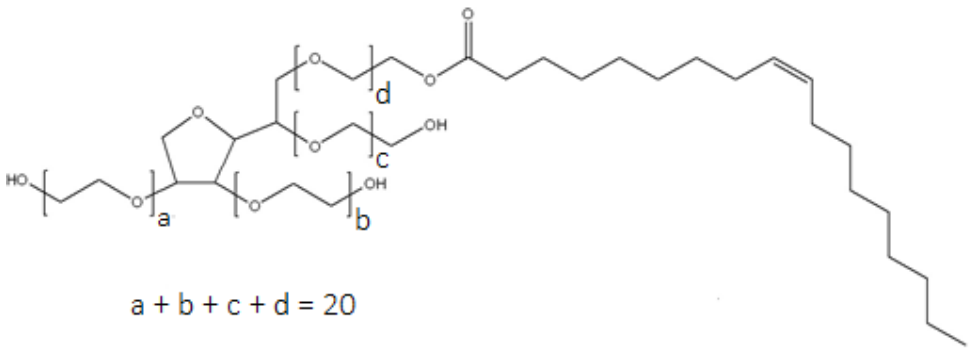

Figure 17. The chemical structure of Tween 80.

Tween 80 (Figure 17) is a nonionic surfactant, which has been used in drug delivery studies and functionalizing GO to enhance GO's biocompatibility.[25] Tween 80-GO reduced the aggregation of blood cells in mice compared with unfunctionalized GO. The effect of the addition of Tween to the GO suspension in PBS was studied for investigating the aggregation of blood cells when treated with GO.[25] GO caused the aggregation of blood cells, but GO treated with Tween prevented blood cell aggregation. Another significant finding was the capability of Tween 80 to change GO's zeta potential. Because of this, the blood cell aggregation was inhibited, as the change in zeta potential inhibited GO from attaching with blood cells. As a result, Tween 80 was also observed to prevent GO accumulation in mice's lungs.

3. The biological behaviour of graphene nanomaterials

The behaviour of graphene-based nanomaterial in the body depends on the properties of graphene material, such as the lateral size and proportion of oxygen and carbon.[26] Also, the biocorona formed after the nanoparticles have entered the body and the administration region of the material affects.[27] The natural features of graphene-based materials impart their accumulation, degradation, biodistribution, clearance, and translocation to secondary organs.[26] The environment, proteins, and ion concentration can change the properties of graphene materials after their entrance to the body. Because the thickness, surface charge, shape, and colloidal stability of the graphene materials can change in the body, their biological behaviour may change. Biotransformation, such as degradation, may alter the natural properties of graphene materials. Therefore the identification of the material in its pristine form as well as *in situ* changes is essential.[26] The preparation of graphene material, the type of the cell, and the type of the experiment are important things considering the use of graphene in a biological system.[1]

3.1 Behaviour in biological fluids

Graphene family nanomaterials (GFN) are capable of interacting in physiological media.[1] The size, surface chemistry and shape of the two-dimensional graphene sheets may change within the physiological media.[11] Salts, ions, and biomolecules can interact with graphene. Hence, aggregation of graphene may appear in the media. For example, graphene oxide is stable in water, but when the environment is changed to cell culture media, graphene oxide may aggregate because ions and salts in the media cover the negatively charged graphene oxide surface.[1]

The lateral size and thickness of graphene flakes are factors that affect graphene's ability to aggregate in physiological media. Bigger graphene flakes are more likely to interact with each other and aggregate than smaller graphene flakes.[28] To avoid aggregation, chemical methods, including centrifugation and washing, can be used.[1] Because thin graphene flakes have smaller aggregation ability, one way to prevent aggregation is making suspensions that contain thin and laterally small graphene flakes.[1] Also, functionalization stabilizes graphene family nanomaterials, provided that there are buffering agents, such as PEG, chitosan, dextran or serum proteins, in the solution.[1]

After nanomaterials have entered the human body, serum proteins adsorb on their surface, resulting in the formation of the protein corona[1] (Figure 18). The protein corona formation depends on the surface properties such as charge, geometry, and chemistry, but also the protein type affects the formation.[29] The protein corona has two parts, a hard corona and a soft corona. The hard corona part has stronger interactions with the nanoparticle surface. Therefore, the soft corona proteins are potentially substituted for the hard corona proteins afterwards.[1] The protein corona possibly increases the stability of the nanoparticles as proteins attach to the nanoparticle's basal plane with hydrophobic regions and the exterior part with charged hydrophilic regions.

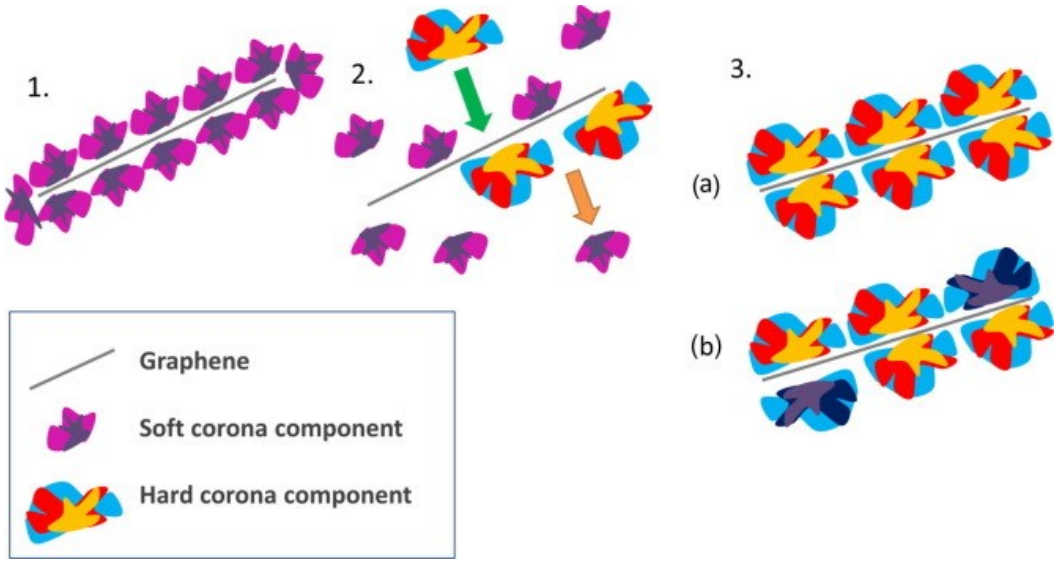

Figure 18. Graphene-based materials are covered with soft and hard corona components after their entrance to the human body. Published in Eur. J. of Pharm. and Biopharm., 104, McCallion, C.; Burthem, J.; Rees-Unwin, K.; Golovanov, A., and Pluen, A., Graphene in therapeutics delivery: Problems, solutions and future opportunities, 235-250, Copyright Elsevier 2016.

3.2 Inflammatory and immune response

Unmodified graphene family nanomaterials and modified graphene family nanomaterials can cause different adverse systemic responses.[1] Tan *et al.*[11] have recognized that graphene oxide can bind and activate the complement protein C3. The complement protein C3 is a part of the complement system, which belongs to the immune system. Certain mechanisms cause the activation of the complement system, which then leads to the activation of products C3a and C3b. As C3a operates, a stimulating

protein, C3a(des-Arg), detaches from its structure.[30] C3a(des-Arg) may cause, for example, cardiovascular diseases or diabetes.[31] Tan *et al*.[11] observed that when GO is functionalized with PEG, the amount of serum proteins attached on its structure and the activation of the complement protein C3 bound is significantly lower compared to unfunctionalized GO.[11]

Macrophages may engulf graphene oxide and pristine graphene, supporting cell activation and secretion of proinflammatory cytokines.[32] The geometry of the graphene flakes affect the cell activation and secretion of proinflammatory cytokines. Studies have also shown that inflammatory response is more significant when lateral flake dimensions are greater. This effect has been recognized *in vitro* and *in vivo*.[32] The secretion of inflammatory cytokines has been studied with two groups of graphene oxide flakes, with dimensions of 350 nm and 2 μm.[32] As a result, the secretion by macrophage has been observed to be more significant when the flakes are larger *in vitro*. Also, a larger flake size causes more macrophages and cytokines to flow into adipose tissues *in vivo.* The secretion of proinflammatory cytokines was noted to be more significant in murine macrophages[32] versus human cells.[33]

Functionalization of graphene family nanomaterials (GFN) has been recognized to impact inflammatory and immunological effects. Zhi *et al*.[34] studied how polyvinylpyrrolidone (PVP) covered GO flakes behave compared to uncovered GO flakes *in vitro*. They used macrophages and immature dendritic cells (DCs) and found that GO and PVP-GO could activate immature DCs. The activation of immature DCs induces biological processes, such as dose-dependent maturation and secretion of inflammatory cytokines.[34] The effect of GO and PVP-GO was also examined on the activity of mitochondria metabolism of human macrophages using the concentrations of 25 μg/ml, 50 μg/ml and 100 μg/ml during 48 h (Figure 19). Increased concentration of PVP-GO was seen to increase the relative activity of the macrophages, while the increased concentration of GO was recognized to reduce the activity.

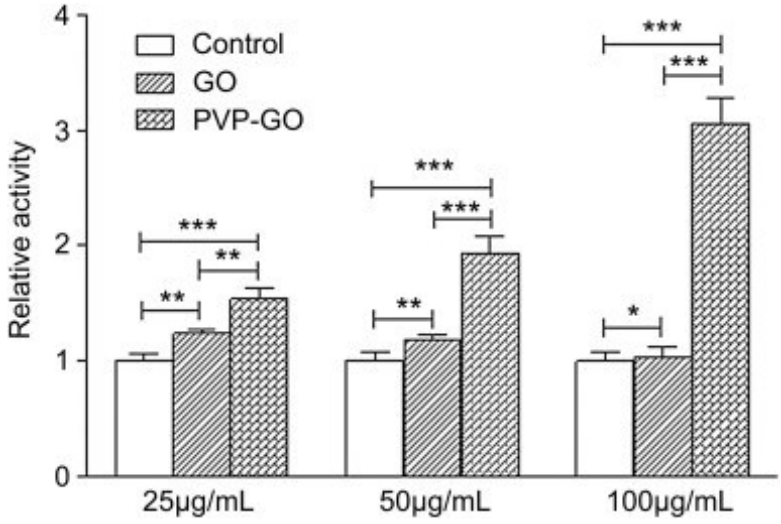

Figure 19. The effect of GO and PVP-GO with concentrations 25 μg/ml, 50 μg/ml and 100 μg/ml on the relative activity of mitochondria metabolism of human macrophages during 48 h. Reprinted from Biomaterials, *34*, Zhi, X.; Fang, H.; Bao, C.; Shen, G.; Zhang, J.; Wang, K.; Guo, S.; Wan, T., and Cui, D., The immunotoxicity of graphene oxides and the effect of PVP-coating, 5254-5261, Copyright 2013, with permission from Elsevier.

3.3 Behaviour with the blood components

Graphene nanomaterials need to be compatible with the blood components to be used as platforms for drug delivery. GFNs may damage the cell membrane and cause hemolysis after the production of reactive oxygen species (ROS).[13]

The ability of pristine graphene and carboxyl-functionalized graphene to cause hemolysis has been studied by Sasidharan *et al*.[35] Both formed aggregates in the cell culture media. When the particles were imaged with TEM, graphene particles were seen to aggregate around the red cells. Pristine graphene or GO, however, did not significantly break the red blood cells when the concentration was from 0 to 75 μg/ml (Figure 20).

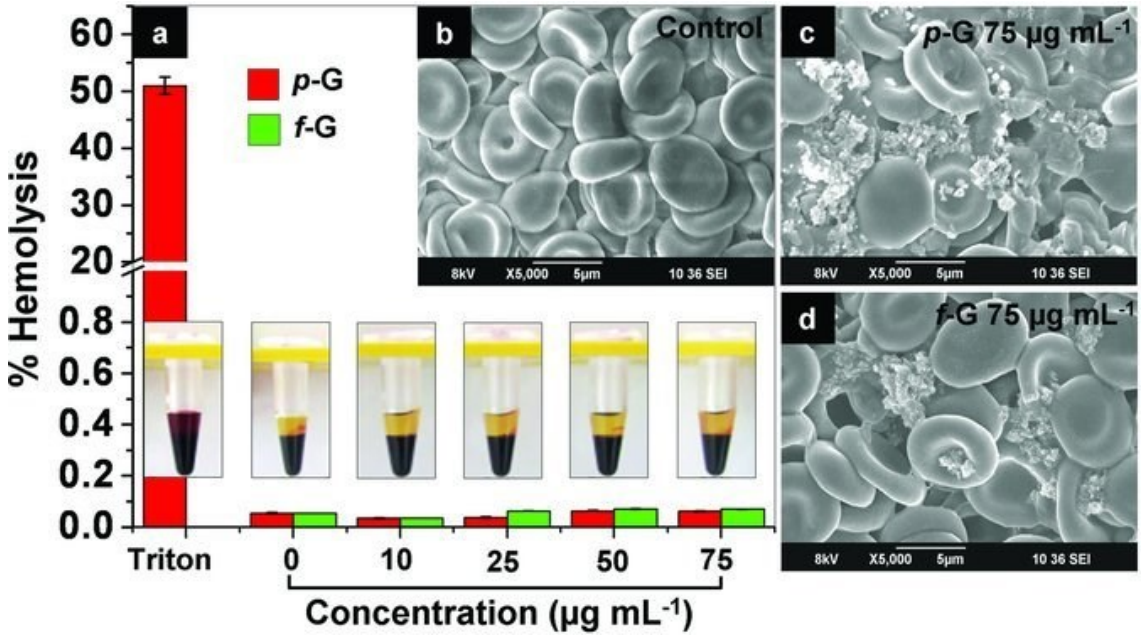

Figure 20. (a) The ability of pristine graphene (*p*-G) and carboxylic-functionalized graphene (*f*-G) with different concentrations to cause hemolysis. Triton was used as a control, and it points out 100% hemolysis. SEM images of (b) red blood cells, (c) red blood cells exposed to pristine graphene, and (d) red blood cells exposed to carboxylic-functionalized graphene.

If foreign compounds enter a human body, platelets are activated *in vitro*, indicating their adverse impact of the substances.[1] In the study of Singh *et al*.,[36] GO was injected into mice to investigate the level of thrombosis caused by GO, as the platelets interacted with GO's negatively charged surface and aggregated. rGO flakes were less thrombogenic because of the smaller amount of negative charges on the rGO's surface.[36] In the other study of Singh *et al*.,[14] the quantity of thrombosis by GO and amine-functionalized graphene, G-NH_2, was studied *in vivo*. The positively charged G-NH_2 was observed to be less thrombogenic compared to GO.[14] When comparing the aggregation effect of GO and G-NH_2, GO caused the aggregation of the platelets with the dose of 10 µg/ml. Conversely, G-NH_2 did not arise aggregation remarkably with the same dose. When 250 µg/kg of GO per body weight was used, thrombosis was as significant as in the case of combining 200 µg/ml of the platelet-activating agent collagen with 250 µg/kg body weight of GO. When 250 µg/kg of G-NH_2 was used, no significant thrombosis arose.[14]

3.3.1 Interaction of graphene oxide and reduced graphene oxide with serum proteins

Interaction with proteins may change the features of GO and rGO. The reduction level of GO and the material concentration imparts to the number and type of the proteins attached to GO or rGO.[29]

The interaction of GO and rGO with the proteins of fetal bovine serum (FBS) has been studied with five GO and rGO suspensions at different concentrations in the range of 10 – 160 µg/ml.[29] The zeta potential measurements of the prepared rGO-protein and GO-protein complexes were conducted. The change in the zeta potential after the conjugation with proteins was concluded to be due to the interaction with proteins. Also, the increase in zeta potential was thought to reduce the repulsive interaction of graphene sheets, which may cause aggregates. If the repulsive interaction of the sheets is reduced, the size of the GO sheets may rise.

In turn, GO's and rGO's ability to quench fluorescence was detected. GO was found to quench the fluorescence of the FBS proteins more significantly than rGO, which may be due to the different plane features of GO and rGO. The quantity of FBS proteins on the surface of GO and rGO was examined, and GO was found to have a higher tendency to bind serum proteins. Additionally, the increased level of reduction either in GO or rGO may prevent the adsorption of proteins.[29]

An essential observation was the effect of concentration on the number of attached proteins on GO's or rGO's surface. When the concentration of GO or rGO was higher, the number of serum proteins on the surface of each unit was smaller. Conversely, the overall number of serum proteins attached was higher. This means that at a lower concentration, the number of proteins on each unit was higher, but the overall amount of the proteins smaller. The reason for the observation is the adsorption efficiency. When the concentration of GO or rGO is smaller, the adsorption efficiency is better and vice versa. The type of proteins bound on GO and rGO was also observed to be different. Generally, proteins may attach to GO mainly with π-π interactions, but proteins to rGO usually attach hydrophobically. The differences in the type of interactions between the proteins and GO and rGO may be why the different types of proteins bound to GO and rGO.[29]

3.4 Bioaccumulation of graphene-based nanomaterials

The nanoparticle size and geometry affect their biodistribution.[27] If the nanoparticle's diameter is over 500 nm, a cell engulfs them, but kidneys excrete them if the diameter is under 30 nm. Nanoparticles with a diameter beyond 500 nm are led to the reticuloendothelial system (RES) after they are engulfed. If the diameter is 30-500 nm, nanoparticles accumulate in the stomach, heart, kidneys, spleen, bone marrow, and liver.[1] Graphene has been observed to behave similarly.

The circulation and secretion of Fe_3O_4 bound graphene sheets have been compared to the properties of GO-Fe_3O_4 nanoparticles using iron level for the circulation and secretion measurements.[1] After 14 days, GO-Fe_3O_4 nanoparticles were observed to reach the standard iron level, whereas the iron levels of GO-Fe_3O_4 nanosheets did not decrease. The concentration of nanoparticle and nanosheet complexes were both measured in the lung, spleen, and liver. The level of nanoparticles decreased after 24 hours in the kidney, but the level of nanosheets in the same organ was only ignoble after the increase after two weeks.[1]

The accumulation and aggregation of indestructible nanoparticles, such as graphene flakes, have also been studied in living organs.[27] The indestructible nanoparticles can activate granuloma production, which is a common process of carbon nanotubes.[37] Carboxyl functionalized graphene has been observed to accumulate and aggregate in mice.[32] After three months, a decreased level of graphene in the lungs was observed. Raman spectroscopy showed the degradation of graphene, and most of the degradation occurred on the outermost part of graphene. Degradation was remarkable in the spleen, which was observed from the graphene aggregates with the help of microscopic pictures and Raman measurements.[32] The degradation of endocytosed graphene flakes in murine macrophages was observed *in vitro* for seven days: half of the graphene flakes were destructed.[32]

PEG can enhance the biocompatibility of GFNs.[1] PEG functionalized graphene materials are also less toxic and degradable, as observed in comparative *in vitro* studies between PEG-GO and GO in human lung fibroblast and liver cells.[10] The toxicity of PEG-GO and GO has been tested *in vitro* in human lung fibroblast and liver cells. Enzymes can separate GO from the PEG functionalized GO system, in which an amino group containing a disulphide bond, SS-NH_2 is employed as a linker. Following the separation of GO from the system, GO can degrade and interact with the target cell.[10]

3.5 Routes of administration of graphene-based materials

3.5.1 Oral administration

Zhang *et al*.,[38] have administered ^{125}I labelled rGO nanoparticles of the size of 87.97 and 472.08 nm orally to mice.[38] The biodistribution of the sheets was tested over 60 days. The rGO sheets of both sizes were found in different organs, such as the heart and kidneys. The amount of rGO in the kidneys was remarkably higher at the end of the experiment than on the first day of the test. Based on the results, the rGO sheets with both sizes are rapidly taken in the gastrointestinal tract and then entered secondary organs via systemic circulation.[38]

Yang *et al*.,[39] functionalized GO sheets with PEG and tested their biodistribution in mice *in vivo*. They used three different materials; nanosized GO, large rGO, and nanosized rGO, and labelled them with ^{125}I. The stomach and intestine were the only organs where radioactivity was observed after four hours of the dosing. The radioactivity was measured again after 24 hours, but no detectable signal was observed, which potentially showed that the PEGylated graphene materials used in the research were not absorbed into the intestine.

The inhalation route has been observed to be a significant factor when studying the biodistribution of graphene-based materials in mice.[40] GO with lateral dimensions of 10-800 nm and 1-2 layers were used by Li *et al*.[40] The layers were labelled with ^{125}I, and the intratracheal instillation was used. Most of the GO sheets were observed in the lungs, and the amount of GO reduced radically from 10 min to 12 h. There was less GO in the other organs, such as the kidneys. Since a significant amount of the material was also observed in the stomach and intestines, it was concluded that GO could have moved to the blood either from the lungs or via intestinal adsorption.[40]

The biodistribution of graphene platelets constituting of a few graphene layers (FLG) labelled with ^{14}C has been studied by Mao *et al*.[41] 28 days after the administration, the material was mostly observed in the lungs (Figure 21) and minor amounts in the stomach and intestines.

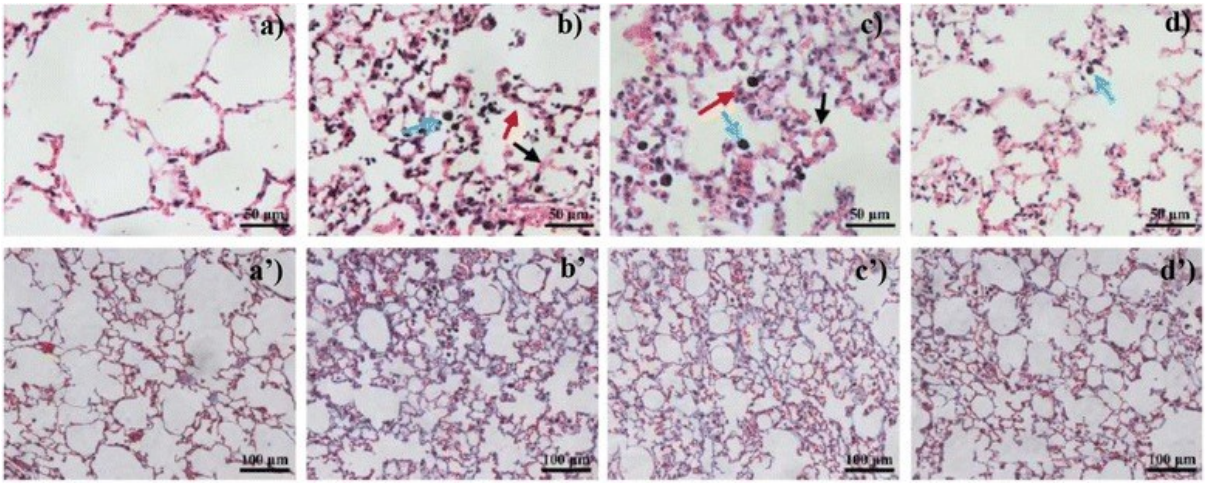

Figure 21. The lungs of six mice after treatment with FLG. a-d present the lungs stained with hematoxylin-eosin, while a'-d' were stained with Masson. The images taken (a) and (a') after the treatments; (b) and (b') one day after the treatments; (c) and (c)' 7 days after the treatments; (d) and (d') 28 days after the treatments. Mao, L.; Hu, M.; Pan, B.; Xie, Y., and Petersen, E.J., Biodistribution and toxicity of radio-labeled few layer graphene in mice after intratracheal instillation, *Particle and Fibre Toxicology*, *13(7)*, **2016**, 1-12. (https://creativecommons.org/licenses/by/4.0)

Based on the findings, it was assumed that a mucociliary clearance mechanism transferred the materials.[41] The material had not significantly moved to the bloodstream, as the quantity of the material was low in the spleen and liver. Also, the decrease of the material in the organs depended on time. The biodistribution of the graphene platelets detected in the experiment is similar to the biodistribution of ^{14}C labelled multiwalled carbon nanotubes after being digested to the pharynx and accumulated in the spleen of mice.[26]

3.5.2 Subcutaneous administration

The biological behaviour of PBS functionalized GO and rGO has been tested by a subcutaneous administration.[42] After administrating GO and rGO, acquisition of monocytes between rGO and the subcutaneous tissue was suspected. After three days, the monocytes were found to be unabsorbed within rGO. Later, at the 7^{th} and 14^{th} days, macrophages and fibroblasts were slightly infiltrated on the GO but completely infiltrated on the rGO. By the 14^{th} day, collagen started to form on the surface of rGO, meaning fibrosis formation. After 29 days, the GO's macrostructure was infiltrated by macrophages, fibroblasts, and large cells, whereas the macrostructure of rGO started to heal and the

tissue to repair. Also, extracellular matrix remodelling was detected, but no fibrosis appeared. The factors that caused the fibrosis may have been the macrophages.

3.5.3 Intraperitoneal administration

After intraperitoneal administration, GO can form aggregates in the peritoneal cavity.[43] The aggregates have not been found to interact with the other organs or blood components or cause toxicity. Following the intraperitoneal injection, less oxidated rGO has been observed to attract fewer monocytes in the peritoneal cavity than GO. The cells restored from the peritoneal cavity tended to form more proinflammatory cytokines and chemokines in GO than rGO. rGO was assumed to be removed faster than GO, meaning that the clearance rate possibly depends on the use of monocytic cells and inflammogenicity of GO and rGO.[43]

Following intraperitoneal administration, PEGylated graphene materials possibly biodistribute less compared to non-nanosized graphene materials.[39] PEGylated forms of nanosized GO (lateral size 10-40 nm), nanosized r-GO (lateral size 50-80 nm), and the non-PEGylated nanosized r-GO (lateral size 10-30 nm), have been found to accumulate in the liver and spleen in mice after one day of the exposure. After seven days of exposure, nanosized forms decreased in the liver and increased in the spleen, but the larger rGO-PEG increased radically between the first and seventh day in the liver and spleen. After macroscopic experiments, non-PEGylated GO was observed to aggregate in the peritoneal cavity. After 30 days of the injection, black materials, assumed to originate from the injections, were found in the histological sections.

PEGylated rGO probably passed over the blood-brain barrier in mice when their biodistribution, clearance, and toxicity were studied.[44] PEGylated rGOs (lateral size 1 μm, thickness 4-9 nm, C/O ratio 3.7) were identified in the kidney, brain, liver, and spleen. On the third day, the material was observed in the spleen in high concentrations. Over time, the amount of the material reduced in the spleen, increased between 7-14 days in the brain, decreased by the 21 days in the brain, and increased radically in the liver by the day 21.[44]

3.5.4 Intravenous administration

Intravenous administration is a commonly used way to administrate nanomaterials.[45] The factors affecting the biodistribution and fate of nanomaterials following intravenous administration are size, shape, and surface charge. GO-PBS accumulated more in the lungs of mice compared to GO-PBS-Tween 80, whereas GO-PBS-Tween 80 accumulated more in the liver.[25] The observations were made with the help of histological sections, where the black colour of organs resulted from treating them with graphene materials. In conclusion, the higher the colloidal stability, the more GO sheets cross the lung capillaries.[25]

The whole-body imaging of mice has been used for the biodistribution evaluation using poly(sodium 4-styrene sulfonate)-GO sheets (lateral size 300-700 nm and thickness 1-4 nm) labelled with the fluorescent Cy7 dye.[46] After 24 hours of treatment, the liver and bladder were the only organs where the fluorescence was found. From day 14 to day 180, the substances were discovered in the liver, lungs, and spleen with the help of histological images.

rGO-PEG sheets (lateral size ~1 µm and thickness 4-9 nm) were observed in the liver and spleen after three days of injection in several studies (Figure 22).[44] After 14 days, the sheets were present in the brain, and the amount decreased by day 21. Oxidized few-layer graphene (FLG) platelets (lateral size 150-220 nm) agglomerated and made 0.5-10 µm constructions in the kidneys, liver, lungs, and spleen. The aggregated forms of FLG platelets were still found after 90 days of the injection, but a little bit of degradation was also detected.

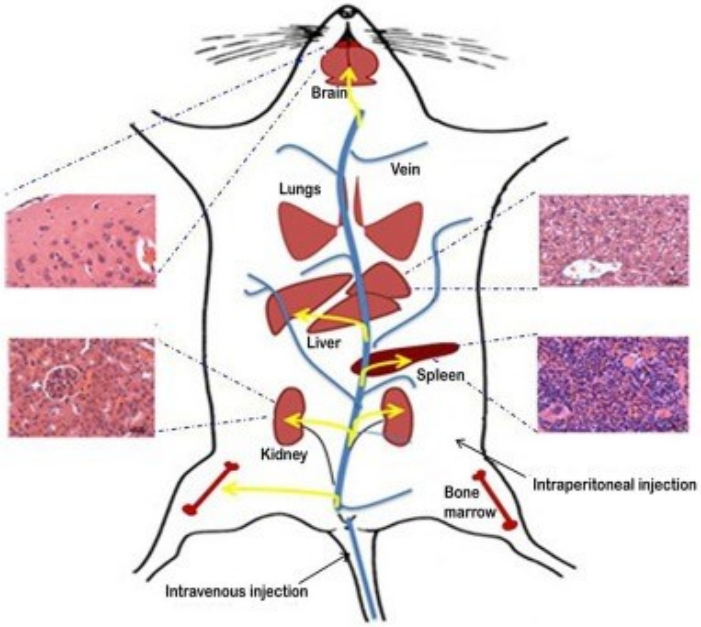

Figure 22. The circulation of GO following intravenous and intraperitoneal administration in the mouse. Reprinted from Biomaterials, *131*, Syama, S.; Paul, W.; Sabareeswaran, A., and Mohanan, P.V., Raman spectroscopy for the detection of organ distribution and clearance of PEGylated reduced graphene oxide and biological consequences, 121-130, Copyright 2017, with permission from Elsevier.

The interaction of GO and rGO with serum proteins can lead to capillary blockage in the case of intravenous administration, as the size of GO and rGO increases when they interact with serum proteins after their administration.[29] Because of this, the impact of the size is remarkable considering the intravenous administration.

3.6 Cell targeting of graphene oxide drug complexes

When using an active targeting mechanism, drugs are delivered to particular cell types or tissues (Figure 23).[1] The active targeting possibly speeds the cell uptake and intracellular trafficking. The amount of drug bound to the platform is greater in active targeting than passive targeting or free drug.

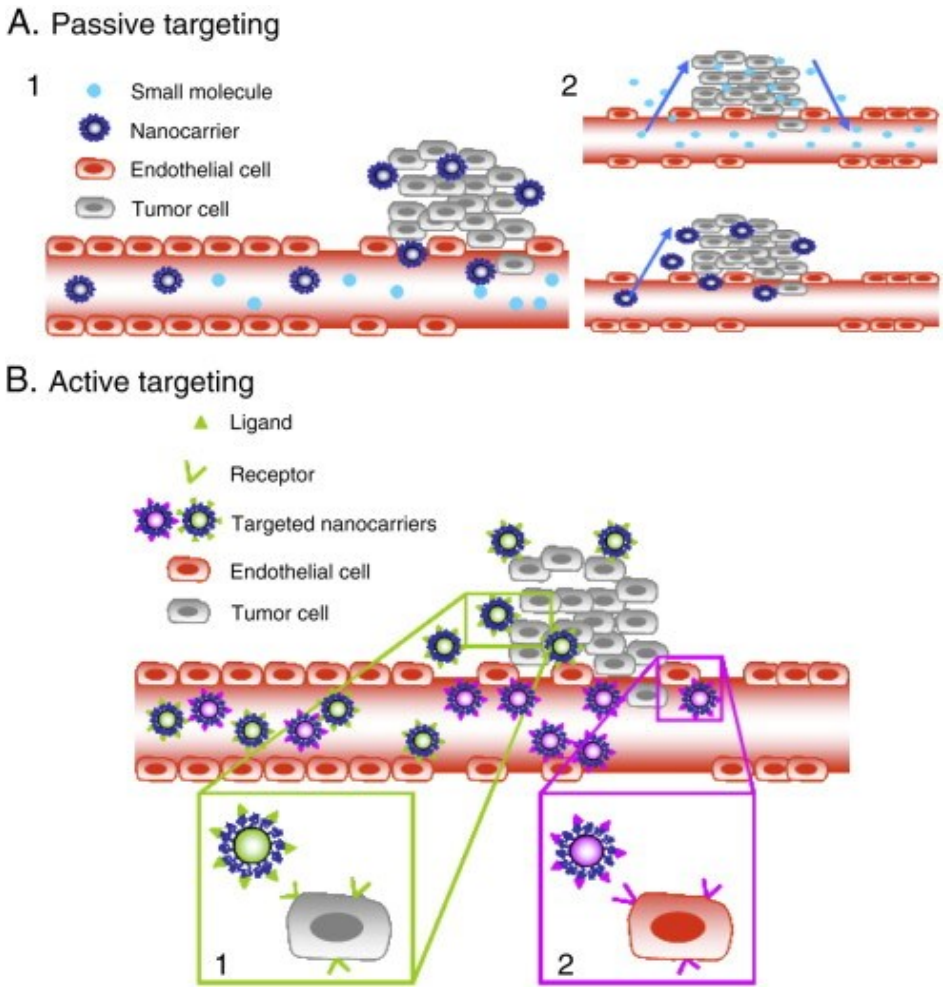

Figure 23. A: Passive targeting. 1. Drugs are delivered to tumors via weak blood vessels. 2. Drug molecules are released from the tumor to the blood vessel and vice versa due to their small size. B: Active targeting. With the help of their ligands, nanocarriers attach to 1. cancer tumor 2. endothelial cells. Reprinted from Journal of Controlled Release, *148*, Danhier, F.; Feron, O., and Préat, V., To exploit the tumor microenvironment: Passive and active tumor targeting of nanocarriers for anti-cancer drug delivery, 135-146, Copyright 2010, with permission from Elsevier.

Following the accumulation within the tumor, covering the nanoparticle's surface with suitable ligands enhances the affinity of the particle and drug efficiency, as the ligands attach to the tumor's overexpressed receptors. Generally used ligands are antibodies, peptides, proteins, aptamers or small molecules.[47] A commonly used ligand is folate acid, which recognizes overexpressed folate receptors on the surface of cancer cells.[1] Folates are naturally non-toxic, and they are possibly taken up through receptor-mediated endocytosis. Additionally, the transferrin receptor is overexpressed on the surface of some cancer cells, and it has been utilized as a ligand on GO's surface with localized heating.

Molecules of which mass is greater than 40-45 kDa are actively targeted, whereas smaller molecules are carried passively (Figure 23).[1] Smaller molecules are capable of going through the nuclear pore complex. For example, in the classical nuclear import cycle, the most well-understood mechanism, a cytoplasmic carrier protein, observes the macromolecules that will be imported. The macromolecule attaches to the target protein and, after that, to the particular receptor in the nuclear pore complex.[1] Then, the trimeric complex translocates into the nucleus. Proteins have a Nuclear Localisation Signal (NLS) sequence in their structure to recognize them. NLS has been employed on the surface of the GO-PEI complex for delivering plasmid DNA, and NLS was observed to enhance the vehicle's efficiency in 293T and HeLa cells compared to the carriers without NLS.

Non-cancerous cells stay alive because cytotoxic substances are targeted only to cancer cells by targeted drug delivery systems (DDS).[48] The complex is targeted to the target cell after the cargo has been loaded to the structure. By using passive targeting mechanisms, broad functionalization is not needed. Graphene platforms have been widely been studied for passive targeting.[1] Graphene family nanomaterials can accumulate successfully within tumors, as cancer cells use the enhanced permeability and retention (EPR) effect, which was found in 1980 by Maeda *et al*.[49] EPR effect means that tumors have overvascularisation, leaky vasculatures and reduced lymphatic drainage. With the help of those properties, graphene family nanoparticles may be delivered to the tumor by blood circulation.[1] Tumors tend to have a more permeable inner surface, endothelium, as inflammation/hypoxia exist within them. Due to hypoxia, tumors associate with new, leaky vessels, which enable nanosystems to enter the tumor. Tumors do not have normal lymphatic drainage, meaning that nanoparticles can stay inside the tumor cells.[48]

In the case of vascular targeting, angiogenic endothelial cells near the tumor cells are targeted. Those cells are connected to blood vessels, which means that the amount of blood circulating to the tumor is decreased. Cancer cells are not able to get oxygen or nutrients, causing hypoxia and necrosis.[50] The advantages of vascular targeting are its capability to restrict poor delivery of drugs and drug resistance. The method may be used for various tumors and in heterogeneous tumours.[51]

EPR effect may be modified either chemically or mechanically, aiming at vascular normalization, which would help nanocarriers to accumulate better.[48] Chemical compounds increasing EPR are bradykinin, nitric oxide, prostaglandins, peroxynitrite, vascular permeability factor (VPF)/ vascular endothelial growth factor (VEGF), and other cytokines. They promote hypertension and vascular normalization, so the tumor perfusion is possibly increased. Alternatively, ultrasound, hyperthermia, radiation, and photo-immunotherapy modify the vessels of tumors, hence enhancing the entrance of

nanosystems to the tumour.[48] The use of hyperthermia, in which the infra-red light is used in the targeted area, is possible because GO has high infra-red absorption.[1] The infrared light has also been recognized to enhance cell permeability and transfection efficiency of the graphene complexes.

The size of nanoparticles and circulation time impart to the targeting of the tumor when EPR is used. The size is also a significant factor for the particle's retention inside the tumor, as tumors commonly have fenestrations with size 200-800 nm in their structure.[48] If the nanoparticle's diameter is less than 6 nm, they are removed by renal excretion (RES), whereas RES remove nanoparticles if their diameter is more than 500 nm. Based on these observations, the most appropriate size of the nanoparticle would be 20-200 nm.[48] Other factors affecting the circulation time are surface chemistry and the charge of the nanoparticle. PEGs are used to make the nanoparticles hydrophilic and slightly anionic or neutral, and PEGs also make particles 'look like water'.[52] PEG can also inhibit aggregation and changes charge and hydration, therefore inhibiting non-specific interactions.[48]

The EPR effect is more effective when circulation time is longer, which results in higher intratumoral accumulation.[53] In the EPR effect, particles can avoid renal clearance, and therefore they flow into the interstitial space of the tumour.[54] The tumors' reduced lymphatic drainage and the nanoparticles' enhanced retention in tumors originate from the fast growth of tumours. The EPR effect has been tested broadly in mice, but their murine tumors have some differences compared to human tumors. It means that the experimental results of the drug carriers may differ between preclinical and clinical tests. Human tumors are formed after cell or cells in a tissue gather mutations. After that, the cells proliferate without control, which commonly takes years to develop the actual tumors, with the right set of mutations.[55] The immune system affects the formed tumors, and the tumors are genetically highly diverse, making treatment challenging. In the experiments, the cells developing into tumors in mice grow without the immune system's influence, and the resulting tumors form up to a few weeks. As mice are smaller than humans, the tumor-to-body weight ratio is remarkably higher in mice. Humans and mice also get chemotherapy at different periods because their metabolism is different. A human patient needs to recover from the toxic effects after treatment. Therefore, the treatment period is commonly between two and four weeks, whereas mice often get dosages every three days.[56] Therefore, human tumors have more time to repair. It is impossible to sort out cancer recurrence in mice in the same period since humans' lives are longer.

3.7 Cellular toxicity of graphene-based materials

3.7.1 Cytotoxicity study of GO-PEG, GO-BSA, rGO-PEG and rGO-BSA

Functionalization is possibly a key factor for the level of cytotoxicity in GO and GO derivatives. In the study of Li *et al.*,[10] pristine GO and GO-PEG, GO-BSA, rGO-PEG and rGO-BSA conjugates were tested in three different human cell lines, liver cell line HL-7702, lung fibroblast line MRC-5 and macrophage line U937, to define the cytotoxicity of the conjugates. Unfunctionalized GO and the conjugates were administrated by using the concentrations 25 µg/ml, 50 µg/ml, 100 µg/ml and 200 µg/ml. The surface functionalization of GO decreases remarkably its cytotoxicity. In the study, the relative cell viability, i.e. the percentual amount of viable cells, was noted to be about 50% when the concentration of unfunctionalized GO was 200 µg/ml. After administration of GO having a concentration of 25 µg/ml, the relative cell viability was 80-90%. The results were similar with all the tested cell lines. The cell viability studies were performed using two different tests, the first being 3-(4,5-dimethylthiazol-2-yl)-2,5-diphenyltetrazolium bromide (MTT) method, in which MTT was utilized to measure the cell viabilities. In the second test, Cell Counting Kit-8 (CCK-8) assay, the solution was added to the cells after treatment with GO and GO conjugates to record the cell viabilities.

GO-PEG, GO-BSA, rGO-PEG and rGO-BSA can decrease the cytotoxicity compared to unfunctionalized GO.[10] The best performance was observed for GO-PEG, which showed the relative cell viability of about 80% after the exposure of 72 h in the case of all three cell lines. This observation was made even in the case of the highest concentration. The CCK-8 assay showed lower relative cell viability values for GO compared to the MTT assay.

The cell viability tests described revealed the importance of GO's surface functionalization. The functionalized GO forms have been noted to cause the least toxicity for the cells, as their cell viability values have been larger compared to unfunctionalized GO.[10]

3.7.2 Cytotoxicity study of G-NH_2

MTT study has been performed for studying the cytotoxicity of amine-functionalized graphene (G-NH_2).[14] In the treatment with human platelets, amine-functionalized graphene-based constructs were tested at concentrations ranging from 2 μg/ml to 20 μg/ml. The MTT study showed that cells stayed alive in all tested concentrations. At the lowest concentration, 2 μg/ml, no platelet aggregation was observed, while 10 μg/ml of G-NH_2 caused a very tiny amount of aggregation. The cytotoxicity towards the THP-1 monocyte cell line of humans was also studied. After one day of treatment, G-NH_2 was not found to cause remarkable cell viability. Based on these results, G-NH_2 can be concluded to be more biocompatible than GO.

3.7.3 Cytotoxicity studies of GO and GO-PEI

CCK8 assay has been performed to examine the GO's cytotoxicity in human fibroblast cells.[57] Human fibroblast cells were treated with GO concentrations of 5 μg/ml, 10 μg/ml, 20 μg/ml, 50 μg/ml and 100 μg/ml. GO with concentrations of 5, 10, and 20 μg/ml showed no significant cytotoxicity, and over 80% of the cells stayed viable. When the cells were exposed to GO of 50 and 100 μg/ml, less than 80% of the cells stayed viable. Based on this study, the lower the concentration of the GO-based material, the less cytotoxicity the construct causes.

GO has been observed to have an insignificant cytotoxic effect on T lymphocytes when GO's concentration is 1.6 – 25 μg/ml.[58] After increasing GO's concentration from 25 μg/ml to 50 μg/ml, the relative viability of the cells reduced. GO was also less cytotoxic than PEI functionalized GO towards T lymphocytes when the concentration is 1.6 – 100 μg/ml. As a conclusion from the study, PEI functionalized GO was more cytotoxic than pristine GO. The reason for the higher cytotoxicity of PEI functionalized form is its positively charged surface, which enhances the electrostatic adsorption with the cell membrane, thus possibly breaking the membrane.

4. Graphene-based nanomaterials in drug delivery

Carbon materials can be utilized in biological environments due to their unique optical and electrical features, and their size is similar to the size of biological macromolecules.[59] They also can transport through the cell membrane, which possibly is achieved by endocytosis.[60]

The idea in the drug delivery (Figure 24) is to expand the bioavailability in a particular area in the body within a required time.[61] The dosage of the drug needed and the adverse side effects originating from the drug can be decreased with the help of carbon nanomaterials, such as graphene.[2] Carbon nanomaterials support the delivery of the drug to a specific location and help the drug accumulate in tumors. Therefore, it is possible to deliver drug molecules to the actual cancer tissue, whereas healthy tissues remain untouchable.[2] Graphene can be utilized as a drug transport vehicle, as small drug substances and biopharmaceuticals can be attached to graphene.[62]

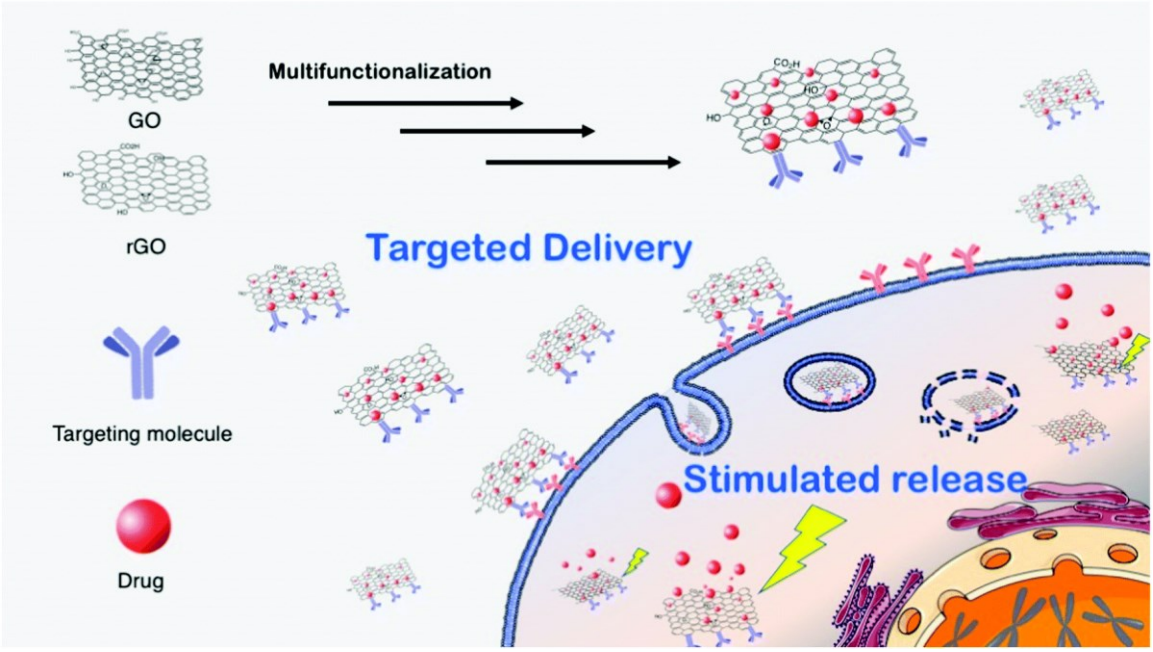

Figure 24. GO and rGO can be used as platforms for drugs and targeting molecules in targeted drug delivery, and the multifunctionalization of the materials can be utilized as well. Drug molecules are released after the graphene-based drug delivery complex is delivered into a cell. Chem. Soc. Rev., **2017**, *46*, 4400-4416 – Published by The Royal Society of Chemistry.

GO is suitable as a therapeutic platform because of the combination of hydrophobicity and hydrophilicity. A negatively charged surface induces high and stable water dispersibility, whereas

hydrophobic interactions or π-π interactions can be utilized to attach drugs.[12] Also, GO has the highest stability at pH values of 7 or 8. Therefore the drug release from the graphene oxide platform is most efficient in mildly acidic environments.[63] The degradation and release of the drug depend on the loading and the size and shape of the graphene-drug complex.[1]

Because GO lacks rigidity, its ability to penetrate the cell is low. GO's lateral dimensions do not restrict drug loading.[64] They may, however, limit blood-brain transport, renal clearance, and biodegradation. The behaviour of the GO as a drug platform depends on three aspects: loading capacity of the drug, degree of toxicity and biocompatibility of the GO drug platform and ability of the platform to release drugs at the target. Multifunctionalized GO may improve the drug's thermal stability and half-life.[64]

4.1 Drug attachment on graphene oxide platforms

4.1.1 Attachment of doxorubicin and camptothecin

An anticancer drug, doxorubicin (DOX), has been bound on the surface of GO.[24] DOX was noted to release more effectively in tumors than healthy tissues. The amount of released DOX depended on the pH and buffer solution's salt concentration. The quantity of glutathione (GSH) and reductive cysteine is greater within cancerous cells, meaning they are more acidic than healthy cells. Therefore, GO is capable of releasing DOX quicker in cancerous cells. Additionally, Zhao *et al*.,[65] used cysteine polymethacrylic acid crosslinked nano-graphene oxide polyethylene glycol, from which DOX release was six times faster in the cancerous tissues with a pH of 5.0 versus healthy tissues with a pH of 7.4. Peptide chlorotoxin-conjugated GO sheets have been noted to kill glioma cells when they were exposed to DOX.[66] The complex was also reported to be more efficient compared to the pristine DOX or GO-DOX complex.

If two or more pharmacological agents are used for targeted drug delivery, the treatment may be more efficient.[24] DOX and anticancer drug camptothecin (CPT) together are more toxic within cells than the complex containing only DOX or CPT. The multidrug complex has also been recognized to target cancerous cells more effectively. To beat the multidrug resistance, adriamycin (ADR) has been attached to the platform consisting of polypropylene glycol (PPG), PEI, poly(sodium 4-styrene sulfonate) (PSS) and GO.[67] After miR-21 targeted small-interfering RNA (siRNA) was bound on the

complex, it was targeted to MCF-7/ADR breast cancer cells that resist ADR drug. The complex showed enhanced accumulation of ADR within the MCF-7/ADR cancer cells because of the PPG, and the complex also had higher cytotoxicity versus pristine ADR. Therefore, PPG possibly reverses ADR resistance taking place in MCF-7/ADR cells.[67]

An aromatic DOX can bind on the surface of nanosized graphene oxide (nGO) by π-π interactions following the use of antibodies to destroy cancer cells.[68] Before the loading of DOX to the nGO, PEG star-polymers were covalently bound to the surfaces, and the edges were chemically activated. The quantity of DOX loaded to the nGO was observed to be significant. With the help of Rituxan CD20+ antibodies on the nGO's surface, DOX was delivered selectively to the cancer cells, as nGO-PEG complexes seem to behave pH-dependently. Since the surroundings of the tissues and micro-environments within lysosomes and endosomes are acidic, drugs could be released effectively from the nGO-PEG platforms.

Nanosized graphene oxide has been used for delivering mixed anticancer drugs for targeting human breast cancer cells (MCF-7).[24] The hydroxyl, epoxide, and ester groups of the nGO structure were altered to COOH groups by treating nGO with $ClCH_2COONa$ in basic environments. Because MCF-7 cells have folate receptors in their structure, nGO was used with folic acid (FA). DOX or CPT was loaded to the nGO surface, resulting in nGO-DOX and nGO-CPT composites, where the drugs were bound hydrophobically or using π-π bonds. FA-nGO/DOX complexes were found to be explicitly uptaken by MCF-7 cells using receptor-mediated endocytosis. FA-nGO was observed to be nontoxic when its concentration was less than 100 μg/ml. The study showed that the drug loading ratio of DOX is significantly greater than that of CPT, as the capacity for DOX was more than 400% and for CPT about 4.5% (Figure 25). The reason for this is likely the different chemical structure of DOX and CPT, meaning they interact unequally with nGO.

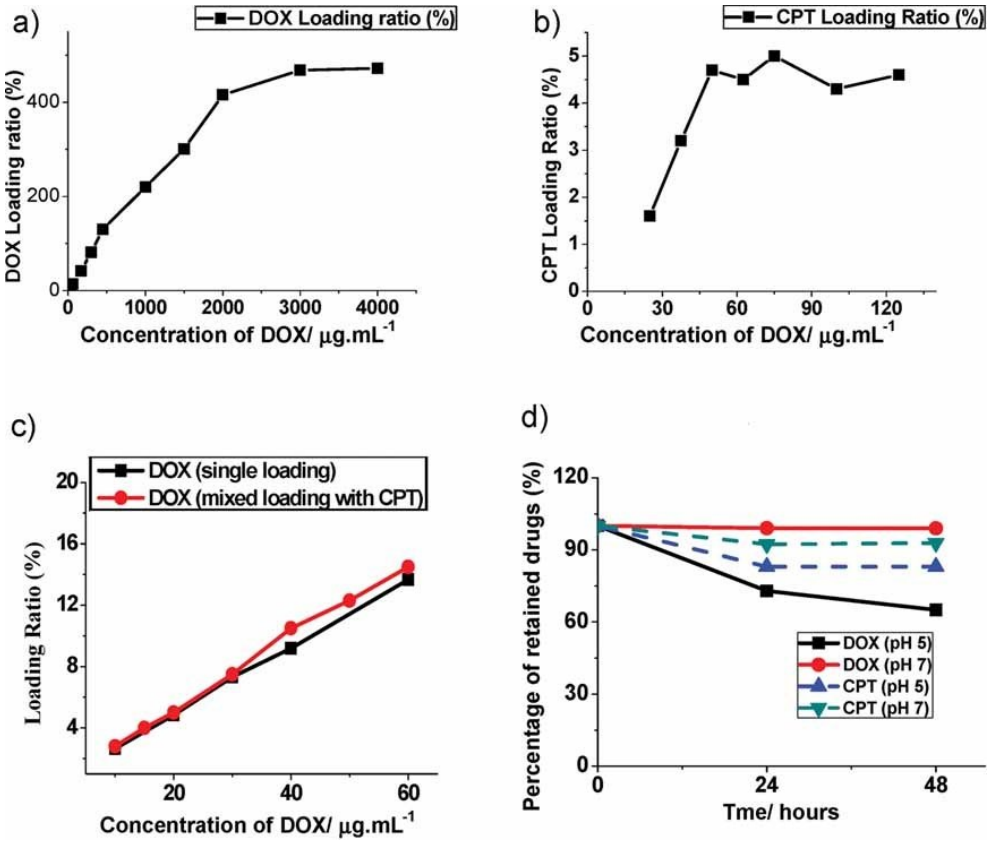

Figure 25. (a) The loading ratio of DOX, (b) the loading ratio of CPT, (c) the loading ratio of DOX compared to the loading with DOX and CPT and (d) the remained DOX and CPT portions on the platforms at pH 5 and 7. Copyright 2010 Wiley. Used with permission from Zhang, L.; Xia, J.; Zhao, Q.; Liu, L, and Zhang, Z., Functional Graphene Oxide as a Nanocarrier for Controlled Loading and Targeted Delivery of Mixed Anticancer Drugs, Small, John Wiley and Sons.

The pH value can impart to the release of the drugs.[24] In the study of Zhang *et al.*,[24] at the pH of 5.0, 35% of DOX and 17% of CPT was released, but at the pH of 7.0, the released quantities of the drugs were remarkably smaller. When pH is lower, CPT and DOX are more hydrophilic and soluble in water and are therefore released more significantly from the platform. Since DOX has an amino group in its structure, DOX releases more efficiently at low pH values. The cytotoxicity of FA-GO/CPT/DOX (20 ng/ml of DOX and CPT) was remarkable, so the multidrug system may overcome the drug resistance of cancer cells.[24] The cytotoxicity of NA-nGO/CPT or FA-nGO/DOX was not significant.

A galactosylated chitosan/graphene oxide/doxorubicin complex has been developed for cell uptake experiments and cell proliferation analysis[22] (Figure 26). The conjugation of chitosan and lactobionic acid to the material was reached by carbodiimide-mediated amide bond formation. DOX was

noncovalently loaded onto the GO using a PBS solution (pH 7.4) and GO-DOX formed with the help of freezing and drying. Noncovalent interactions were utilized to load DOX onto the GO and galactosylated chitosan onto the GO-DOX nanoparticle.

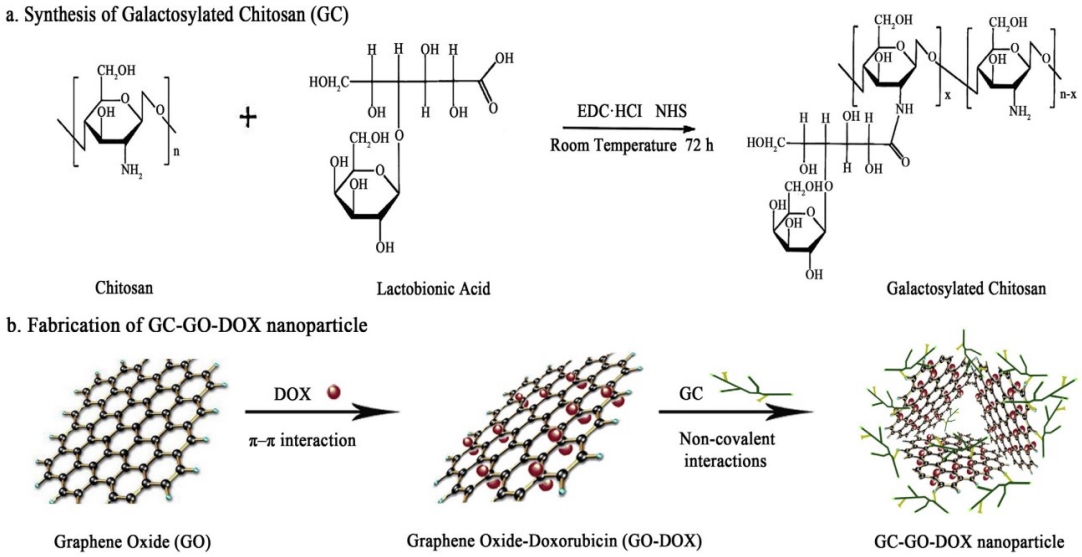

Figure 26. (a) Preparation of galactosylated chitosan in the presence of EDC and NHS. (b) The noncovalent attachment of DOX on the surface of GO and galactosylated chitosan. Reprinted from Journal of Colloid and Interface Science, *516*, Wang, C.; Zhang, Z.; Chen, B.; Gu, L.; Li, Y, and Yu, S., Design and evaluation of galactosylated chitosan/graphene oxide nanoparticles as a drug delivery system, 332-341, Copyright 2018, with permission from Elsevier.

PEGylated folate (FA-PEG) and peptide-decorated GO nanovehicle has been constructed for treating cancer cells (Figure 27).[69]

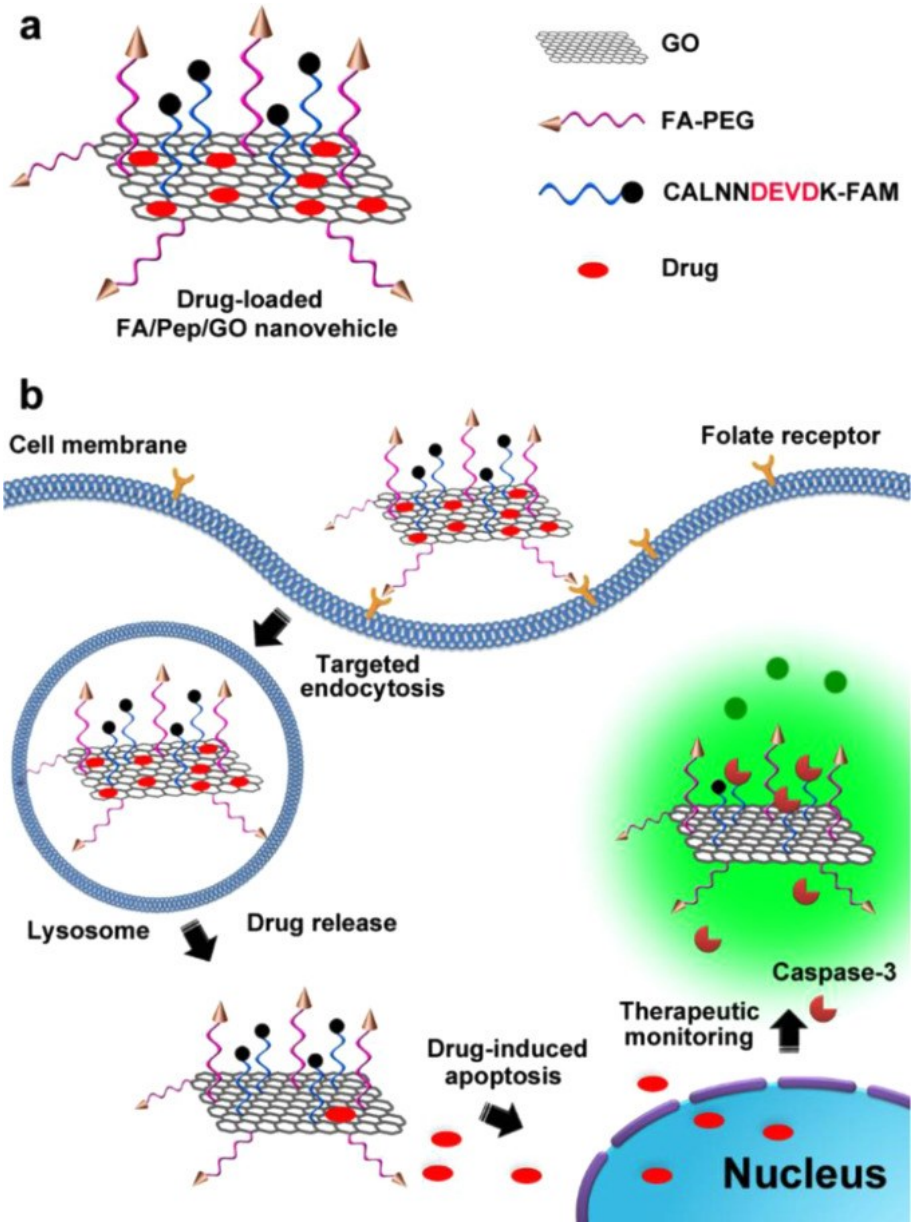

Figure 27. Folic acid and polyethylene glycol functionalized GO drug complex can be delivered into a cell with the help of the folate receptors on the cell membrane. Reprinted from Biosensors and Bioelectronics, *80*, Tian, J.; Luo, Y.; Huang, L.; Feng, Y.; Ju, H., and Yu, B., Pegylated folate and peptide-decorated graphene oxide nanovehicle for *in vivo* targeted delivery of anticancer drugs and therapeutic self-monitoring, 519-524, Copyright 2016, with permission from Elsevier.

Before using the complex for targeting, GO sheets were shown to disperse significantly. Camptothecin, curcumin, evodiamine and silyblin were loaded to the FA/Pep/GO's surface. The drug loading capacity (LC) was measured to be more than 1.7 mg/mg, and the loading efficiency (LE) 90%.[69] The release of camptothecin depended on the physiological pH. At a pH of 5.0, more camptothecin was released than at pH 7.4. In more acidic conditions, camptothecin is more

hydrophilic because of the protonation of nitrogen. Therefore, hydrophobic interactions between camptothecin and FA/Pep/GO are minimized.

Human cervical carcinoma, HeLa cells, were handled with CPT, /CPT/Pep/GO or FA/CPT/Pep/GO for studying their cytotoxicity. FA/Pep/GO was recognized to be biocompatible and CPT cytotoxic. Its cytotoxicity depended on its concentration; at higher CPT concentrations, cytotoxicity was more remarkable. The CPT/Pep/GO showed less toxicity than FA/CPT/Pep/GO. Thus, FA was indicated to be significant in CPT's targeted delivery into HeLa cells. The behaviour of folate receptor (FR) against FA was studied as well. On the membrane of several cancer cells, FR's high affinity for FA is up-adjusted, therefore using PEGylated FA on the GO's surface supported the delivery of the complex to the cancer cells. To summarise, nanocomplex had high loading capacity (LC) and loading efficiency (LE) values and the possibility to load aromatic and hydrophobic drugs on its surface. By using FA-PEG on the surface, the nanovehicle targeted the cancer cells containing FR.[69]

Acidic tumour environments have been exploited for altering graphene-based flakes charge.[70] After loading DOX to graphene-based flakes and functionalizing the flakes with PEG, the flakes are negatively charged in normal environments. Conversely, in acidic environments, such as in tumours, flakes change their charge to positive (Figure 28). That enables the interaction with the negatively charged cell membrane and endocytosis occurring after it.[1] It is possible to use additional factors such as fluorescence imaging, flow cytometry, and photothermal ablation to enhance cell death.

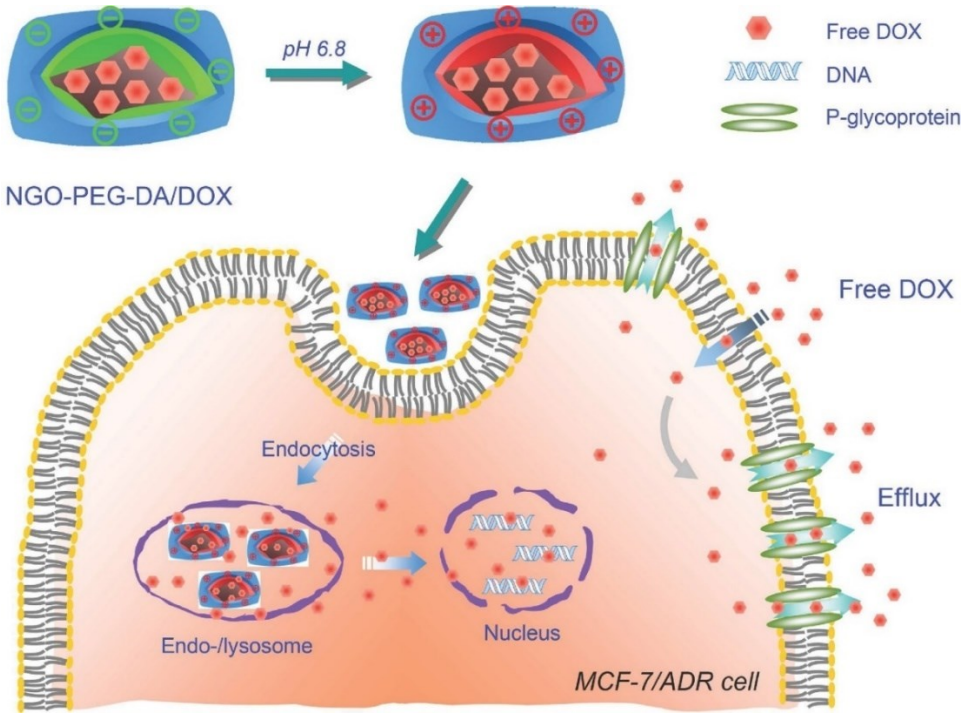

Figure 28. After the negatively charged nGO-PEG-DA/DOX is changed to positively charged in the tumor's surroundings (pH 6.8), the complex enters the tumor and DOX is released from the platform due to the acidity. Copyright 2014 Wiley. Used with permission from Feng, L.; Li, K.; Shi, X.; Gao, M.; Liu, J., and Liu, Z., Smart pH-Responsive Nanocarriers Based on Nano-Graphene Oxide for Combined Chemo- and Photothermal Therapy Overcoming Drug Resistance, Advanced Healthcare Materials, John Wiley and Sons.

4.1.2 Attachment of dopamine and methotrexate

Graphene oxide has been used in the therapeutic delivery of dopamine (DA) and the anticancer drug methotrexate (MTX).[71] Nanosized graphene oxide was synthesized using the modified Hummer's method, and DA was functionalized onto nGO using amide bonds (EDC/NHS coupling). The carboxylated DA-nGO was synthesized by treatment with NaOH and chloroacetic acid. By sonication and using -CH_2COOH linker, epoxide and hydroxyl groups changed to carboxyl groups. MTX was added to the DA-nGO dispersion, and after stirring, purification, and lyophilization, DA was successfully loaded (Figure 29).[71]

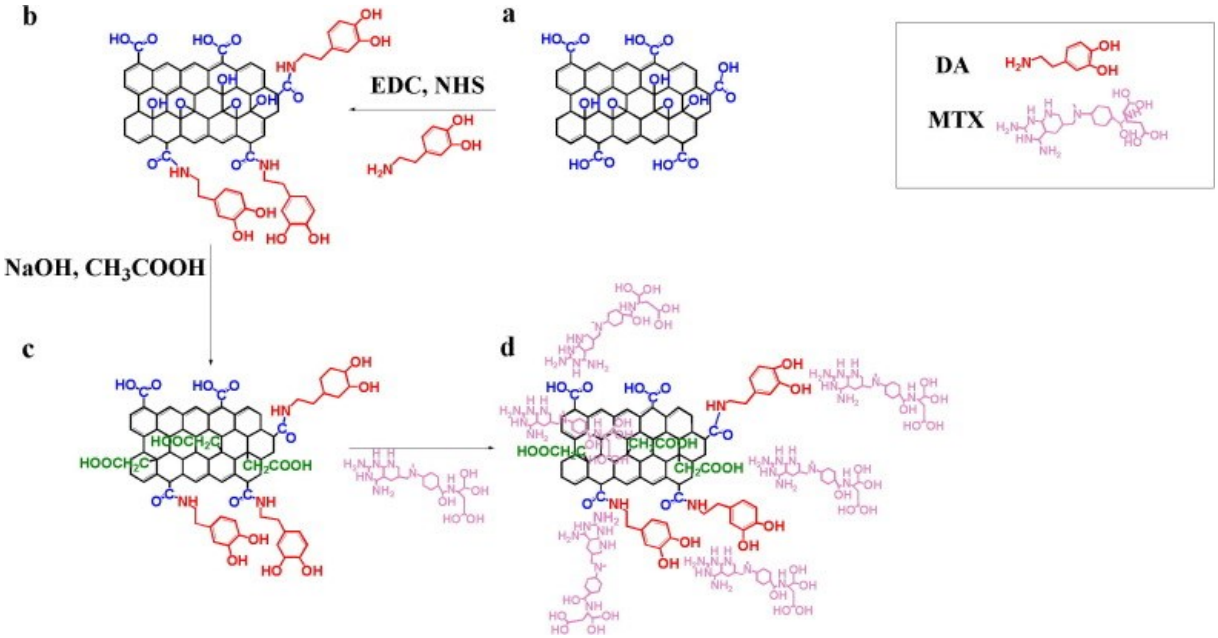

Figure 29. Functionalization of (a) GO with (b) dopamine, (c) oxygenated functional groups and (d) MTX drug. Reprinted from Chem. Phys. Lett., *668*, Masoudipour, E.; Kashanian, S., and Maleki, N., A targeted drug delivery system based on dopamine functionalized nano graphene oxide, 56-63, Copyright 2017, with permission from Elsevier.

When the drug release was studied, MTX was observed to release at pH 7.4, and 80% of the MTX was released in 24 hours. MCF-7 cells and HEK-293 cells were used to analyze the cytotoxicity of MTX, MTX-nGO, and MTX-DA-nGO. MCF-7 cells have DA receptors, whereas HEK-293 cells do not. DA induced the nanocarrier to target the cells with DA receptors, and it may enhance the cell entrance as well. DA did not remarkably affect the DA receptor-negative cells.

4.1.3 Attachment of paclitaxel

GO can be functionalized with amine, following the functionalization with albumin-conjugated polyethylene glycol cyanuric chloride (APC).[72] After the APC-amino-GO formation, paclitaxel (PTX) can be loaded to the complex, resulting in APC-amino-GO-PTX, and PTX can be released from the surface. The release of PTX depends on pH value; at lower pH values, the release of PTX is faster.

PTX has also been used with poly(lactide) (PLA) and PEG for the covalent functionalization of nanosized graphene (Figure 30).[73]

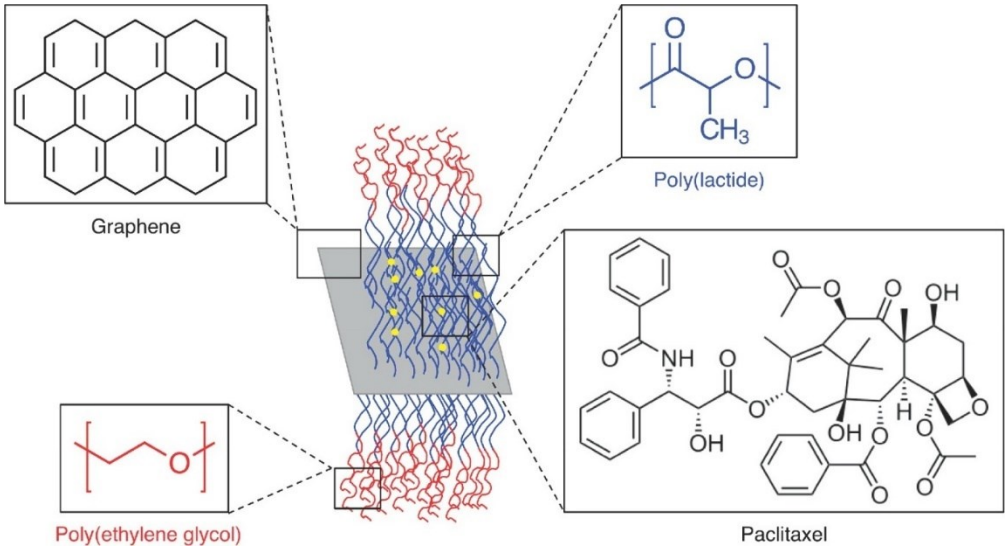

Figure 30. The construction of the PLA and PEG functionalized GO complex, to which PTX drug was bound. Copyright 2014 Wiley. Used with permission from Moore, T.L., Podilakrishna, R.; Rao A., and Alexis, F., Systemic Administration of Polymer-Coated Nano-Graphene to Deliver Drugs to Glioblastoma, Particle & Particle Systems Characterization, John Wiley and Sons.

As pristine graphene is a hydrophobic material, drugs may bind on its surface if they interact physically with graphene. Utilizing PLA-PEG makes it possible to attach hydrophobic drugs, such as PTX, to pristine graphene. PLA is attached to nGr by ring-opening polymerization, and nGr-PLA-PED formed by the reaction between a hetero-bifunctional methoxy-PEG-isocyanate (Mpeg-ISC) and PLA's terminal hydroxyl groups. nGr-PLA-PEG was used for delivering PTX to U-138 glioblastoma cells.[73] nGr-PLA-PEG was observed to encase PTX at 4.15 w-%. In the complex, PLA encases PTX and PEG stabilizes the complex.

4.1.4 Attachment of 1,3-bis(2-chloroethyl)-1-nitrosourea (BCNU)

Polyacrylic acid (PAA) has been used for functionalizing nanosized graphene oxide.[20] PAA can enhance the nanocarrier's water solubility and cell entrance and potentially improve the thermal stability of 1,3-bis(2-chloroethyl)-1-nitrosourea BCNU. Graphene oxide was prepared by a modified

Hummers' method and PAA-GO by free radical polymerization. The nanocarrier's size and topography were analyzed using AFM. 1,3-bis(2-chloroethyl)-1-nitrosourea (BCNU) was immobilized onto the surface of PAA-GO by using covalent bonds. One of the advantages of using the PAA-GO complex for delivering BCNU to GL261 cancer cells *in vitro* was the elongation of BCNU's half-life from 19 to 43 hours. The intracellular uptake was also effective. The anticancer efficacy raised 30%, whereas the IC50 value toward GL261 reduced by 77%. The nanocarrier may transport 198 μg BCNU/mg PAA-GO (70% retention of drug activity). Resulting from the effective intracellular uptake of PAA-GO within cancer cells, BCNU's concentration on the nanocarrier could be raised.

4.2 Drug release from graphene oxide carriers

The preparation of graphene and techniques used for binding affect how the drug is released.[1] For example, the bonding-affinity of DOX, bound by hydrogen bonds onto the GO's surface, has been changed by altering the pH in the cell environment.[1] From functionalized graphene family nanomaterials (GFNs), the drug is released based on the cargo's binding method and the functionalization methods used for enhancing cell targeting.[1]

External aspects affect the release of a drug from its carrier.[61] Factors, such as ultrasound, magnetic, and electric fields, provoke the release. A magnetic field has been successfully employed for drug release from a nanocomposite consisting of graphene and Fe_3O_4. A drug used with pristine graphene (0.2 mg/ml) and methacrylic acid released successfully when low electrical voltages were used. Because graphene is a conductive material, the graphene methacrylic acid hydrogel reduced the hydrogel's resistive heat and necrosis to the skin and tissue around the treated area.[61]

4.2.1 Release of doxorubicin from graphene oxide platform

The drug release from the nanocarrier has commonly been studied using dialysis chambers, such as in the drug release experiment by Yang *et al*.[74] In this particular study, the release of DXR was studied by taking samples for the UV-Vis characterization from the dialysis chamber.

11% of DXR was released at pH 7 during 30 h, as DXR is attached to GO by hydrogen bonds, which are not broken down at pH 7 as easily as in more acidic conditions. At pH 10, 25% was released, and at pH 2, 71% was released during 30 h. The interaction between DXR and GO is stronger in basic conditions, and in more acidic conditions, hydrogen bonds can dissociate, enhancing the drug release. Also, at pH 2, the OH bonds are the only possible bonds between DXR and GO, but at pH 7 and 10, NH_2 bonds exist as well.[74]

4.2.2 Ciprofloxacin release from the polyethylenimine graphene oxide hybrid film

The release of ciprofloxacin (CF) *in vitro* has been observed to be pH-dependent when tested with PBS buffer.[18] At pH 5.5, the release was faster than at pH 7.4. The reason for the slower release in less acidic pH values could be the stronger interaction between CF and PEI, which was used as a linker in the experiment. At a lower pH value, repulsive electrostatic interactions produce positive ionization for CF and PEI. PEI also has amine groups in its structure, and these groups can form positively charged ions in more acidic conditions. The positive ions of the amine groups weaken the interaction between PEI molecules, which then drives GO layers farther from each other and enhances the release of CF from the nanocarrier. It was also noted that the release in more acidic conditions was less cumulative, as the hydrogen interaction between the COOH groups of CF and OH groups of GO is stronger in a more acidic environment. As a result, CF does not release as effectively from the platform as at a pH of 7.4. Additionally, CF was not observed to release explosively at the beginning, which has been noticed to be normal in the case of some developed drug carriers.[18]

4.2.3 Release of methotrexate from dopamine functionalized graphene oxide carrier

In the research by Masoudipour *et al*.,[71] it was observed that 80 % of the methotrexate (MTX) from the dopamine functionalized GO drug carrier was released in one day. They also observed that MTX's positively charged NH_3^+ ions can form more hydrogen bonds to GO or dopamine by becoming NH_2, preventing the drug release from the carrier.

A significant factor affecting the drug release from graphene oxide carrier is environment pH. As concluded earlier, the physiological pH value of a human body is about 7.4. Instead of that, the pH in a tumor environment most commonly is approximately 5.5. The less drug is released from the drug carrier before it enters the tumor, the more effective the carrier is. The preparation method of graphene and the method used for binding the drug affect the drug release. Thus, these factors have a significant role when creating effective graphene-based drug carriers.

Experimental part

Synthesis and characterization of graphene oxide and reduced graphene oxide conjugates with phenylalanine *tert*-butyl ester

KEMS5800 Miniproject

5. Aim of the miniproject

The current project was undertaken from 2.11.2020 until 12.11.2020 and supervised by Dr Efstratios Sitsanidis and Doctoral Student Romain Chevigny. The project aimed to make graphene oxide (GO) and reduced graphene oxide (rGO) conjugates with phenylalanine *tert*-butyl ester (GO-PheO*t*Bu and rGO-PheO*t*Bu). GO conjugates have several potential biomedical applications, such as platforms of anticancer drugs for targeted drug delivery.[1] The research work focused on the synthesis of GO-PheO*t*Bu and rGO-PheO*t*Bu conjugates. The conjugates were prepared by stirring GO flakes and rGO powder with 1-ethyl-3-(3-dimethylaminopropyl)carbodiimide hydrochloride (EDC), *N*-hydroxysuccinimide (NHS) and PheO*t*Bu powder in phosphate-buffered saline (PBS) solution, followed by centrifugation, washings and drying.[66] The preparation of conjugates was based on forming an amide bond between the amine group of phenylalanine ester and the carboxylic groups of GO and rGO (Figure 31).

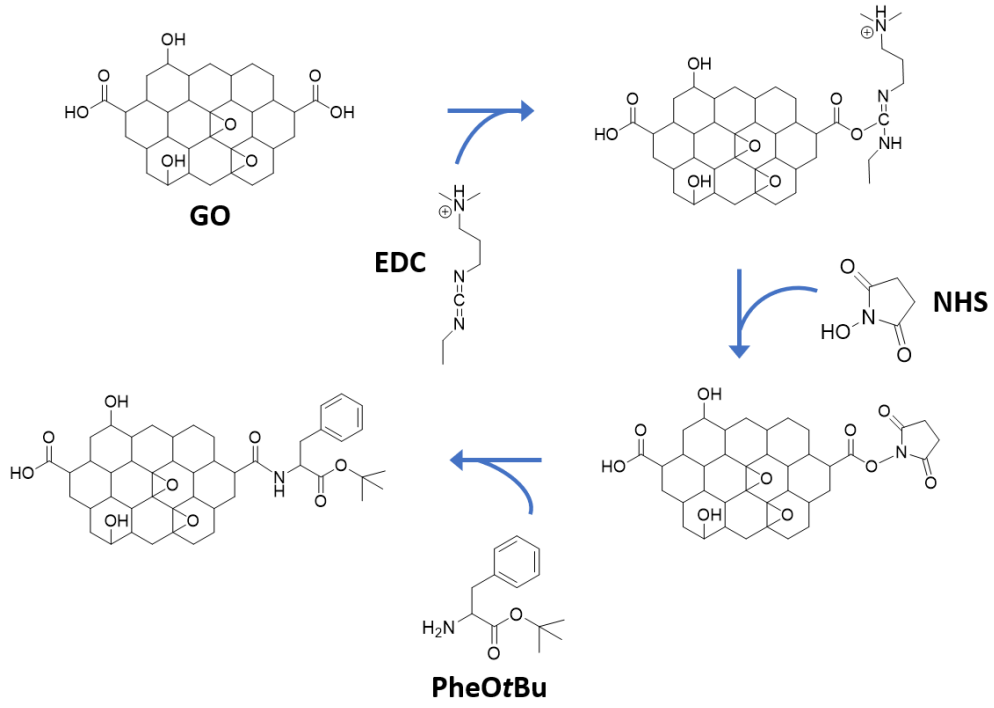

Figure 31. The reaction mechanism for the synthesis of GO-PheO*t*Bu conjugate. The same mechanism applies to the preparation of rGO-PheO*t*Bu conjugate.

GO is a two-dimensional (2D) material that consists of sp^2 hybridized carbon atoms bond together in a honeycomb lattice.[75] Due to its aromaticity, compounds can be attached to its lattice *via* non-covalent interactions such as π-π stacking, H-bonding, Van der Waals and Coulombic forces or by covalent bonding. Indeed, several functional groups on the surface and GO's lattice edges, such as epoxy, carboxylic, and hydroxyl groups, enable its versatile functionalization. The current project is based on Wang *et al*.[66] on the preparation of GO-Chlorotoxin conjugate as an anticancer drug delivery system.

GO-based materials can be used for biomedical applications due to graphene's supreme physicochemical properties, such as biocompatibility, the facility of functionalization, and large surface area.[2] Owing to its unique electrical and optical properties, GO conjugates can serve as main components for biosensor devices to detect biomolecules. Additionally, such materials can act as bio-imaging probes. GO composites have been used, for example, in magnetic resonance imaging and imaging of live cells. GO materials can enhance both photothermal (PTT) and photodynamic (PDT) therapies for treating several diseases due to the high optical absorption of graphene.

The structure of rGO is similar to GO, but there are less oxygenated groups.[6] rGO is prepared by thermal or chemical treatment of GO using reducing agents, such as hydrazine or hydrogen. By using ascorbic acid, rGO can be produced at higher yields.[76]

6. Materials and methods

All chemical reagents were used without any further purification unless stated otherwise (Table 1). Denver Instrument APX-200 balance was used to measure weights and Heraeus Megafuge 16 Centrifuge to centrifugate the reaction suspensions (13000 rpm for 20 min). NMR spectra were recorded by a Bruker Avance III HD 300 NMR Spectrometer while the samples were prepared in deuterated d_6-DMSO. Raith e-LINE Scanning Electron Microscope (SEM) instrument and Olympus BX51M Optical Microscope were used to produce the images of the specimens. FT-IR spectra were recorded by a Bruker Alpha FT-IR spectroscope.

Table 1. Used reagents and their purities.

Reagent	Producer	Purity
EDC	Thermo Fisher	*
Graphene oxide	Graphenea	> 95%
NHS	Sigma Aldrich	98%
PheO*t*Bu	CarboSynth	*
Reduced graphene oxide	Sigma Aldrich	98-99%

*The value of purity is unknown.

PBS solution (0.1 M, pH 6) for the synthesis was prepared. Na_2HPO_4 (0.3565 g, 2.51 mmol) was dissolved in deionized water (10 mL). The second solution of NaH_2PO_4 (1.5600 g, 13.0 mmol) was also prepared in deionized water (50 mL). The two solutions were then mixed (6.15 mL of Na_2HPO_4 and 43.85 mL of NaH_2PO_4 solution) and diluted after that with deionized water (100 mL).

7. Synthesis of conjugates

7.1 rGO-PheOtBu conjugate

rGO (150 mg) was dissolved in PBS solution (20 ml) in a round-bottomed flask. EDC (6.0 mg, 0.039 mmol) and NHS (4.09 mg, 0.035 mmol) were then added, and the mixture was left to stir for 30 min. After stirring, the pH value of the reaction mixture was increased to 8.0 by the addition of NaOH aqueous solution (2M) followed by the addition of PheO*t*Bu (15 mg, 0.058 mmol). The reaction was then left to stir for 48 h at rt.

After 48 h, the suspension was transferred into two Falcon tubes and centrifuged for 20 min. The supernatant was removed from the precipitate and kept to a reagent bottle while the precipitate was further washed with deionized water. Centrifugations and washings were performed at three cycles, and the obtained rGO-PheO*t*Bu conjugate was finally dried under a vacuum.

7.2 GO-PheOtBu conjugate

GO (150 mg) was dissolved in PBS solution (20 mL) in a round-bottomed flask. EDC (6.0 mg, 0.039 mmol) and NHS (4.09 mg, 0.035 mmol) were then added, and the mixture was left to stir for 30 min. After stirring, the pH value of the reaction mixture was increased to 8.0 by the addition of NaOH aqueous solution (2M) followed by the addition of PheO*t*Bu (15 mg, 0.058 mmol). The reaction was then left to stir for 48 h at rt.

After 48 h, the suspension was transferred into two Falcon tubes and centrifuged for 20 min. The supernatant was removed from the precipitate and kept to a reagent bottle while the precipitate was further washed with deionized water. Centrifugations and washings were performed at three cycles, and the obtained GO-PheO*t*Bu conjugate was finally dried under a vacuum.

8. Characterization of conjugates

8.1 NMR spectroscopy

^{1}H NMR spectra of GO, rGO, PheO*t*Bu, GO-PheO*t*Bu, and rGO-PheO*t*Bu were recorded (Figures 32 and 33). ^{13}C NMR spectra of GO and rGO were also recorded (Figure 34).

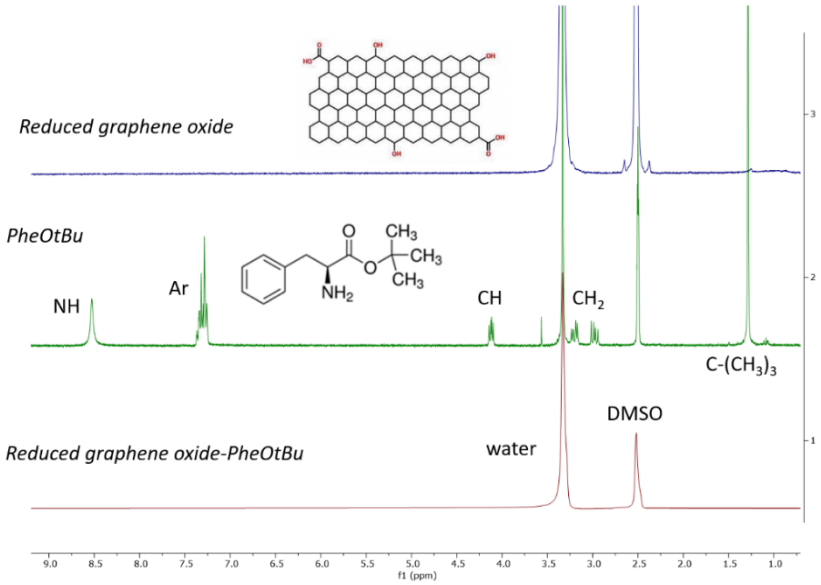

Figure 32. The ^{1}H NMR spectra of rGO starting material, PheO*t*Bu starting material and rGO-PheO*t*Bu reaction product.

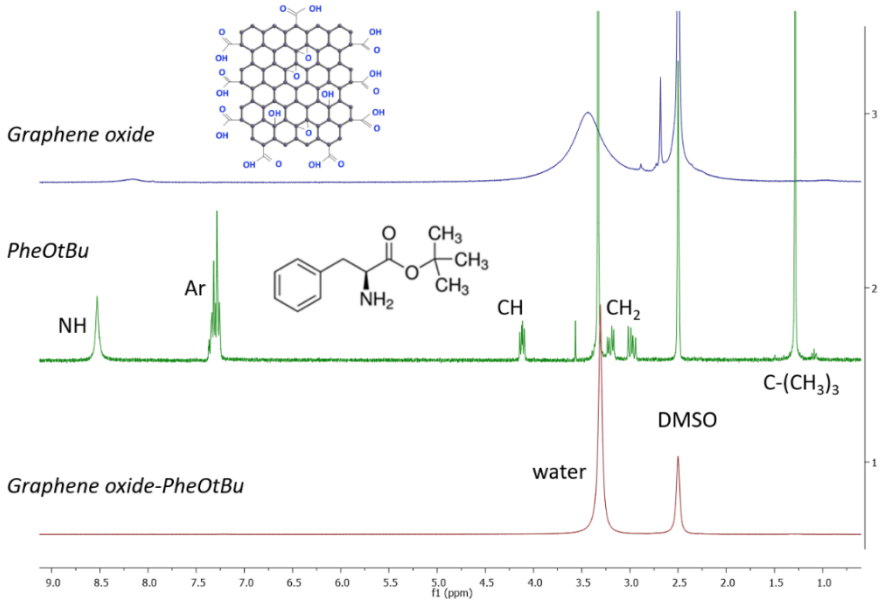

Figure 33. The ^{1}H NMR spectra of GO starting material, PheO*t*Bu starting material and GO-PheO*t*Bu reaction product.

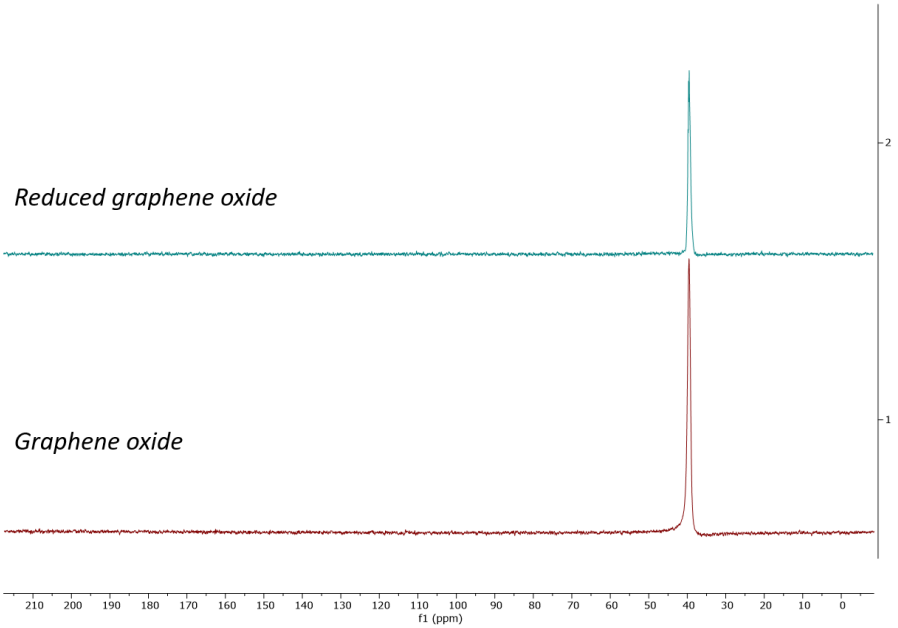

Figure 34. The ^{13}C NMR spectra of rGO and GO starting materials.

By observation of the ^{1}H NMR spectra of rGO, GO, rGO-PheO*t*Bu, and GO-PheO*t*Bu samples (Figures 2 and 3), the only noticeable peaks are attributed to water (3.3 ppm) and d_6-DMSO solvent (2.5 ppm). The peak observed in ^{13}C NMR spectra of rGO and GO samples (Figure 4) corresponds to d_6-DMSO (40 ppm) solvent. The lack of NMR signals is due to the poor solubility of the samples to organic solvents. Indeed, based on the literature, solid-state NMR spectra of graphene samples are mainly reported.[77] The peaks shown at PheO*t*Bu starting material ^{1}H NMR spectrum are given below: ^{1}H NMR (300 MHz, DMSO) δ 8.53 (s, 3H, NH), 7,29 (dd, J = 11.0, 5H, Ar), 4.12 (dd, J = 8.4, 1H, CH), 3.23 – 3.05 (m, 1H, CH_2), 3.01 – 2.82 (m, 1H, CH_2), 1.29 (s, 9H, CH_3)

8.2 IR spectroscopy

Figures 35 and 36 show the FT-IR spectra of rGO, PheO*t*Bu, rGO-PheO*t*Bu, GO, and GO-PheO*t*Bu.

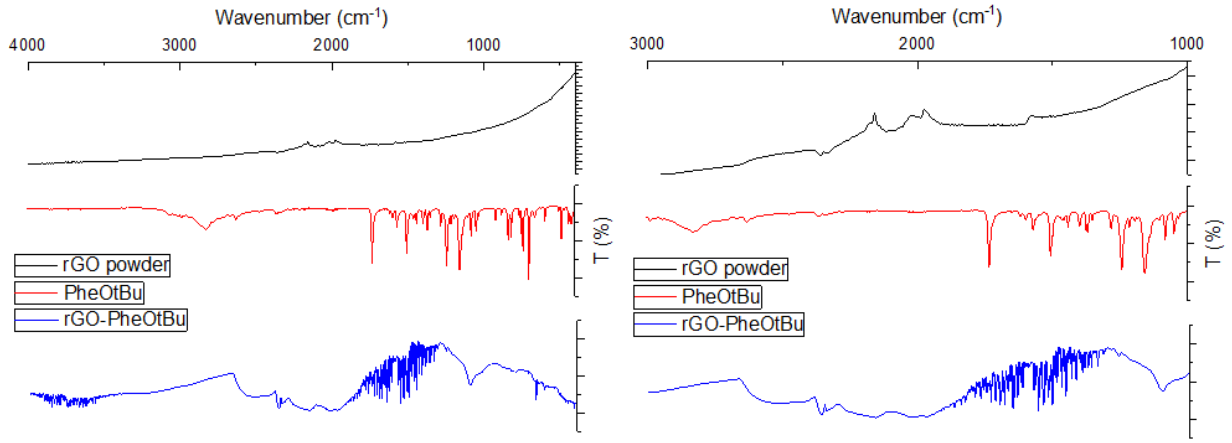

Figure 35. The IR spectra of rGO and rGO-PheO*t*Bu.

In the IR spectrum of rGO, OH stretching is observed at 3000 cm^{-1}, C-O-C at 1090 cm^{-1} and C=C bond at 1600 cm^{-1}. The spectrum of rGO-PheO*t*Bu has a peak at 1700 cm^{-1} due to the stretching of the C=O amide bond. The C-N stretching of rGO-PheO*t*Bu's amide bond is observed at 1300 cm^{-1}. Peaks at 1700 cm^{-1} and 1300 cm^{-1} are not observed in the spectrum of rGO, which indicates that amide bonds between rGO and PheO*t*Bu have formed.

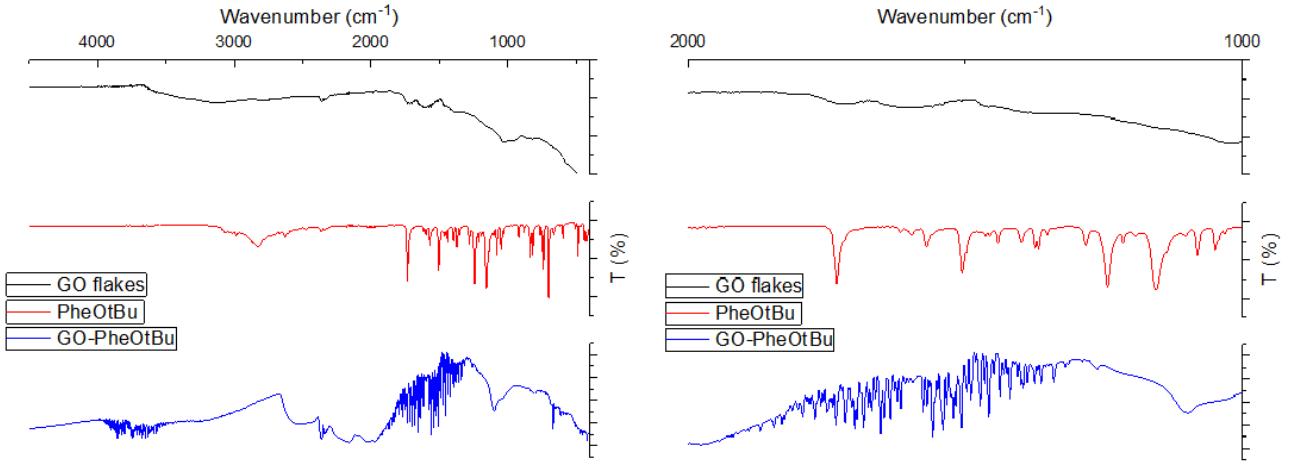

Figure 36. The IR spectra of GO, PheO*t*Bu, and GO-PheO*t*Bu.

In the IR spectrum of GO, OH stretching is observed at 3300-3000 cm^{-1}. C=O stretching is observed at 1724 cm^{-1} and C=C bond at 1600 cm-1. GO's IR spectrum also shows signals at 1398 cm^{-1}, 1179 cm^{-1} and 1030 cm^{-1} due to OH bending, C-O-C, and C-O stretching, respectively.

Differences between the IR spectra of GO and GO-PheO*t*Bu are also observed. GO-PheO*t*Bu shows a strong peak at 1680 cm^{-1} due to the stretching of the C=O bond, which is characteristic for amides. The peak at 1300 cm^{-1}, characteristic for the C-N stretching of the amide bond, is observed as well. The signals at 1680 cm^{-1} and 1300 cm^{-1} are not observed in GO's IR spectrum. These observations indicate that amide bonds between PheO*t*Bu and GO have formed.

8.3 SEM and optical microscopy

Scanning electron microscopy (SEM) images of GO, GO-PheO*t*Bu, rGO and rGO-PheO*t*Bu specimens are given below (Figure 37). The samples were prepared by adding a drop of the material's suspension on a carbon-coated copper grid (Figure 38) with a pipette. Then the grid was left to dry for SEM imaging.

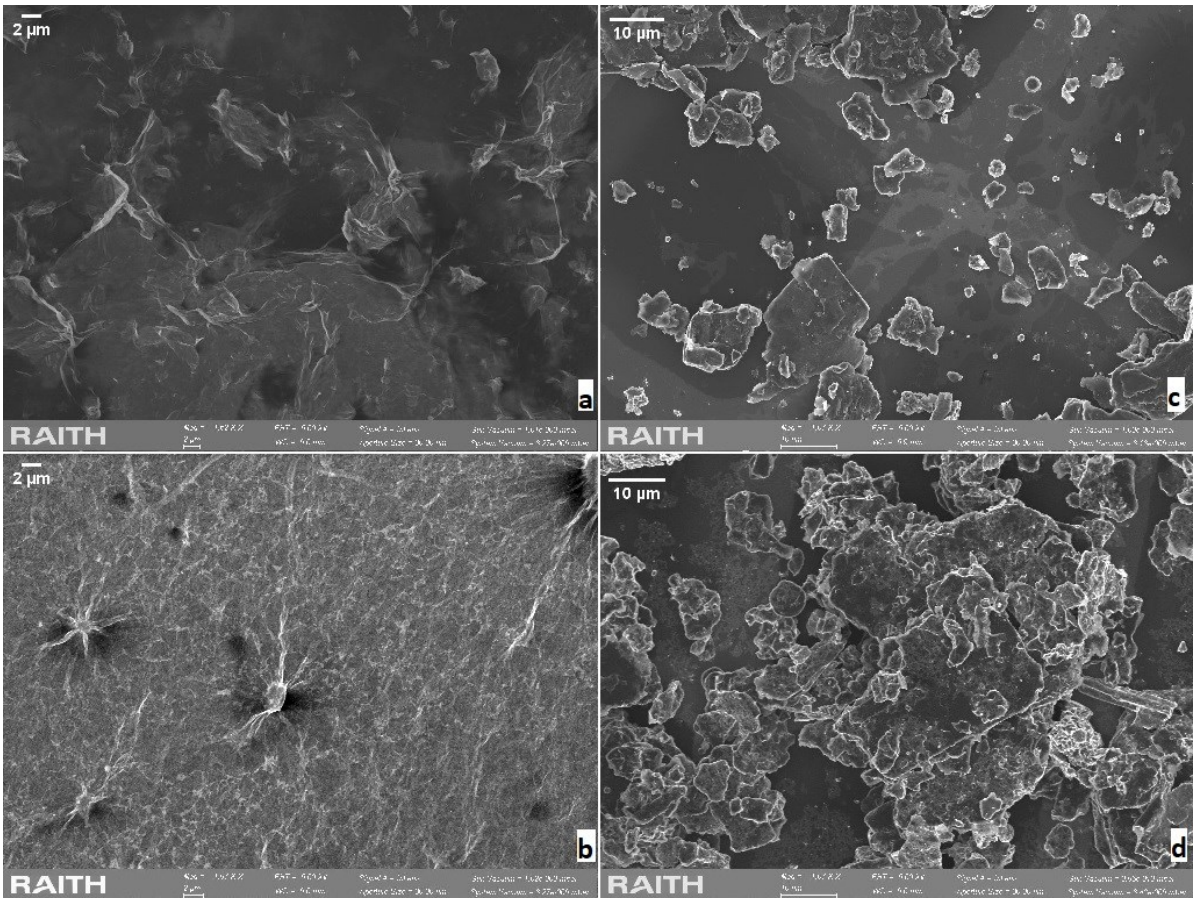

Figure 37. SEM images of (a) GO, (b) GO-PheO*t*Bu, (c) rGO and (d) rGO-PheO*t*Bu.

Figure 38. Carbon coated copper grid used for SEM imaging.

Figures 37 a and 37 c show the structural differences between GO and rGO. rGO has sharper edges, and it is more aggregated compared to GO flakes. Star-shaped objects are observed in figure 37 b, which are potential nucleation points of PheO*t*Bu upon the GO surface. rGO-PheO*t*Bu is observed as aggregated structures in figure 37 d. rGO-PheO*t*Bu was also viewed by optical microscope in bright and dark field mode to observe potential structural differences of the functionalized graphene-flakes (Figure 39).

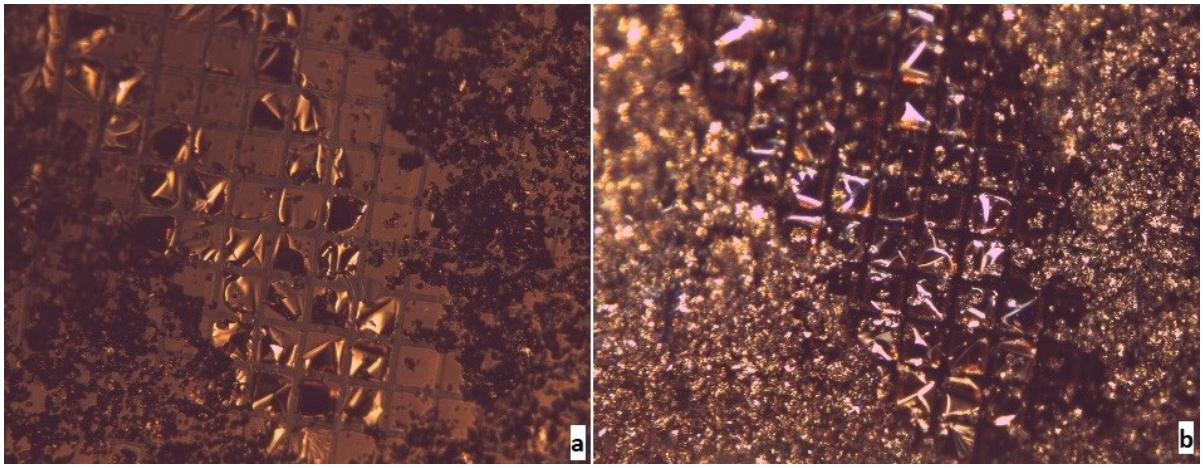

Figure 39. Optical microscope images of rGO-PheO*t*Bu using (a) bright field and (b) dark field.

9. Summary of the miniproject

GO and rGO composites (GO-PheO*t*Bu and rGO-PheO*t*Bu respectively) were synthesized. Based on the FT-IR data, the synthesis of GO-PheO*t*Bu and rGO-PheO*t*Bu was successful, as the formation of an amide bond between rGO and GO and phenylalanine ester was observed. Based on research results, IR spectroscopy has been proven a valuable characterization method to observe the formation of conjugates.

rGO and GO do not give any visible signals in their ^{1}H and ^{13}C NMR spectra since they are insoluble in DMSO. For the same reason, rGO-PheO*t*Bu and GO-PheO*t*Bu conjugates gave no signals at their corresponding ^{1}H NMR spectra. NMR characterization of graphene oxide is challenging, as graphene oxide is not soluble in deuterated NMR solvents.

SEM images revealed useful information about the graphene oxide flakes and their corresponding composites. Atomic force microscopy (AFM) and transmission electron microscopy (TEM) are two promising imaging techniques for characterizing graphene materials alongside SEM and optical microscopy. Due to the short duration of the project and the laboratory restrictions because of the Covid-19 pandemic outbreak, AFM and TEM imaging were not performed. According to the regulations of the University of Jyväskylä, only a limited number of staff could access the corresponding lab premises as a precautionary measure against the spread of the virus.

Preparation, characterization and reactivity tests of graphene – linker constructs designed for strain promoted alkyne-azide cycloaddition (SPAAC)

10. Aim of the project

The experimental project "Preparation, characterization and reactivity tests of graphene – linker constructs designed for strain promoted alkyne-azide cycloaddition (SPAAC)" was conducted at Orion Corporation in the Medicine Design department from November 2020 until March 2021.

The project aimed to synthesize graphene oxide-based constructs with a covalently bound linker for SPAAC (Figure 40).[78] Bicyclononyne (BCN) and dibenzocyclooctyne (DBCO) (Figure 40) are strained cyclic alkyne moieties commonly used in click reactions with azide moiety.[79]

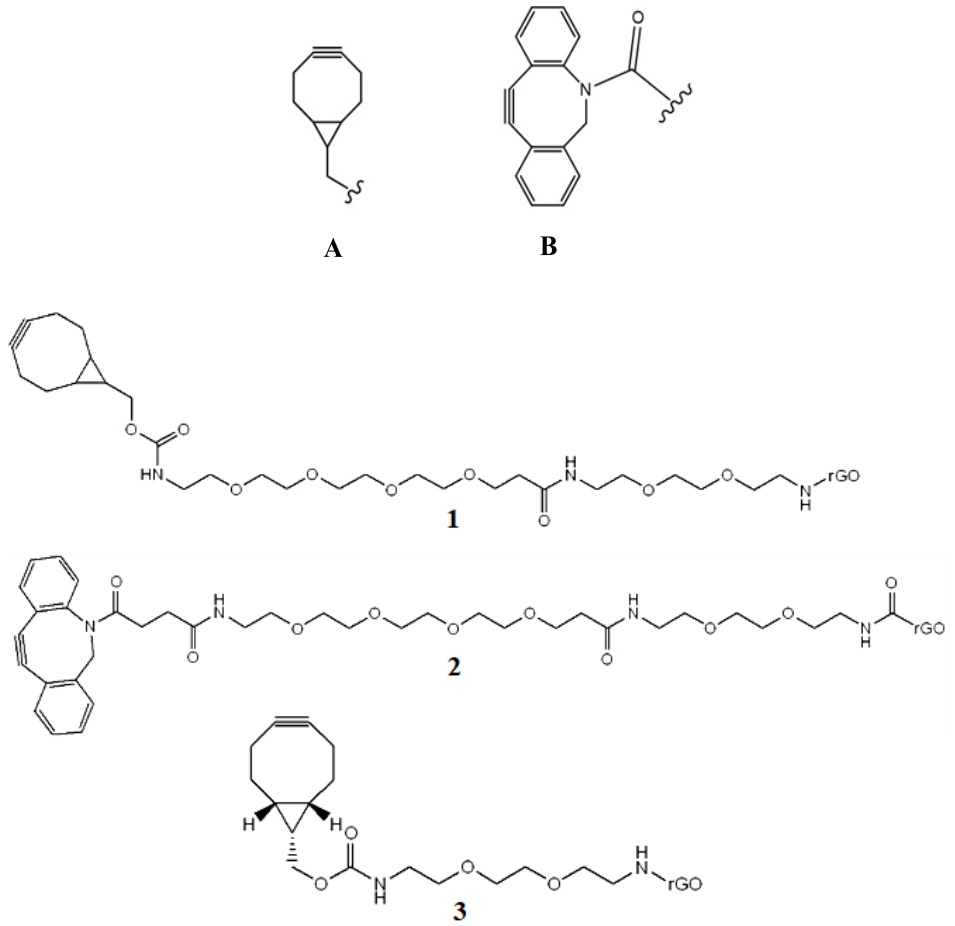

Figure 40. The chemical structure of A: BCN moiety, B: DBCO moiety, rGO-amine-endo-BCN-PEG4 conjugate **1**, rGO-amine-DBCO-PEG4 conjugate **2**, and rGO-amine-BCN conjugate **3**.

The formation of the prepared constructs was analyzed by FT-IR analysis. In addition, the synthesis of rGO-amine-BCN conjugate **3** (Figure 40) was attempted.

The reactivity of the synthesized rGO-amine-endo-BCN-PEG4 **1** conjugate was further tested by SPAAC test reaction[78]. In the test reaction, the aim was to form 1,2,3-triazole. Selected analysis methods for the characterization of the SPAAC test reaction products were ^{1}H NMR, ^{19}F NMR and FT-IR. The goal in the ^{19}F NMR measurement was to observe a fluorine signal of the trifluoromethyl group originating from the 1-(azidomethyl)-4-(trifluoromethyl)benzene **10**.

Small molecules, such as drug molecules, can be further attached covalently or noncovalently to the structure of graphene-based materials.[1] For instance, anticancer drugs doxorubicin and camptothecin could be bound by π-π or hydrophobic interactions on the basal plane of graphene oxide for targeted drug delivery, as shown by Zhang *et al*.[24]

11. Synthesis of rGO amine-based conjugates

11.1 rGO-amine-endo-BCN-PEG4 conjugate 1

Since polyethylene glycol (PEG) enhances the biocompatibility and solubility of graphene-based nanomaterials[10], endo-BCN-PEG4-NHS ester **6** bearing the four-unit PEG chain was used for the synthesis of rGO-amine-endo-BCN-PEG4 conjugate (**1**; Scheme 1).

As the disappearance of endo-BCN-PEG4-NHS ester **6** by LC-MS monitoring was observed during a stirring compound in a PBS solution (Figure 41), PBS was not used as a reaction solvent. However, in the literature, DMSO has commonly been used in click reactions.[80] Therefore, DMSO was used for the synthesis of rGO-amine-endo-BCN-PEG4 conjugate **1**.

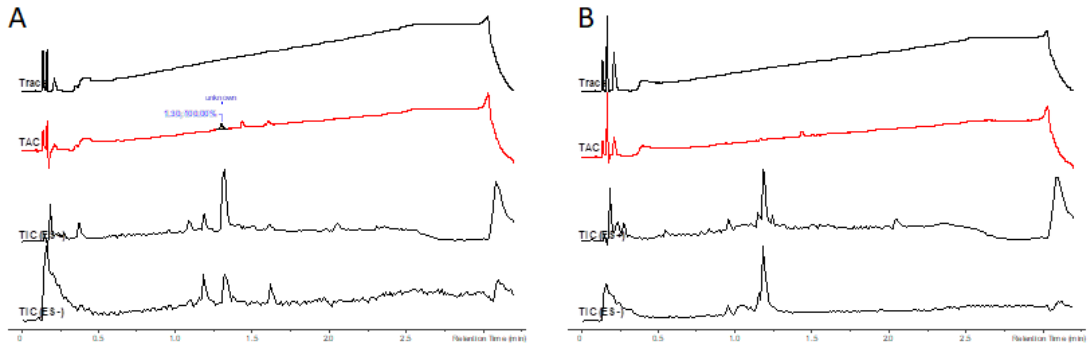

Figure 41. LC-MS monitoring of endo-BCN-PEG4-NHS ester **6** starting material in a PBS solution. The retention time of endo-BCN-PEG4-NHS ester is 1.3 min. (A) Starting material was still observed at 0.5 h (B) No more starting material at 4 h.

The rGO-amine-endo-BCN-PEG4 conjugate **1** was succesfully synthesized once (Scheme 1). 80% of **6** was noted to be consumed after 3.5 h from the beginning of the reaction.

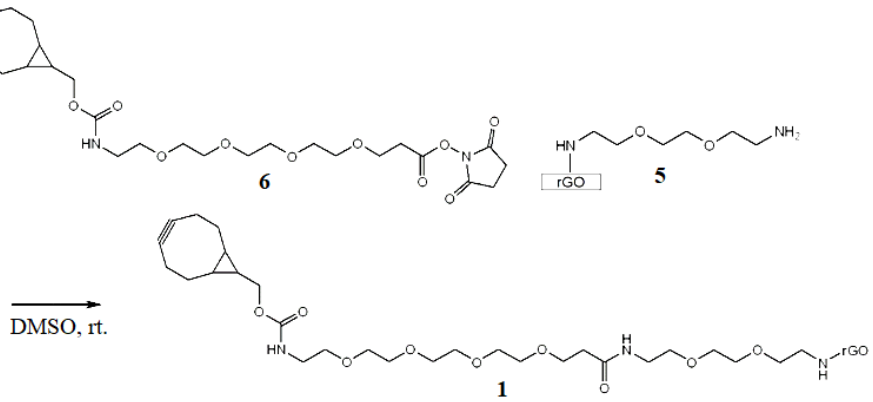

Scheme 1. Synthesis of rGO-amine-endo-BCN-PEG4-amide **1** without DIPEA and heating.

The formation of rGO-amine-endo-BCN-PEG4 amide **1** is observed in the FT-IR spectrum (Figure 42). The N-H stretching band of the amide bond is observed at 3300 cm^{-1}, while the C=O stretching band of the amide bond is seen at 1633 cm^{-1}. The peak at 1573 cm^{-1} corresponds to the C-N and N-H of the formed amide bond. Moreover, the lack of the peaks at 1521 cm^{-1} and 1361 cm^{-1}, which corresponds to the N-O of the NHS group, confirms that the NHS of **6** has been removed and the amide product is formed.

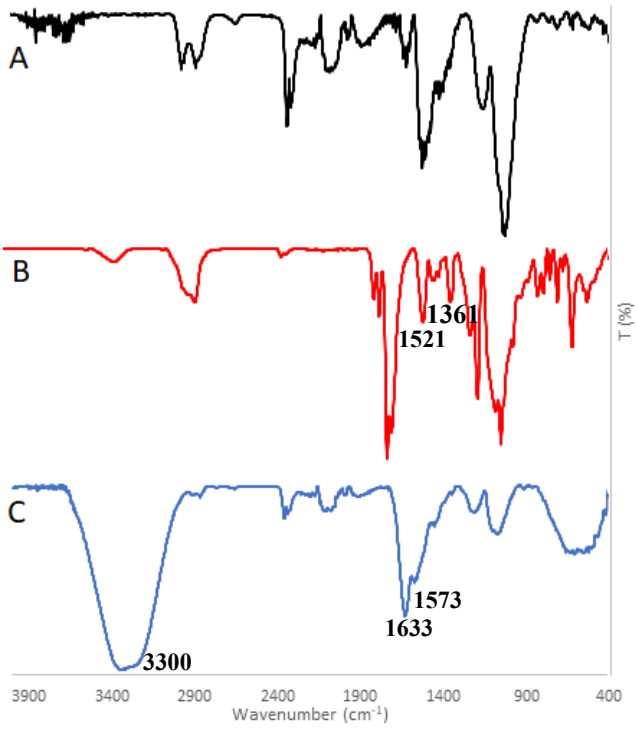

Figure 42. The FT-IR spectrum of (a) rGO amine starting material, (b) endo-BCN-PEG4-NHS ester starting material and (c) rGO-amine-BCN-PEG amide.

The synthesis of the rGO-amine-endo-BCN-PEG4 conjugate **1** was attempted twice using *N,N*-diisopropylethylamine (DIPEA) and heating to promote the reaction (Scheme 2).

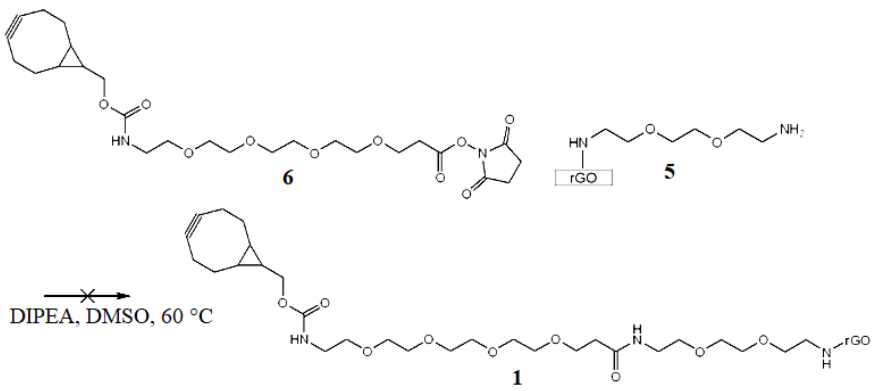

Scheme 2. Synthesis of rGO-amine-endo-BCN-PEG4-amide **1**.

During the first synthesis with DIPEA and heating, the concentration of endo-BCN-PEG4-NHS ester **6** in the reaction mixture was observed to decrease effectively (Figure 43), based on the LC-MS monitoring. After 0.5 h from the start of the reaction, 90% of endo-BCN-PEG4-NHS ester **6** was consumed.

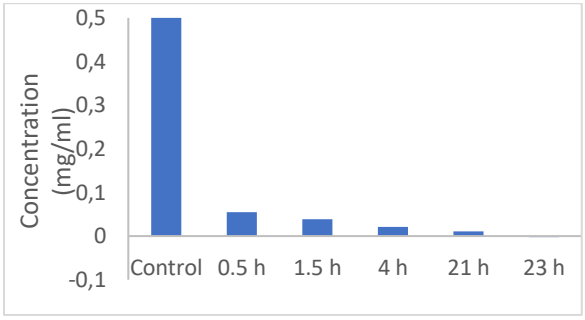

Figure 43. The concentration of endo-BCN-PEG4-NHS ester **6** in the reaction mixture.

In the second experiment, 1 eq of DIPEA was added into the reaction mixture after 21 h, and 3 eq of DIPEA after 26 h. To further support the reaction, heating at 40 °C was started after 55 h. Temperature was raised to 50°C after 56 h. As observed from Figure 44, heating was effective.

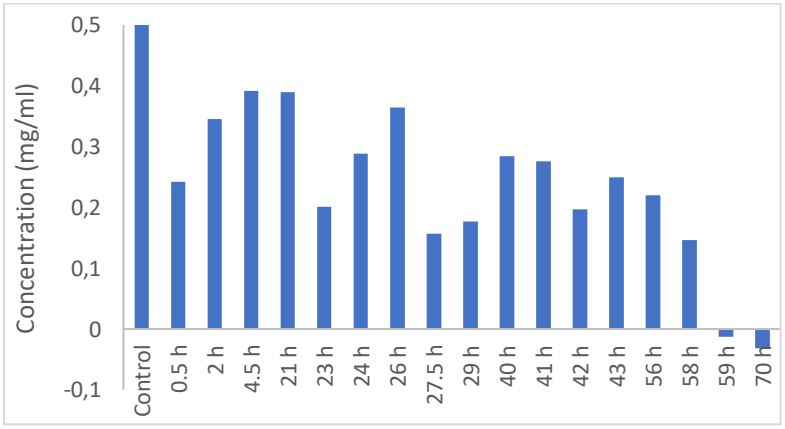

Figure 44. The concentration of endo-BCN-PEG4-NHS ester **6** in the reaction mixture.

Based on the FT-IR analysis of the products (Figure 45), the rGO-amine-endo-BCN-PEG4 conjugate **1** did not form. The observed signals correspond to the spectra of rGO-amine **5**. Any signals indicating amide bond formation are absent.

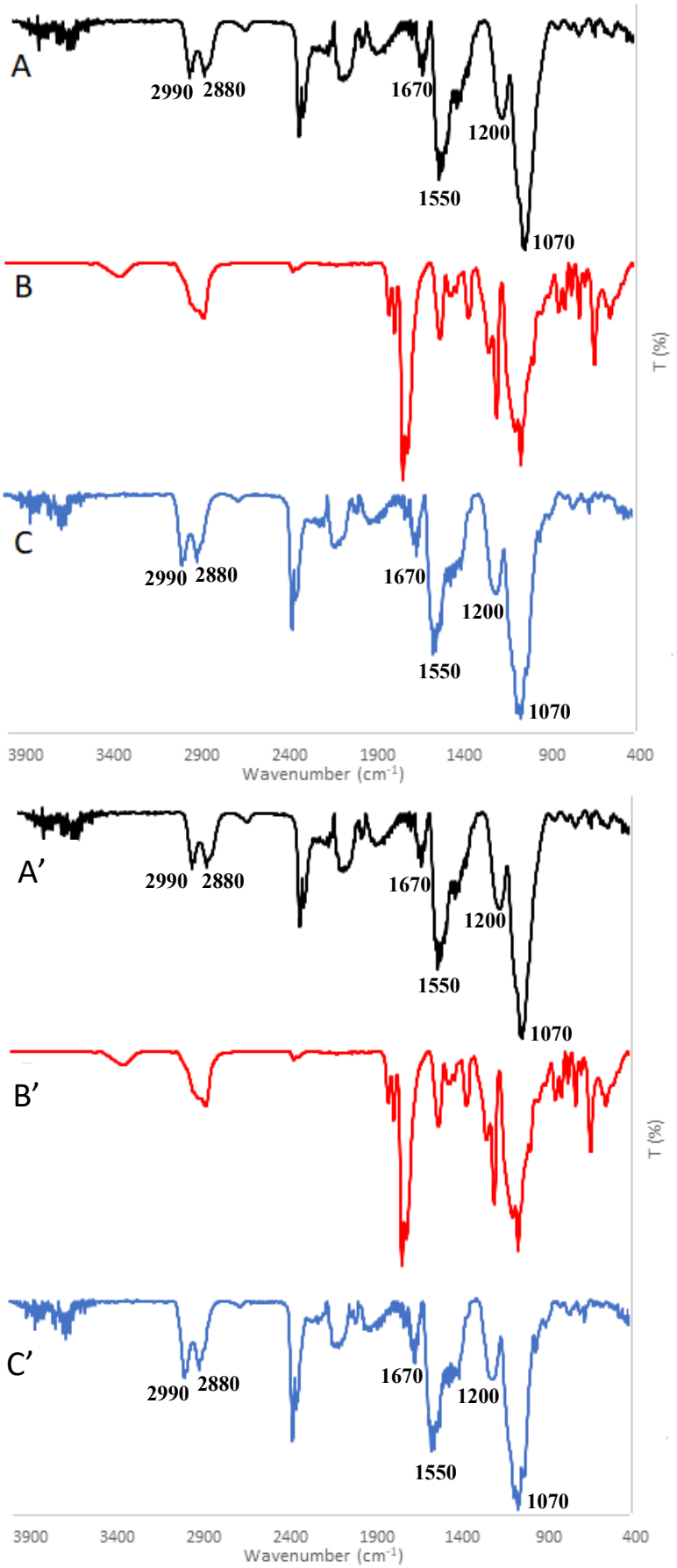

Figure 45. Comparison of FT-IR spectra of the two synthetic approaches. (A) and (A'): rGO amine starting material; (B) and (B'): endo-BCN-PEG4-NHS ester starting material, and (C) and (C'): the reaction product from the first and second synthesis, respectively.

11.2 rGO-amine-DBCO-PEG conjugate 2

Based on the LC-MS monitoring, DBCO-PEG4-NHS ester **7** is more chromophoric than endo-BCN-PEG4-NHS ester **6** (Figure 46). This facilitates the reaction monitoring with LC-MS.

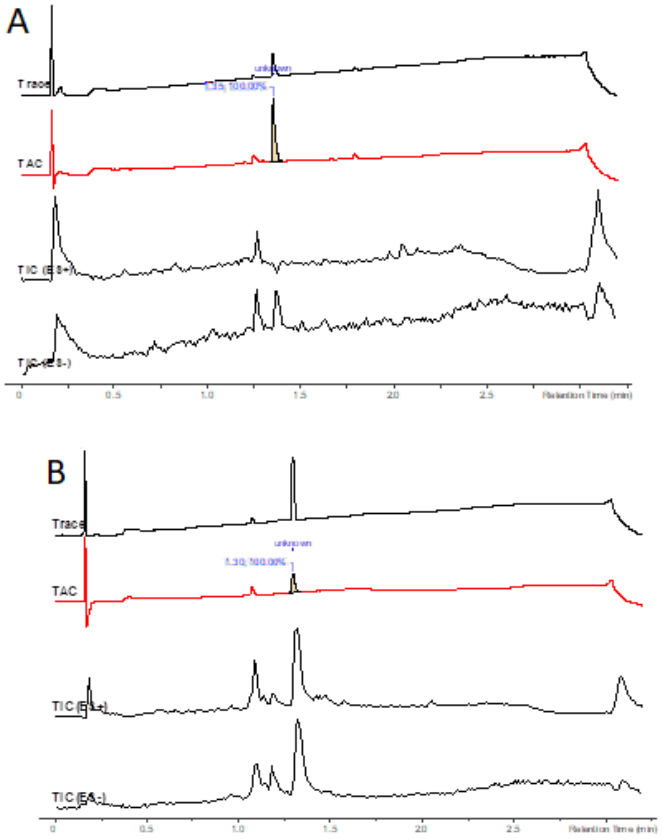

Figure 46. (a) The LC-MS gram of DBCO-PEG4-NHS ester **7**, 0.5 mg/ml in DMSO and (b) the LC-MS gram of endo-BCN-PEG4-NHS ester **6**, 0.5 mg/ml in DMSO.

The synthesis of rGO-amine-DBCO-PEG4 conjugate **2** was performed several times (Scheme 3). In the syntheses, DIPEA and heating were used as promoters, while the concentration of DBCO-PEG4-NHS ester **7** starting material in the reaction mixture was monitored by LC-MS (Figure 47). As observed from the diagrams, the combination of DIPEA and heating seem to facilitate the reaction more than the DIPEA additions without heating.

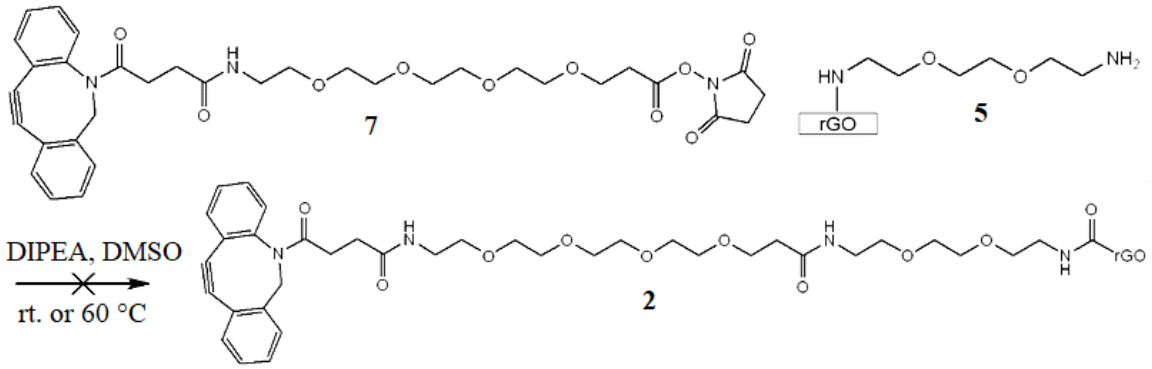

Scheme 3. Synthesis of rGO-amine-DBCO-PEG-amide.

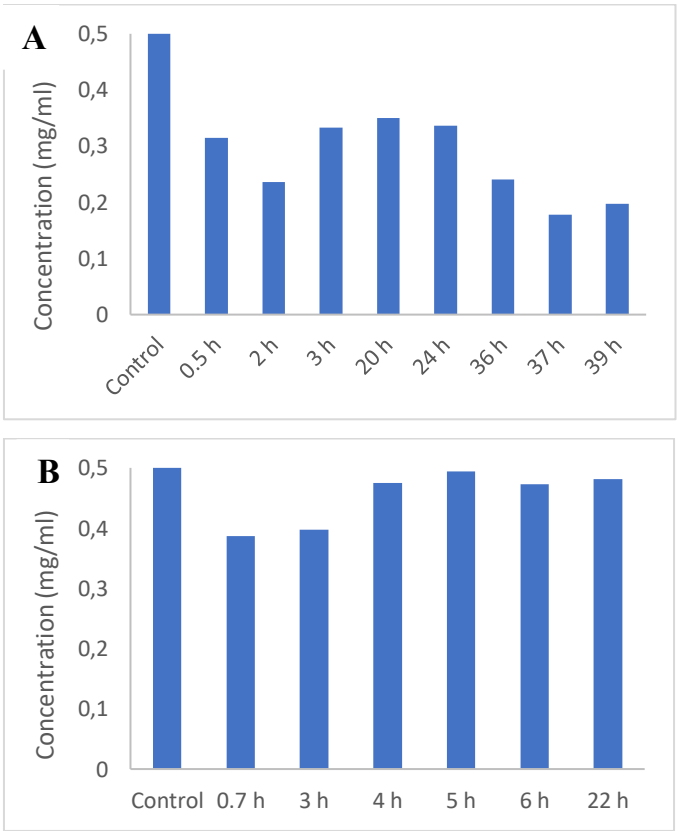

Figure 47. (a) The concentration of DBCO-PEG4-NHS ester **7** in the reaction mixture when DIPEA and heating were used in the synthesis. 1 eq of DIPEA was added after 20 h and 3 eq of DIPEA after 24.5 h. Heating up to 50°C was started after 36 h, and the temperature was raised to 60°C after 37 h. (b) The concentration of DBCO-PEG4-NHS ester **7** in the reaction mixture when DIPEA was used in the synthesis. 1 eq of DIPEA was added after 4.5 h and 3 eq of DIPEA after 5.5 h.

The reaction products were characterized by FT-IR (Figure 48). The spectra show that the amide products had not formed, as the IR absorptions of the amide bond are not observed.

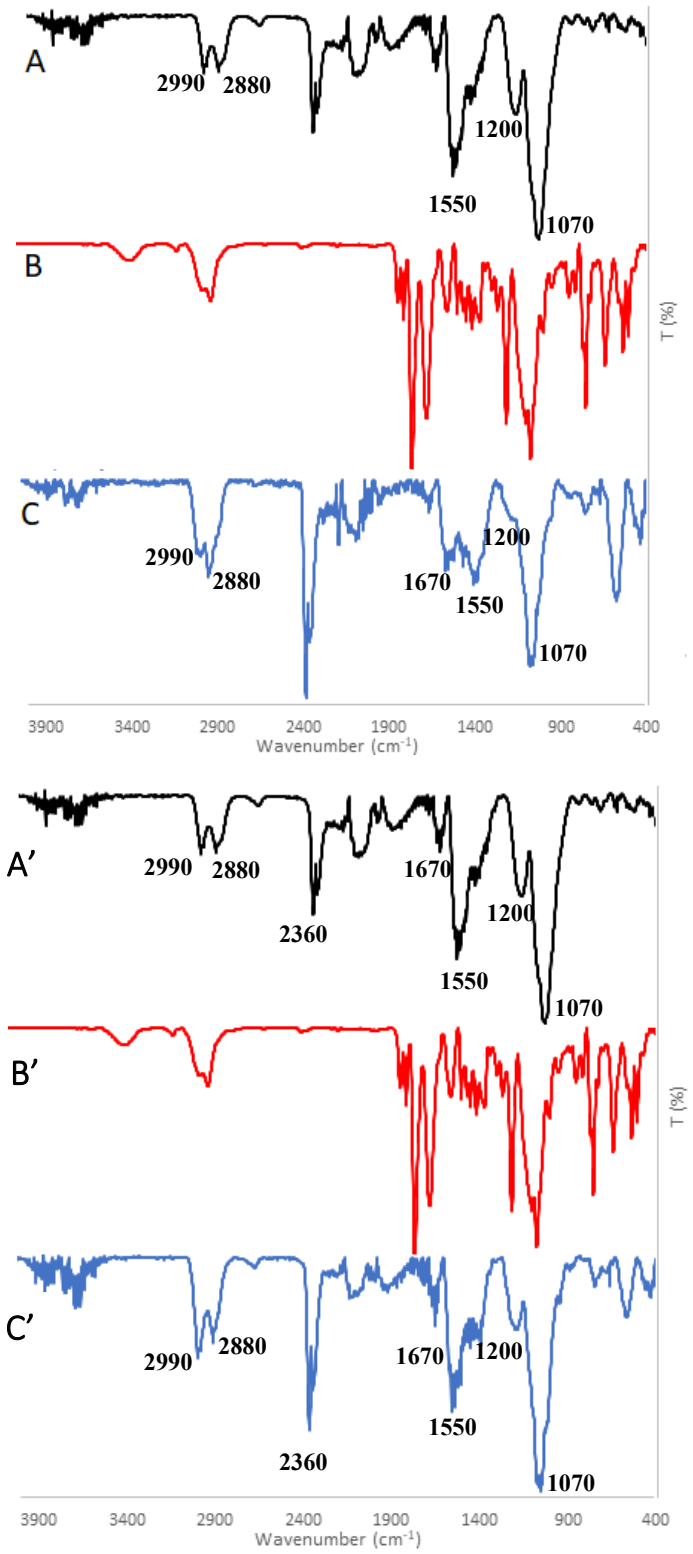

Figure 48. Comparison of FT-IR spectra of the two synthetic approaches. (A) and (A'): rGO amine starting material; (B) and (B'): DBCO-PEG4-NHS ester starting material, and (C) and (C'): the reaction product from the first and second synthesis, respectively.

11.3 rGO-amine-BCN conjugate 3

The synthesis of rGO-amine-BCN-carbamate (Scheme 4) was performed using phosphate-buffered saline (PBS) with a pH value of 7.4 as a reaction solvent. PBS buffer was utilized, as PEGylated reduced graphene oxide (rGO) has been observed to be stable in a PBS solution.[10] The pH value 7.4 of human plasma, was used for the PBS buffer.[29]

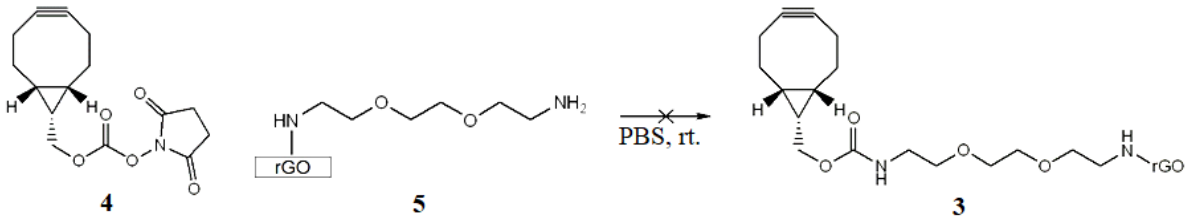

Scheme 4. Synthesis of rGO-amine-BCN-carbamate **3**.

The reaction was performed by stirring the mixture of BCN-succinimidyl ester **4** and rGO amine **5** in 0.1 mM PBS at room temperature. The consumption of BCN-succinimidyl ester **4** in the reaction mixture was monitored by LC-MS. BCN-succinimidyl ester **4** was observed to be consumed efficiently (Figure 49).

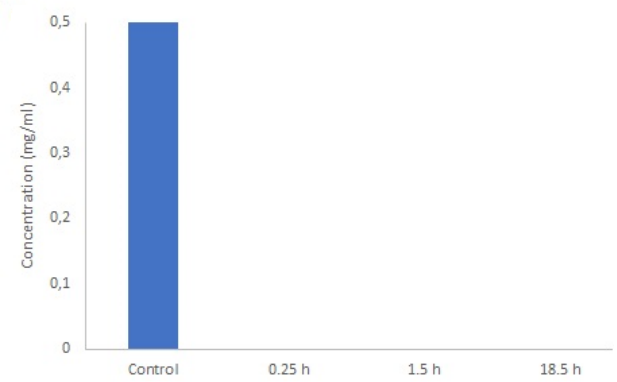

Figure 49. The concentration of BCN-succinimidyl ester starting material in the reaction mixture.

The obtained product was characterized by FT-IR. Based on the observation from the product spectrum (Figure 50), rGO-amine-BCN-carbamate **3** did not form, as the product's spectrum is almost identical to the spectrum of rGO-amine starting material **5**. In the spectrum of rGO-amine **5**, a C-O-C signal of the PEG chain is observed at 1070 cm^{-1}, C-N at 1200 cm^{-1}, C=C at 1550 cm^{-1}, C=O at 1670 cm^{-1} and N-H stretching bands at 2880 cm^{-1} and 2990 cm^{-1}. These signals are also observed in the spectra of the reaction product.

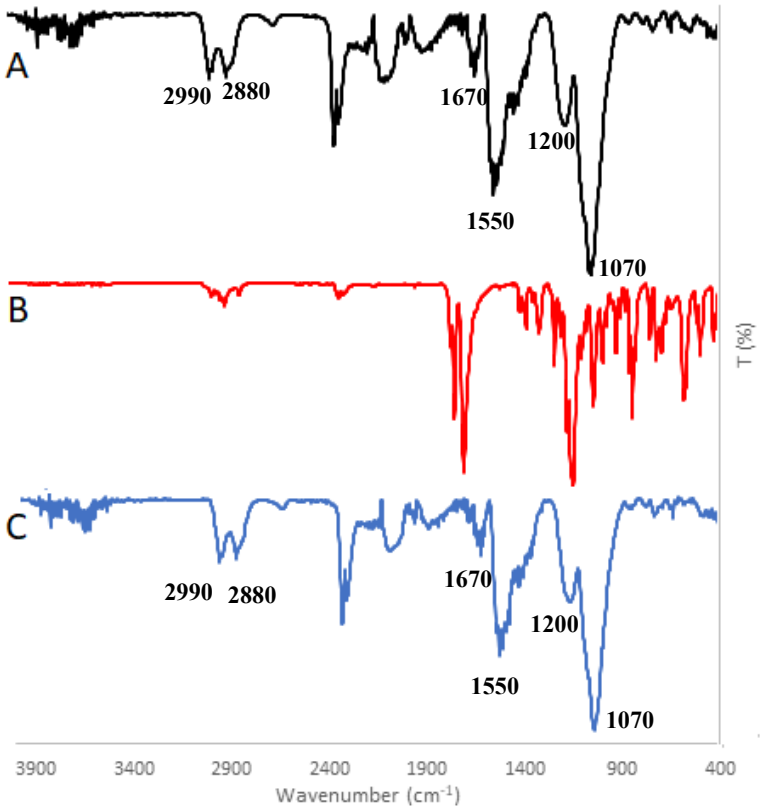

Figure 50. FT-IR spectra of (a) rGO-amine starting material, (b) BCN-succinimidyl ester starting material and (c) the reaction product.

12. SPAAC reactivity test

12.1 Preparation of 1-(azidomethyl)-4-(trifluoromethyl)benzene 10 for SPAAC test reaction

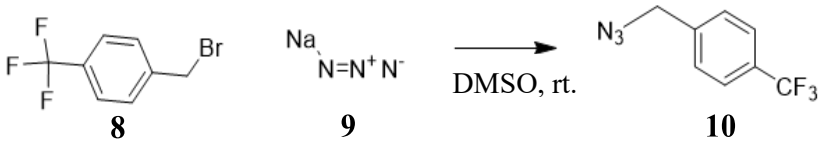

Scheme 5. Synthesis of 1-(azidomethyl)-4-(trifluoromethyl)benzene **10**.

The synthesis of 1-(azidomethyl)-4-(trifluoromethyl)benzene **10** (Scheme 5) was performed by the reaction between 4-(trifluoromethyl)benzyl bromide **8** and sodium azide **9**. The formation of the reaction product can be seen from the ^{1}H NMR and ^{19}F NMR spectra of the product (Appendices 1 and 2).

The applicability of the synthesized 1-(azidomethyl)-4-(trifluoromethyl)benzene **10** for SPAAC was confirmed by the reaction between **10** and BCN alcohol **11**, resulting in the formation of BCN-alcohol-1-[(4-trifluoromethyl)benzyl]-1,2,3-triazole **12** (Scheme 6). The data is not shown.

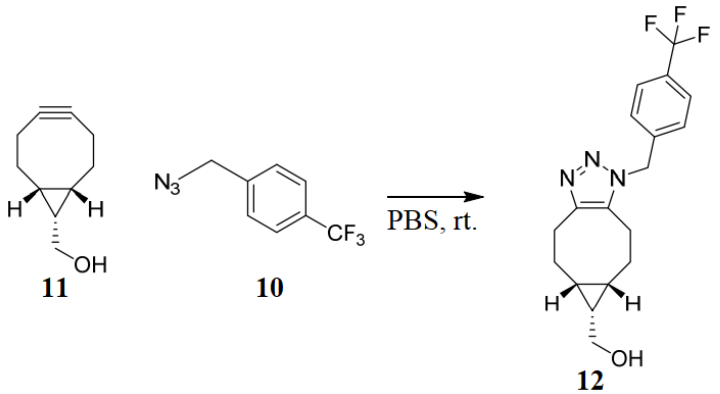

Scheme 6. Synthesis of BCN-alcohol-1-[(4-trifluoromethyl)benzyl]-1,2,3-triazole **12**.

The reactivity of the rGO-amine-endo-BCN-PEG4-amide product was tested by conducting SPAAC reaction[81], in which the synthesized 1-(azidomethyl)-4-(trifluoromethyl)benzene **10** was used.

12.2 Reactivity test of rGO-amine-endo-BCN-PEG4 conjugate 1

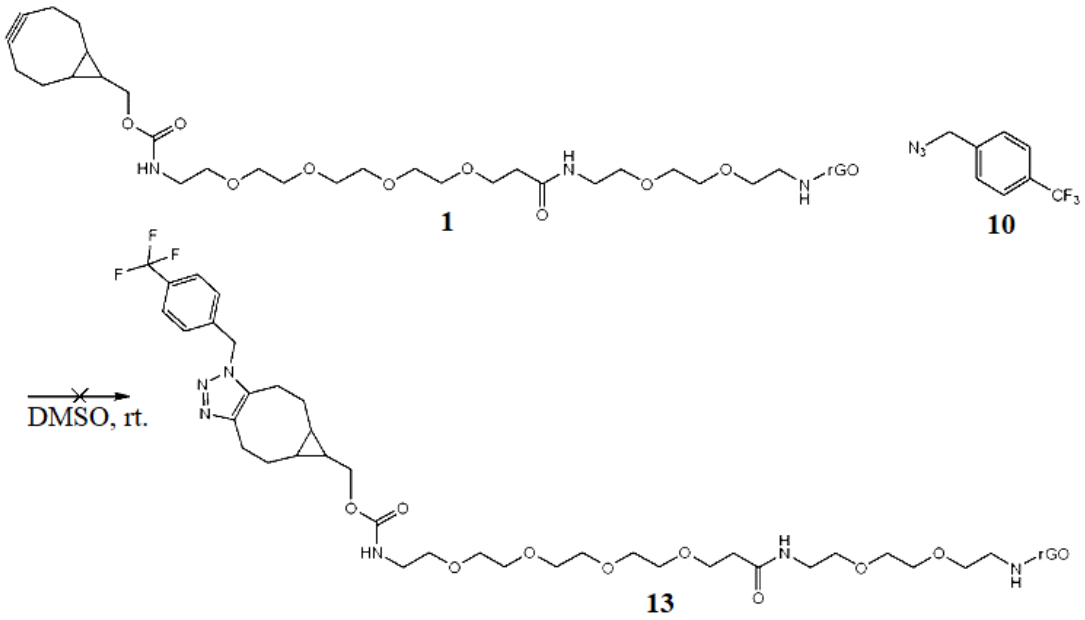

Scheme 7. Synthesis of rGO-amine-endo-BCN-PEG4-1-[(4-trifluoromethyl)benzyl]-1,2,3-triazole **13**.

The reactivity of the synthesized rGO-amine-endo-BCN-PEG4 conjugate **1** was tested by the reaction of rGO-amine-endo-BCN-PEG-4-amide-trifluoromethyl-benzyl-triazole **13** (Scheme 7). The concentration of 1-(azidomethyl)-4-(trifluoromethyl)benzene starting material **10** in the reaction is shown in Figure 51.

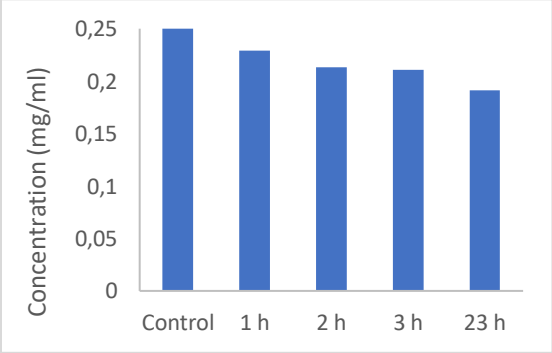

Figure 51. The concentration of 1-(azidomethyl)-4-(trifluoromethyl)benzene **10** in the reaction.

The ^{1}H NMR (Appendix 3) and ^{19}F NMR (Appendix 4) spectra of the product were recorded. The only visible peaks in the ^{1}H NMR spectrum of the product are due to water (3.3 ppm) and DMSO (2.5 ppm). The peak observed at -61 ppm in the ^{19}F NMR spectrum is due to the 1-

(azidomethyl)-4-(trifluoromethyl)benzene starting material **10**. FT-IR characterization of the product was also performed (Figure 52).

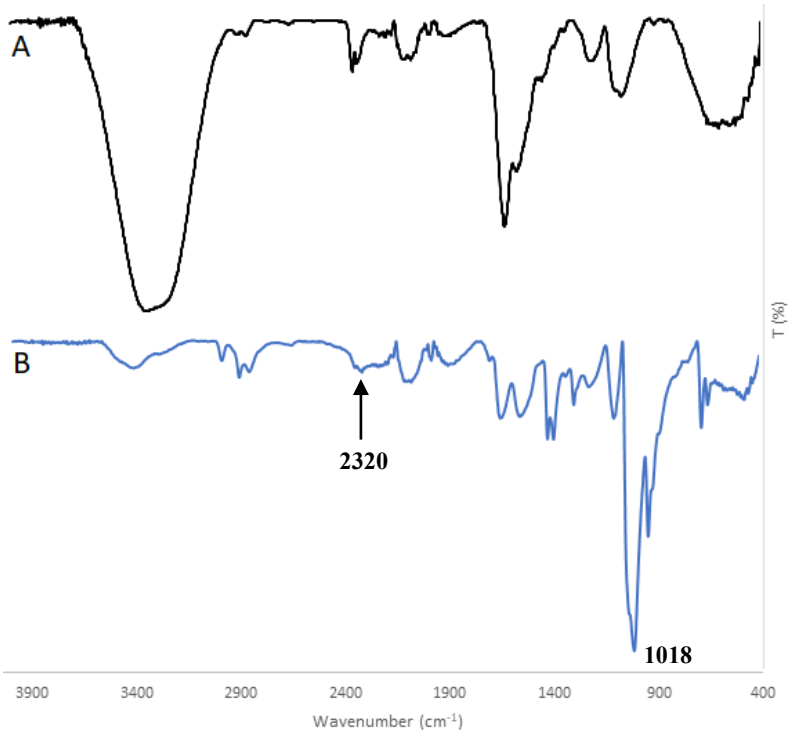

Figure 52. FT-IR spectra of (a) rGO-amine-endo-BCN-PEG4-amide and (b) the reaction product.

As seen from the FT-IR spectrum of the SPAAC reaction product, the N=N=N stretching of the 1-(azidomethyl)-4-(trifluoromethyl)benzene starting material **10**, that commonly absorbs as a strong peak at 2094 cm^{-1} is not observed.[82] This could indicate that the unreacted starting material has been successfully removed during the purification of the obtained product. The C≡C bond of endo-BCN-PEG4-NHS ester **6** starting material generally absorbs at 2200 cm^{-1}, and this signal is seen in the spectrum of the rGO-amine-endo-BCN-PEG4 conjugate **1**. As this peak of the C≡C bond was present in the spectrum of the product at 2320 cm^{-1}, the formation of the triazole product can not be confirmed. The strong peak at 1018 cm^{-1} is due to the trifluoromethyl group attached to the benzene ring of 1-(azidomethyl)-4-(trifluoromethyl)benzene **10**.

13. Equipment and materials

All chemical and reagents were used without any further purification unless stated otherwise (Table 1). Mettler Toledo XSE 204 was used to measure weights and Eppendorf Centrifuge 5810 R to centrifugate the reaction suspensions (13000 rpm for 5 min). NMR spectra were recorded by a Bruker Avance NEO 600 MHz. Finnsonic m03 sonicator was used to dissolve solid graphene oxide particles into NMR solvents for the NMR measurements. FT-IR spectra were recorded by a Bruker Tensor 27 FTIR spectrometer at the University of Jyväskylä. Waters Acquity Ultra Performance LC was used for the LC-MS measurements. Laborota 4000 Heidolph rotavapor was used to evaporate the solvents. During the syntheses, the reaction monitoring samples for LC-MS were prepared by taking 100 µl of the reaction mixture with an automatic pipet, mixing it with 100 µl of acetonitrile by Vortex and filtrating the solid graphene oxide material with Minisart SRP 4 0.45 µm PTFE – membrane filter. An injection volume of 1 µl was used unless stated otherwise.

Table 2. Used reagents and their purities.

Reagent	Vendor	Purity	CAS number
Reduced graphene oxide amine	Sigma Aldrich	*	
Trifluoromethyl benzyl bromide	Acros Organics	*	402-49-3
Sodium azide	Sigma Aldrich	99.5%	26628-22-8
BCN-succinimidyl ester	Sigma Aldrich	*	1516551-46-4
endo-BCN-PEG4-NHS ester	BroadPharm LCC	98%	1702356-19-1
DBCO-PEG4-NHS ester	BroadPharm LCC	97%	1427004-19-0

*The value of purity is unknown.

14. Experimental procedures

14.1 rGO-amine-BCN-carbamate 3

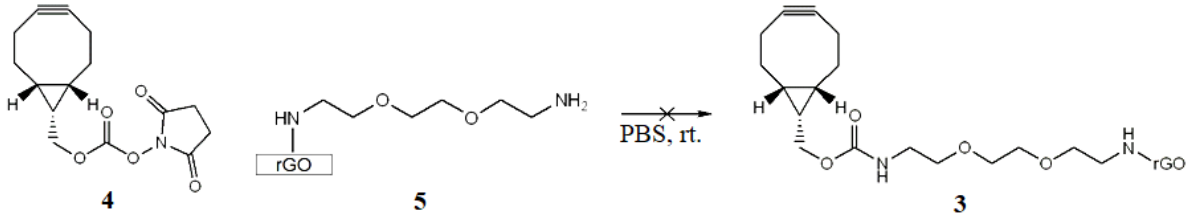

4 5 3

Amine functionalized reduced graphene oxide **5** (40 mg, 1.0 eq), with the amount of 0.22 mmol/g of amine groups, was dissolved in a PBS solution (pH 7.4, 2.5 ml) in a round-bottomed flask. BCN-succinimidyl ester **4** (2.6 mg, 8.8 µmol, 1.0 eq) was added into the flask, and the mixture was sonicated for 15 min. The reaction mixture was stirred at room temperature for 18 h. During the stirring, the concentration of **4** was followed by LC-MS monitoring. The LC-MS measurements were performed with an injection volume of 3 µl. The LC-MS monitoring was performed at 15 min, 1.5 h and 18.5 h from the initiation of the reaction.

After **4** was not observed in the reaction mixture anymore, the reaction suspension was transferred from the flask into two Eppendorf tubes. The reaction suspension was washed in five cycles, including centrifugations (13 000 rpm, 5 min), to separate and purify the obtained product, as done in the study by Wang *et al.*[66] The supernatant was removed from the precipitate after each centrifugation, while the precipitate was washed. The precipitate was washed with 1 ml of deionized water after the first and second centrifugation, and the rest of the washings were done with 1 ml of MeCN. The obtained product was dried in the vacuum oven overnight (40 °C) resulting in 32 mg of rGO-amine as a black powder. Thus, rGO-amine-BCN-carbamate was not synthesized.

14.2 1-(Azidomethyl)-4-(trifluoromethyl)benzene 10

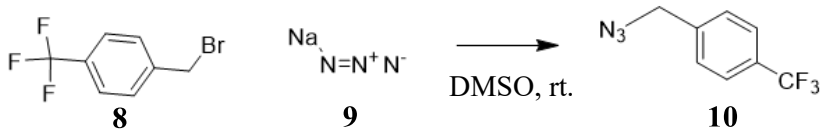

8 **9** **10**

4-(trifluoromethyl)benzyl bromide **8** (239 mg, 1.0 mmol, 1.0 eq) and sodium azide **9** (72 mg, 1.1 mmol, 1.1 eq) were dissolved in DMSO (3 ml). The reaction mixture was left to stir overnight under a nitrogen atmosphere at room temperature.

LC-MS sample (5 µl) was taken from the reaction mixture to observe whether the 1-(azidomethyl)-4-(trifluoromethyl)benzene **10** formed in the reaction mixture. During stirring, the concentration of **8** was followed by LC-MS monitoring.

6 ml of water was added to the reaction mixture. Sediment was not formed. Therefore, the mixture was left to stir for 15 min, following the addition of 14 ml of water. The reaction mixture was transferred into a separating funnel and extracted twice with ethyl acetate (2 x 20 ml). The organic phases were combined, washed with NaCl brine and dried with Na_2SO_4. Ethyl acetate was evaporated with a rotavapor, and the product was left to dry under vacuum overnight resulting in 121 mg of the product as a colourless oil.

^{1}H NMR (600 MHz, $CDCl_3$): δ ppm 4.43 (s, 2H) 7.44-7.46 (m, 2H) 7.64-7.67 (m, 2H).

^{19}F NMR (600 MHz, $CDCl_3$): δ ppm -61.00

14.3 BCN-alcohol-1-[(4-trifluoromethyl)benzyl]-1,2,3-triazole 12

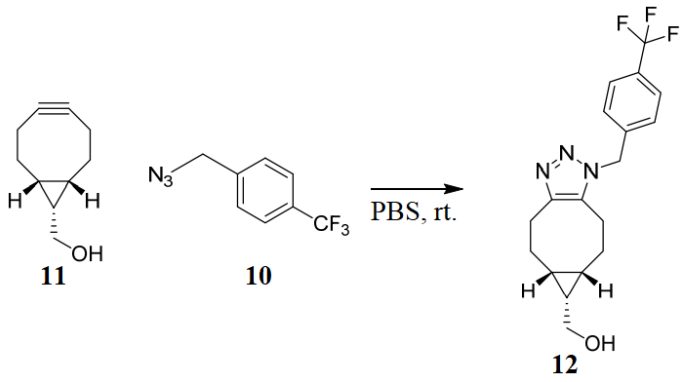

BCN alcohol **11** (3.7 mg, 25 µmol, 1 eq) and 1-(azidomethyl)-4-(trifluoromethyl)benzene **10** (5 mg, 25 µmol, 1 eq) were weighed and added into a flask. PBS solution (5 ml, pH 7.4) was added into the flask. The reaction mixture was stirred with a magnetic bar. The concentration of BCN alcohol was followed by LC-MS. The reaction monitoring samples were measured by LC-MS with an injection volume of 3 µl. The LC-MS samples from the reaction mixture were taken at 50 min, 4 h and 21 h. At 21 h, **11** was completely consumed, thus stirring was stopped. The reaction mixture was extracted twice with diethyl ether (2 x 10 ml). The organic phases were combined, washed with NaCl brine and dried with Na_2SO_4. Na_2SO_4 was filtered and diethyl ether was evaporated with a rotavapor. The product was left to dry under vacuum overnight resulting in 2.2 mg of the product as a colourless oil.

14.4 rGO-amine-endo-BCN-PEG4-amide 1

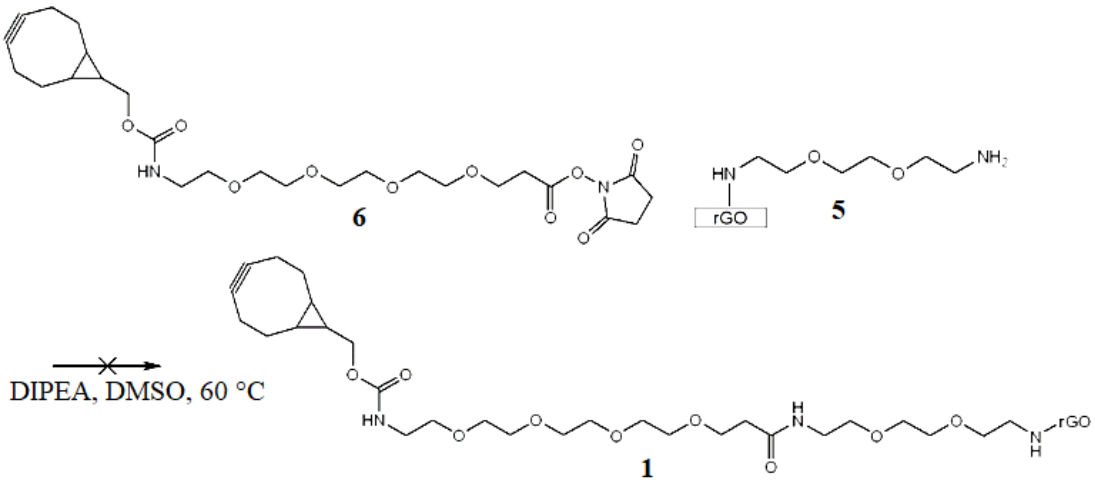

Amine functionalized reduced graphene oxide **5** (45 mg, 1 eq) and endo-BCN-PEG4-NHS ester **6** (5.3 mg, 9.90 µmol, 1 eq) were weighed and added into a flask. DMSO solvent (5.3 ml) was added and the reaction mixture was stirred with a magnetic bar. The concentration of **6** was followed by LC-MS. The reaction monitoring samples were measured by LC-MS with an injection volume of 3 µl. The LC-MS samples from the reaction mixture were taken after 0.5 h, 2 h, 4.5 h, 21 h, 23 h, 24 h, 26 h, 27.5 h, 29 h, 40 h, 41 h, 42 h, 43 h, 56 h, 58 h, 59 h and 70 h from the beginning of the reaction. *N,N*-diisopropylethylamine (1.7 µl, 1 eq) was added into the reaction mixture after 23 h, and a new portion (1.7 µl, 1 eq) after 48 h. After 55 h from the start of stirring of the reaction mixture, heating of the reaction mixture was started (40 °C), and the temperature was increased to 50 °C after 56 h and to 60 °C after 59 h.

After **6** was consumed completely, the stirring was stopped, and the reaction suspension was transferred from the flask into four Eppendorf tubes. The reaction suspension was washed in five cycles, including centrifugations (13 000 rpm, 5 min). The supernatant was removed from the precipitate after each centrifugation while the precipitate was washed. The precipitate was washed with 1 ml of deionized water after the first and second centrifugation, and the rest of the washings were done with 1 ml of MeCN. The obtained product was dried in the vacuum oven overnight (40 °C) resulting in 26 mg of rGO-amine as a black powder. Thus, rGO-amine-BCN-PEG4-amide was not synthesized.

14.5 rGO-amine-endo-BCN-PEG4-amide 1

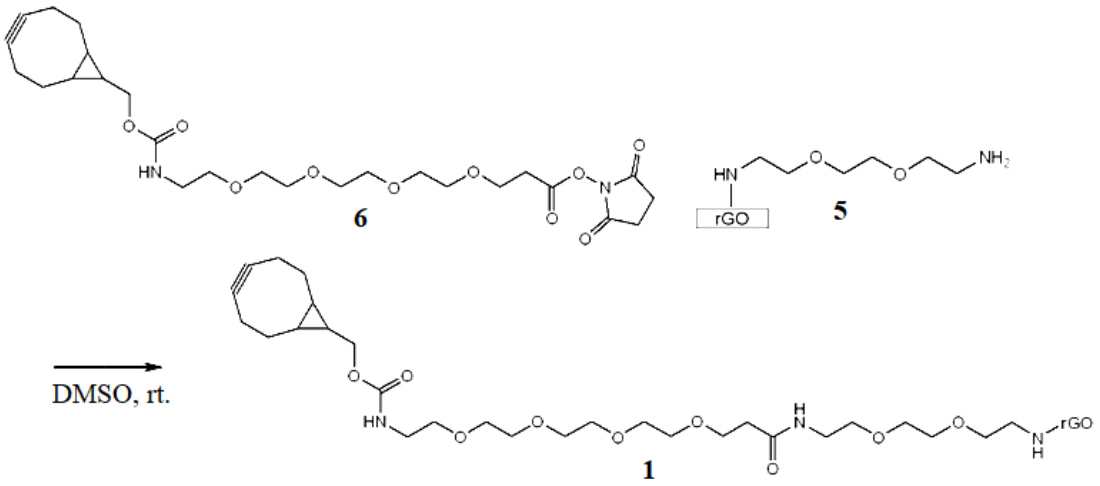

Amine functionalized reduced graphene oxide **5** (75 mg, 1 eq) and endo-BCN-PEG4-NHS ester **6** (8.8 mg, 0.017 mol, 1 eq) were weighed and added into a flask. 8.8 ml of DMSO was measured and added into the flask. Stirring of the reaction mixture by using a magnetic bar was started. A sample (100 µl) for LC-MS measurement was taken after 3.5 h from the start of the reaction, to follow the concentration of endo-BCN-PEG4-NHS ester in the reaction mixture. The LC-MS sample was measured using the injection volume of 3 µl. As the compound was not observed in the reaction mixture, stirring was terminated and the reaction suspension was transferred into a sinter for vacuum filtration. During the filtration, the obtained product was washed five times with water (5 x 10 ml), MeCN (5 x 10 ml) and MeOH (5 x 10 ml). The product was left to dry in a vacuum oven overnight (40 °C) resulting in 63 mg of black powder.

14.6 rGO-amine-endo-BCN-PEG4-1-[(4-trifluoromethyl)benzyl]-1,2,3-triazole 13

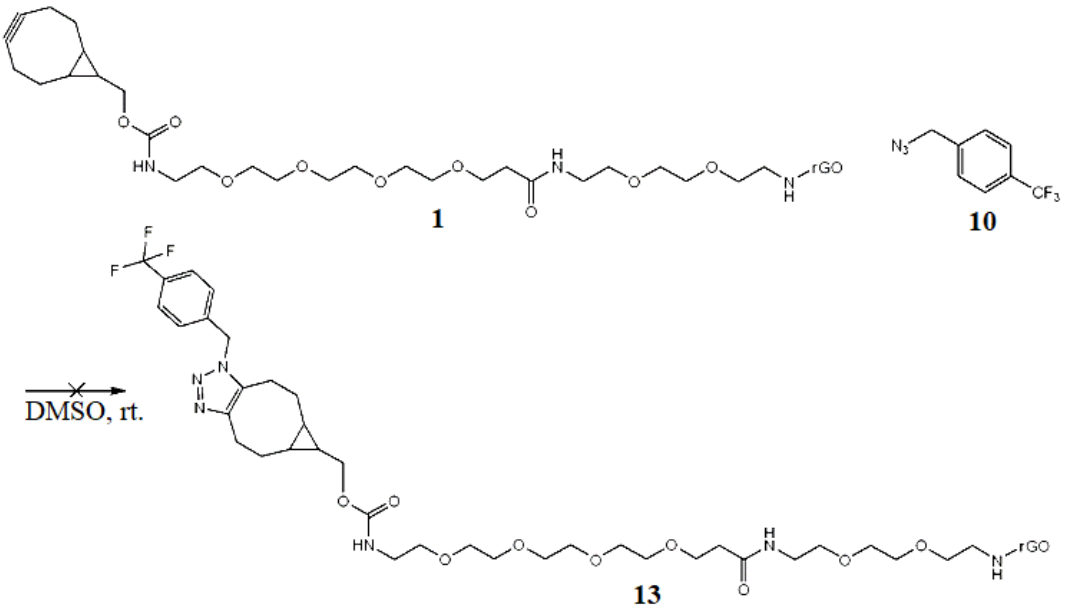

rGO-amine-BCN-PEG-amide **1** (30 mg, 1 eq) and 1-(azidomethyl)-4-(trifluoromethyl)benzene **10** (1.3 mg, 1 eq, 0.007 mmol) were weighed and added into a flask. 2.6 ml of DMSO was added and stirring of the reaction suspension with a magnetic bar was started. The concentration of **10** in the reaction was followed by LC-MS monitoring. The LC-MS measurements were performed after 1 h, 2 h, 3 h and 23 h from the start of the reaction. After 23 h, the stirring was terminated, and the reaction suspension was transferred from the flask into a sinter, vacuum filtrated and washed three times with water (3 x 10 ml), MeCN (3 x 10 ml) and MeOH (3 x 10 ml). The obtained product was dried in the vacuum oven overnight (40 °C) resulting in 29 mg of rGO-amine as a black powder. Thus, rGO-amine-endo-BCN-PEG4-1-[(4-trifluoromethyl)benzyl]-1,2,3-triazole was not synthesized.

14.7 rGO-amine-DBCO-PEG4-amide 2

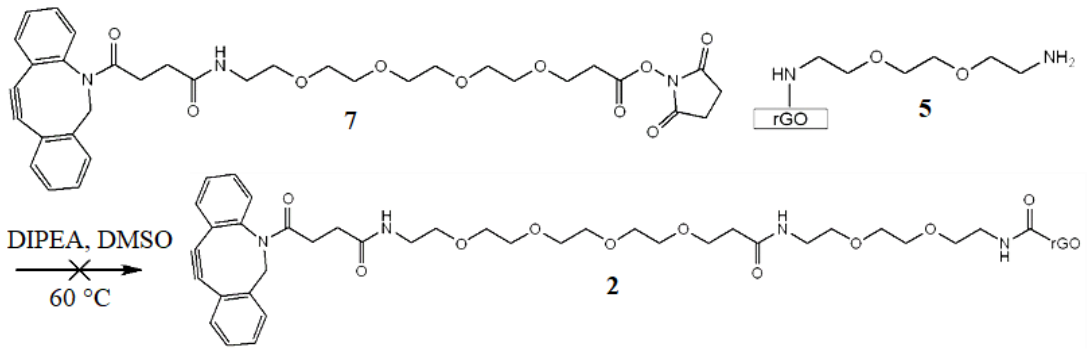

Amine functionalized reduced graphene oxide **5** (40 mg, 1 eq) and DBCO-PEG4-NHS ester **7** (5.7 mg, 0.009 mmol, 1 eq) were weighed and added into a flask. 5.7 ml of DMSO was added and stirring of the reaction mixture with a magnetic bar was started. The concentration of DBCO-PEG4-NHS ester in the reaction mixture was followed by LC-MS. The LC-MS samples were measured after 0.5 h, 2 h, 3 h, 20 h, 24 h, 36 h, 37 h and 39 h. 1 eq of *N,N*-diisopropylethylamine (1.5 µl) was added into the reaction mixture to support the reaction after 20 h and 2 eq after 24.5 h from the start of the reaction. The heating of the reaction mixture up to 50 °C was started after 36 h from the beginning of the stirring, and the temperature was increased to 60 °C after 37 h.

After 39 h from the start of the reaction, the stirring was terminated, and the reaction suspension was transferred into six Eppendorf tubes. The reaction suspension was washed in five cycles, including centrifugations (13 000 rpm, 5 min). The supernatant was removed from the precipitate after each centrifugation, while the precipitate was washed. The precipitate was washed with 1 ml of deionized water after the first and second centrifugation, and the rest of washings were done with 1 ml of MeCN. The obtained product was dried in the vacuum oven overnight (40 °C) resulting in 27 mg of rGO-amine as a black powder. Thus, rGO-amine-DBCO-PEG4-amide was not synthesized.

14.8 rGO-amine-DBCO-PEG4-amide 2

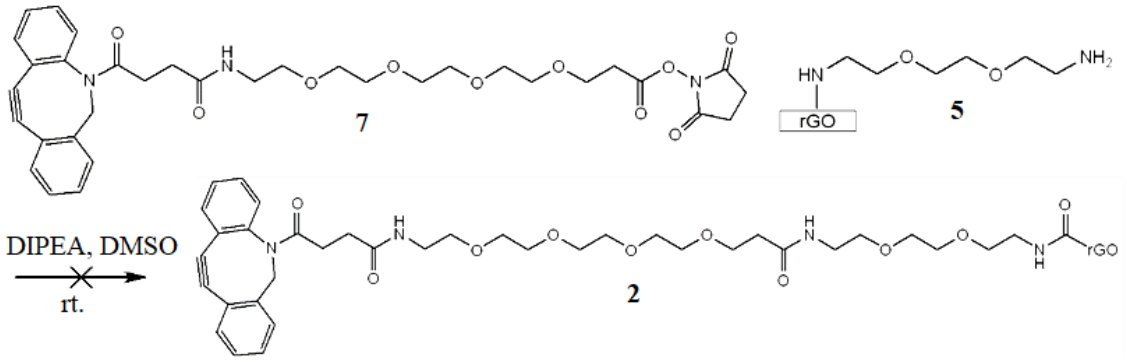

rGO-amine **5** (80 mg, 1 eq) and DBCO-PEG4-NHS ester **7** (11.4 mg, 0.018 mmol, 1 eq) were weighed and added into a flask. 11.4 ml of DMSO was added into the flask and stirring with a magnetic bar was started. The concentration of **7** was followed by LC-MS samples taken from the reaction mixture. The LC-MS samples were measured after 40 min, 3 h, 4 h, 4.5 h, 5.5 h, 6 h and 22 h. *N,N*-isopropylethylamine (3.1 µl, 1 eq) was added after 4.5 h and 5.5 h (6.2 µl, 2 eq) to promote the reaction. After 22 h, stirring was terminated and the reaction mixture was transferred from the flask into a sinter, vacuum filtrated and washed three times with water (3 x 10 ml), MeCN (3 x 10 ml) and MeOH (3 x 10 ml). The product was dried in a vacuum oven (40 °C) overnight resulting in 61 mg of rGO-amine as a black powder. Thus, the rGO-amine-endo-DBCO-PEG4-amide was not synthesized.

15. Conclusions

Graphene-based materials are promising carriers for the targeted delivery of drugs due to the unique properties of graphene that allow drugs to attach efficiently on the surface of graphene. Since the prepared drug systems may have adverse biological effects, such as thrombosis or hemolysis, focusing on the biological behaviour of the graphene-based materials is highly essential. Functionalization enhances the biocompatibility, physiological stability and water-solubility of the materials. Effective and non-toxic graphene-based drug delivery systems could be delivered to the target with passive or active targeting. Hence, healthy cells would remain untouchable and adverse side effects would be reduced.

In the experimental part, GO-PheO*t*Bu and rGO-PheO*t*Bu conjugates were synthesized during the miniproject preceding the thesis project. The products were confirmed by FT-IR. In the thesis project, the rGO-amine-endo-BCN-PEG4 conjugate was synthesized, which is confirmed from the IR spectrum of the product. Conversely, rGO-amine-BCN-carbamate or rGO-DBCO-PEG4-amide were not formed, based on the observations from the FT-IR spectra of the reaction products.

One possible reason for the unsuccessful formation of the rGO-amine-BCN-carbamate and rGO-amine-DBCO-PEG4-amide conjugates is the insolubility of graphene-based materials. The starting materials were not sonicated in the reaction solvent before every reaction. Sonication commonly enhances the dispersibility of graphene-based materials into an organic solvent.[83] In the case of the successful reaction of rGO-amine-endo-BCN-PEG4-amide, the starting materials were sonicated before the stirring was started. Since both rGO-amine and DBCO-PEG4-NHS ester compounds are relatively large in size, steric hindrance may also be a factor for preventing the reaction.

Theoretically, the click chemistry reagents may bind noncovalently to the basal plane of rGO-amine. If so, one should see IR absorptions of the click chemistry reagent in the FT-IR spectrum of a reaction product. As the signals of the click chemistry reagents are absent in the FT-IR spectra of the unsuccessful reaction products, it is unlikely that noncovalent binding occurred.

Both projects aimed to synthesize graphene oxide-based conjugates having an amide bond. In the miniproject, PheO*t*Bu was attached to the carboxylic group of GO or rGO using EDC and NHS as activators. In the latter project, amine-functionalized reduced graphene oxide bearing the PEG chain was used as a starting material.

The projects showed that NMR characterization of graphene oxide-based constructs is challenging due to the poor solubility of graphene oxide-based materials in organic solvents. Based on the literature, solid state NMR has been successful for the characterization of graphene-based materials.

References

1. McCallion, C.; Burthem, J.; Rees-Unwin, K.; Golovanov, A., and Pluen, A., Graphene in therapeutics delivery: Problems, solutions and future opportunities, *Eur. J. Pharm. Biopharm*., **2016**, *104*, 235–250.

2. Yang, Y.; Asiri, A. M.; Tang, Z.; Du, D., and Lin, Y., Graphene based materials for biomedical applications, *Mater. Today*, **2013**, *16(10)*, 365–373.

3. Priyadarsini, S.; Mohanty, S.; Mukherjee, S.; Basu, S., and Mishra, M., Graphene and graphene oxide as nanomaterials for medicine and biology application, *J. Nanostructure Chem*., **2018**, *8(2)*, 123–137.

4. Bhuyan, M. S. A.; Uddin, M. N.; Islam, M. M.; Bipasha, F. A., and Hossain, S. S., Synthesis of graphene, *Int. Nano Lett*., **2016**, *6(2)*, 65–83.

5. Hummers, W. S. and Offeman, R. E., Preparation of Graphitic Oxide, *J. Am. Chem. Soc*., **1958**, *80(6)*, 1339.

6. Lu, N.; Wang, L.; Lv, M.; Tang, Z, and Fan, C., Graphene-based nanomaterials in biosystems, *Nano Res*., **2019**, *12(2)*, 247–64.

7. Lerf, A.; He, H.; Forster, M., and Klinowski, J., Structure of Graphite Oxide Revisited, *J. Phys. Chem. B*., **1998**, *102*, 4477–4482.

8. Dreyer, D. R.; Park, S.; Bielawski, C. W., and Ruoff, R. S., The chemistry of graphene oxide, *Chem. Soc. Rev*., **2010**, *39(1)*, 228–240.

9. Rourke, J. P.; Pandey, P. A.; Moore, J. J.; Bates, M.; Kinloch, I. A.; Young, R. J., and Wilson, N. R., The Real Graphene Oxide Revealed: Stripping the Oxidative Debris from the Graphene-like Sheets, *Angew. Chem. Int. Ed.*, **2011**, *50*, 3173-3177.

10. Li, Y; Feng, L.; Shi, X.; Wang, X.; Yang, Y.; Yang, K.; Liu, T.; Yang, G, and Liu, Z., Surface Coating-Dependent Cytotoxicity and Degradation of Graphene Derivatives: Towards the Design of Non-toxic, Degradable Nano-graphene, *Small*, **2014**, *10(8)*, 1544–1554.

11. Tan, X.; Feng, L.; Zhang, J.; Yang, K.; Zhang, S.; Liu, Z., and Peng, R., Functionalization of Graphene Oxide Generates a Unique Interface for Selective Serum Protein Interactions, *ACS Appl. Mater. Interfaces*, **2013**, *5(4)*, 1370–1377.

12. Liu, Z.; Robinson, J. T.; Sun, X., and Dai H., PEGylated Nano-Graphene Oxide for Delivery of Water Insoluble Cancer Drugs, *J. Am. Chem. Soc*., **2008**, *130(33)*, 10876-10877.

13. Chowdhury, S. M.; Kanakia, S.; Toussaint, J. D.; Frame, M.D.: Dewar, A.M.; Shroyer K.R., Moore, W., and Sitharaman, B., In Vitro Hematological and In Vivo Vasoactivity Assessment of Dextran Functionalized Graphene, *Sci*. *Rep*., **2013**, *3(2584)*, 1-10.

14. Singh, S. K.; Singh, M. K.; Kulkarni, P. P.; Sonkar, V. K.; Grácio, J. J. A., and Dash, D., Amine-Modified Graphene: Thrombo-Protective Safer Alternative to Graphene Oxide for Biomedical Applications, *ACS Nano*, **2012**, *6(3)*, 2731–2740.

15. Shan, C.; Yang, H.; Han, D.; Zhang, Q.; Ivaska, A., and Niu, L., Water-Soluble Graphene Covalently Functionalized by Biocompatible Poly-L-lysine, *Langmuir*, **2009**, *25(20)*, 12030–12033.

16. Park, S.; Dikin, D. A.; Nguyen, S. T., and Ruoff, R. S., Graphene Oxide Sheets Chemically Cross-Linked by Polyallylamine, *J. Phys. Chem. C.*, **2009**, *113(36)*, 15801–15804.

17. Salavagione, H. J.; Gómez, M. A., and Martínez, G., Polymeric Modification of Graphene through Esterification of Graphite Oxide and Poly(vinyl alcohol), *Macromolecules*, **2009**, *42(17)*, 6331–6334.

18. Huang, T.; Zhang, L.; Chen, H., and Gao, C., A cross-linking graphene oxide-polyethyleneimine hybrid film containing ciprofloxacin: One-step preparation, controlled drug release and antibacterial performance, *J. Mater. Chem. B.*, **2015**, *3(8)*, 1605–1611.

19. Yan, L.; Chang, Y. N.; Zhao, L.; Gu, Z.; Liu, X.; Tian, G.; Zhou, L.; Ren, W.; Jin, S.; Yin, W.; Chang, H.; Xing, G.; Gao, X., and Zhao, Y., The use of polyethylenimine-modified graphene oxide as a nanocarrier for transferring hydrophobic nanocrystals into water to produce water-dispersible hybrids for use in drug delivery, *Carbon*, **2013**, *57*, 120–129.

20. Lu, Y. J.; Yang, H. W.; Hung, S. C.; Huang, C. Y.; Li, S. M.; Ma, C. C. M.; Chen, P. Y.; Tsai, H. C.; Wei, K. C., and Chen, J. P., Improving thermal stability and efficacy of BCNU in treating glioma cells using PAA-functionalized graphene oxide, *Int. J. Nanomedicine*, **2012**, *7*, 1737–1747.

21. Gollavelli, G. and Ling, Y. C., Multi-functional graphene as an *in vitro* and *in vivo* imaging probe, *Biomaterials*, **2012**, *33*, 2532-2545.

22. Wang, C.; Zhang, Z.; Chen, B.; Gu, L.; Li, Y., and Yu, S., Design and evaluation of galactosylated chitosan/graphene oxide nanoparticles as a drug delivery system, *J. Colloid. Interface Sci*., **2018**, *516*, 332–341.

23. Suneetha, R. B., Spectral, Thermal and Morphological Characterization of Biodegradable Graphene Oxide-Chitosan Nanocomposites, *J. Nanosci. Technol*., **2018**, *4(2)*, 342–344.

24. Zhang, L.; Xia, J.; Zhao, Q.; Liu, L., and Zhang, Z., Functional Graphene Oxide as a Nanocarrier for Controlled Loading and Targeted Delivery of Mixed Anticancer Drugs, *Small*, **2010**, *6(4)*, 537–544.

25. Qu, G.; Wang, X.; Liu, Q.; Liu, R.; Yin, N.; Ma, J.; Chen, L.; He, J.; Liu, S., and Jiang, G., The ex vivo and in vivo biological performances of graphene oxide and the impact of surfactant on graphene oxide's biocompatibility, *J. Environ. Sci*., **2013**, *25(5)*, 873–881.

26. Fadeel, B.; Bussy, C.; Merino, S.; Vázquez, E.; Flahaut, E.; Mouchet, F.; Evariste, L.; Gauthier, L.; Koivisto, A.J.; Vogel, U.; Martín, C.; Delogu, L.G.; Buerki-Thurnherr, T.; Wick, P.; Beloin-Saint-Pierre, D.; Hischier, R.; Pelin, M.; Carniel, F. C.; Tretiach, M.; Cesca, F.; Benfenati, F.; Scaini, D.; Ballerini, L.; Kostarelos, K.; Prato, M., and Bianco, A., Safety Assessment of Graphene-Based Materials: Focus on Human Health and the Environment, *ACS Nano*, **2018**, *12(11)*, 10582–10620.

27. Bhattacharya, K.; Mukherjee, S. P.; Gallud, A.; Burkert, S. C.; Bistarelli, S.; Bellucci, S.; Bottini, M.; Star, A., and Fadeel B., Biological Interactions of Carbon-Based Nanomaterials: From Coronation to Degradation, *Nanomedicine*, **2016**, *12(2)*, 333–351.

28. Khan, U.; O'Neill, A.; Lotya, M.; De, S., and Coleman, J. N., High-Concentration Solvent Exfoliation of Graphene, *Small*, **2010**, *6(7)*, 864–871.

29. Wei, X. Q.; Hao, L. Y.; Shao, X. R.; Zhang, Q.; Jia, X. Q.; Zhang, Z. R., Lin, Y .F., and Peng, Q., Insight into the Interaction of Graphene Oxide with Serum Proteins and the Impact of the Degree of Reduction and Concentration, *ACS Appl. Mater. Interfaces*, **2015**, *7(24)*, 13367–13374.

30. Kohl, J., Anaphylatoxins and infectious and non-infectious inflammatory diseases, *Mol. Immunol*., **2001**, *38(2–3)*, 175–187.

31. Onat, A.; Can, G.; Rezvani, R., and Cianflone, K., Complement C3 and cleavage products in cardiometabolic risk, *Clin. Chim. Acta*, **2011**, *412(13–14)*, 1171–1179.

32. Girish, C. M.; Sasidharan, A.; Gowd, G. S.; Nair, S., and Koyakutty, M., Confocal Raman Imaging Study Showing Macrophage Mediated Biodegradation of Graphene In Vivo, *Adv. Healthc. Mater.*, **2013**, *2(11)*, 1489–1500.

33. Russier, J.; Treossi, E.; Scarsi, A.; Perrozzi, F.; Dumortier, H.; Ottaviano, L.; Meneghetti, M.; Palermo, V., and Bianco, A., Evidencing the mask effect of graphene oxide: A comparative study on primary human and murine phagocytic cells, *Nanoscale*, **2013**, *5(22)*, 11234–11247.

34. Zhi, X.; Fang, H.; Bao, C.; Shen, G.; Zhang, J.; Wang, K.; Guo, S.; Wan, T., and Cui, D., The immunotoxicity of graphene oxides and the effect of PVP-coating, *Biomaterials*, **2013**, *34(21)*, 5254–5261.

35. Sasidharan, A.; Panchakarla, L.S.; Sadanandan, A. R.; Ashokan, A.; Chandran, P.; Girish, C. M., Menon, D.; Nair, S. V., Rao, C. N. R., and Koyakutty, M., Hemocompatibility and Macrophage Response of Pristine and Functionalized Graphene, *Small*, **2012**, *8(8)*, 1251–1263.

36. Singh, S. K.; Singh, M. K.; Nayak, M. K.; Kumari, S.; Shrivastava, S.; Grácio J. J. A., and Dash, D., Thrombus Inducing Property of Atomically Thin Graphene Oxide Sheets, *ACS Nano*, **2011**, *5(6)*, 4987–4996.

37. Brown, D. M.; Kinloch, I. A.; Bangert, U.; Windle, A. H.; Walter, D. M.; Walker, G. S., Scotchford, C. A., Donaldson, K., and Stone, V., An in vitro study of the potential of carbon nanotubes and nanofibres to induce inflammatory mediators and frustrated phagocytosis, *Carbon*, **2007**, *45(9)*, 1743–1756.

38. Zhang, D.; Zhang Z.; Liu, Y.; Chu, M.; Yang, C.; Li, W.; Shao, Y.; Yue, Y., and Xu, R., The short- and long-term effects of orally administered high-dose reduced graphene oxide nanosheets on mouse behaviors, *Biomaterials*, **2015**, *68*, 100–113.

39. Yang, K.; Gong, H.; Shi, X.; Wan, J.; Zhang, Y., and Liu, Z., In vivo biodistribution and toxicology of functionalized nano-graphene oxide in mice after oral and intraperitoneal administration, *Biomaterials*, **2013**, *34(11)*, 2787–2795.

40. Li, B.; Yang, J.; Huang, Q.; Zhang, Y.; Peng, C.; Zhang, Y.; He, Y.; Shi, J.; Li, W.; Hu, J., and Fan, C., Biodistribution and pulmonary toxicity of intratracheally instilled graphene oxide in mice, *NPG Asia Mater.*, **2013**, *5(4)*, 1–8.

41. Mao, L.; Hu, M.; Pan, B.; Xie, Y., and Petersen, E. J., Biodistribution and toxicity of radio-labeled few layer graphene in mice after intratracheal instillation, *Part. Fibre Toxicol.*, **2016**, *13(1)*, 1–12.

42. Sydlik, S. A.; Jhunjhunwala, S.; Webber, M. J.; Anderson, D. G., and Langer, R., In Vivo Compatibility of Graphene Oxide with Differing Oxidation States, *ACS Nano*, **2015**, *9(4)*, 3866–3874.

43. Kurantowicz, N.; Strojny, B.; Sawosz, E.; Jaworski, S.; Kutwin, M.; Grodzik, M.; Wierzbicki, M.; Lipinska, L.; Mitura, K., and Chwalibog, A., Biodistribution of a High Dose of Diamond, Graphite, and Graphene Oxide Nanoparticles After Multiple Intraperitoneal Injections in Rats, *Nanoscale Res. Lett.*, **2015**, *10(1)*, 1-14.

44. Syama, S.; Paul, W.; Sabareeswaran, A., and Mohanan, P. V., Raman spectroscopy for the detection of organ distribution and clearance of PEGylated reduced graphene oxide and biological consequences, *Biomaterials*, **2017**, *131*, 121–130.

45. Blanco, E.; Shen, H., and Ferrari, M., Principles of nanoparticle design for overcoming biological barriers to drug delivery, *Nat. Biotechnol.,* **2015**, *33(9)*, 941–951.

46. Wen, K. P.; Chen, Y. C.; Chuang, C. H.; Chang, H. Y.; Lee, C. Y., and Tai, N. H., Accumulation and toxicity of intravenously-injected functionalized graphene oxide in mice, *J. Appl. Toxicol.*, **2015**, *35(10)*, 1211–1218.

47. Chithrani, B. D.; Ghazani, A. A., and Chan, W. C. W., Determining the Size and Shape Dependence of Gold Nanoparticle Uptake into Mammalian Cells, *Nano Lett.*, **2006**, *6(4)*, 662–668.

48. Attia, M. F.; Anton, N.; Wallyn, J.; Omran, Z., and Vandamme, T. F., An overview of active and passive targeting strategies to improve the nanocarriers efficiency to tumour sites, *J. Pharm. Pharmacol.*, **2019**, *71(8)*, 1185–1198.

49. Matsumura, Y and Maeda, H., A New Concept for Macromolecular Therapeutics in Cancer Chemotherapy: Mechanism of Tumoritropic Accumulation of Proteins and the Antitumor Agent Smancs, *Cancer Res*., **1986**, *46(8)*, 6387–6392.

50. Lammers, T.; Hennink, W.E., and Storm, G., Tumour-targeted nanomedicines: principles and practice, *Br. J. Cancer*, **2008**, *99(3)*, 392–397.

51. Seon, B.K.; Haba, A.; Matsuno, F.; Takahashi, N.; Tsujie, M.; She, X.; Harada, N.; Uneda, S.; Tsujie, T.; Toi, H.; Tsai, H., and Haruta Y., Endoglin-Targeted Cancer Therapy, *Curr. Drug Deliv*., **2011**, *8(1)*, 135–143.

52. Torchilin, V., Tumor delivery of macromolecular drugs based on the EPR effect, *Adv. Drug Deliv. Rev.,* **2011**, *63*, 131-135.

53. Danhier, F., To exploit the tumor microenvironment: Since the EPR effect fails in the clinic, what is the future of nanomedicine?, *J. Control. Release*, **2016**, *244*, 108–121.

54. Nichols, J. W. and Bae, Y. H., EPR: Evidence and fallacy, *J. Control. Release*, **2014**, *190*, 451–464.

55. ten Tije, A.J.; Verweij, J.; Loos, W.J., and Sparreboom, A., Pharmacological Effects of Formulation Vehicles, *Clin. Pharmacokinet*., **2003**, *42(7)*, 665–685.

56. Lee, K. S.; Chung, H. C.; Im, S. A.; Park, Y. H.; Kim, C. S.; Kim, S. B., Rha, S. Y., Lee, M. Y., and Ro, J., Multicenter phase II trial of Genexol-PM, a Cremophor-free, polymeric micelle formulation of paclitaxel, in patients with metastatic breast cancer, *Breast Cancer Res. Treat*, **2008**, *108(2)*, 241–250.

57. Wang, K.; Ruan, J.; Song, H.; Zhang, J.; Wo, Y.; Guo, S., and Cui, D., Biocompatibility of Graphene Oxide, *Nanoscale Res. Lett.*, **2010**, *6(1)*, 1-8.

58. Ding, Z.; Zhang, Z.; Ma, H., and Chen, Y., In Vitro Hemocompatibility and Toxic Mechanism of Graphene Oxide on Human Peripheral Blood T Lymphocytes and Serum Albumin, *ACS Appl. Mater. Interfaces*, **2014**, *6(22)*, 19797–19807.

59. Liu, Z.; Robinson, J.T.; Tabakman, S. M.; Yang, K., and Dai H., Carbon materials for drug delivery & cancer therapy, *Mater. Today,* **2011**, *14(7–8)*, 316–323.

60. Kam, N. W. S.; Liu, Z., and Dai, H., Carbon Nanotubes as Intracellular Transporters for Proteins and DNA: An Investigation of the Uptake Mechanism and Pathway, *Angew. Chem. Int. Ed.*, **2006**, *45(4)*, 577–581.

61. Liu, Z.; Chen, K.; Davis, C.; Sherlock, S.; Cao, Q.; Chen, X., and Dai H., Drug delivery with carbon nanotubes for in vivo cancer treatment, *Cancer Res*., **2008**, *68(16)*, 6652–6660.

62. Bates, K. and Kostarelos, K., Carbon nanotubes as vectors for gene therapy: Past achievements, present challenges and future goals, *Adv. Drug Deliv. Rev.*, **2013**, *65(15)*, 2023–2033.

63. Daniyal, M.; Liu, B., and Wang, W., Comprehensive Review on Graphene Oxide for Use in Drug Delivery System, *Curr. Med. Chem*., **2020**, *26*, 3665–3685.

64. Wu, S.Y.; An, S. S. A., and Hulme, J., Current applications of graphene oxide in nanomedicine, *Int. J. Nanomedicine*, **2015**, *10*, 9–24.

65. Zhao X, Yang L, Li X, Jia X, Liu L, Zeng J., Guo, J., and Liu, P., Functionalized Graphene Oxide Nanoparticles for Cancer Cell-Specific Delivery of Antitumor Drug, *Bioconjug. Chem.,* **2015**, *26(1)*, 128–136.

66. Wang, H.; Gu, W.; Xiao, N.; Ye, L., and Xu, Q., Chlorotoxin-conjugated graphene oxide for targeted delivery of an anticancer drug, *Int. J. Nanomedicine*, **2014**, *9*, 1433-1442.

67. Zhi, F.; Dong, H.; Jia, X.; Guo, W.; Lu, H.; Yang, Y.; Ju, H.; Zhang, X., and Hu, Y., Functionalized Graphene Oxide Mediated Adriamycin Delivery and miR-21 Gene Silencing to Overcome Tumor Multidrug Resistance *In Vitro*, *PLOS One*, **2013**, *8(3)*, 1–9.

68. Sun, X.; Liu, Z.; Welsher, K.; Robinson, J.T.; Goodwin, A.; Zaric, S., and Dai, H., Nano-Graphene Oxide for Cellular Imaging and Drug Delivery, *Nano Res.* **2008**, *1(3)*, 203–212.

69. Tian, J.; Luo, Y.; Huang, L.; Feng, Y.; Ju, H., and Yu, B.Y., Pegylated folate and peptide-decorated graphene oxide nanovehicle for *in vivo* targeted delivery of anticancer drugs and therapeutic self-monitoring, *Biosens. Bioelectron.*, **2016**, *80*, 519–524.

70. Feng, L.; Li, K.; Shi, X.; Gao, M.; Liu J., and Liu Z., Smart pH-Responsive Nanocarriers Based on Nano-Graphene Oxide for Combined Chemo- and Photothermal Therapy Overcoming Drug Resistance, *Adv. Healthc. Mater.,* **2014**, *3(8)*, 1261–1271.

71. Masoudipour, E.; Kashanian, S., and Maleki, N., A targeted drug delivery system based on dopamine functionalized nano graphene oxide, *Chem. Phys. Lett*., **2017**, *668*, 56–63.

72. Jokar, S.; Pourjavadi, A., and Adeli, M., Albumin-graphene oxide conjugates; carriers for anticancer drugs, *RSC Adv*., **2014**, *4(62)*, 33001–33006.

73. Moore, T. L.; Podilakrishna, R.; Rao, A., and Alexis, F., Systemic Administration of Polymer-Coated Nano-Graphene to Deliver Drugs to Glioblastoma, *Part. Part. Syst. Charact.*, **2014**, *31(8)*, 886–894.

74. Yang, X.; Zhang, X.; Liu, Z.; Ma, Y.; Huang, Y., and Chen, Y., High-Efficiency Loading and Controlled Release of Doxorubicin Hydrochloride on Graphene Oxide, *J. Phys. Chem. C.*, **2008**, *112(45)*, 17554–17558.

75. Smith, A. T.; LaChance, A. M.; Zeng, S.; Liu, B., and Sun L., Synthesis, properties and applications of graphene oxide/reduced graphene oxide and their nanocomposites, *NMS*, **2019**, *1*, 31-47.

76. Ickecan, D.; Zan, R, and Nezir, S., Eco-Friendly Synthesis and Characterization of Reduced Graphene Oxide, *J. Phys.*, **2017**, *902(1)*, 1-4.

77. Macintosh, A. R.; Harris, K. J., and Goward, G. R., Structure and Dynamics in Functionalized Graphene Oxides through Solid-State NMR, *Chem. Mater*. **2016**, *28(1)*, 360–367.

78. Singh, M. S.; Chowdhury, S., and Koley, S., Advances of azide-alkyne cycloaddition-click chemistry over the recent decade, *Tetrahedron*, **2016**, *72(35)*, 5257–5283.

79. Smeenk, M. L. W. J. ; Agramunt, J., and Bonger, K. M., Recent developments in bioorthogonal chemistry and the orthogonality within, *Curr. Opin. Chem. Biol.*, **2021**, *60*, 79–88.

80. Riomet, M.; Porte, K.; Wijkhuisen, A.; Audisio, D., and Taran, F., Fluorogenic iminosydnones: Bioorthogonal tools for double turn-on click-and-release reactions, *Chem. Commun*., **2020**, *56(52)*, 7183–7186.

81. Agard, N. J.; Prescher, J. A., and Bertozzi, C. R., A Strain-Promoted [3 + 2] Azide-Alkyne Cycloaddition for Covalent Modification of Biomolecules in Living Systems, *J. Am. Chem. Soc*., **2004**, *126(46)*, 15046–15047.

82. Kumar, P.; Joshi, C.; Srivastava, A. K.; Gupta, P; Boukherroub, R., and Jain, S. L., Visible Light Assisted Photocatalytic [3 + 2] Azide-Alkyne "Click" Reaction for the Synthesis of 1,4-Substituted 1,2,3-Triazoles Using a Novel Bimetallic Ru-Mn Complex, *ACS Sustain. Chem. Eng.*, **2016**, *4(1)*, 69–75.

83. Paredes, J. I.; Villar-Rodil, S.; Martínez-Alonso, A., and Tascón, J.M.D, Graphene Oxide Dispersions in Organic Solvents, *Langmuir*, **2008**, *24*, 10560-10564.

Appendices

Appendix 1: ^{1}H NMR spectrum of 1-(azidomethyl)-4-(trifluoromethyl)benzene

Appendix 2: ^{19}F NMR spectrum of 1-(azidomethyl)-4-(trifluoromethyl)benzene

Appendix 3: ^{1}H NMR spectrum of the SPAAC test reaction product

Appendix 4: ^{19}F NMR spectrum of the SPAAC test reaction product

APPENDIX 1

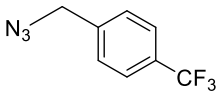
N3
CF3

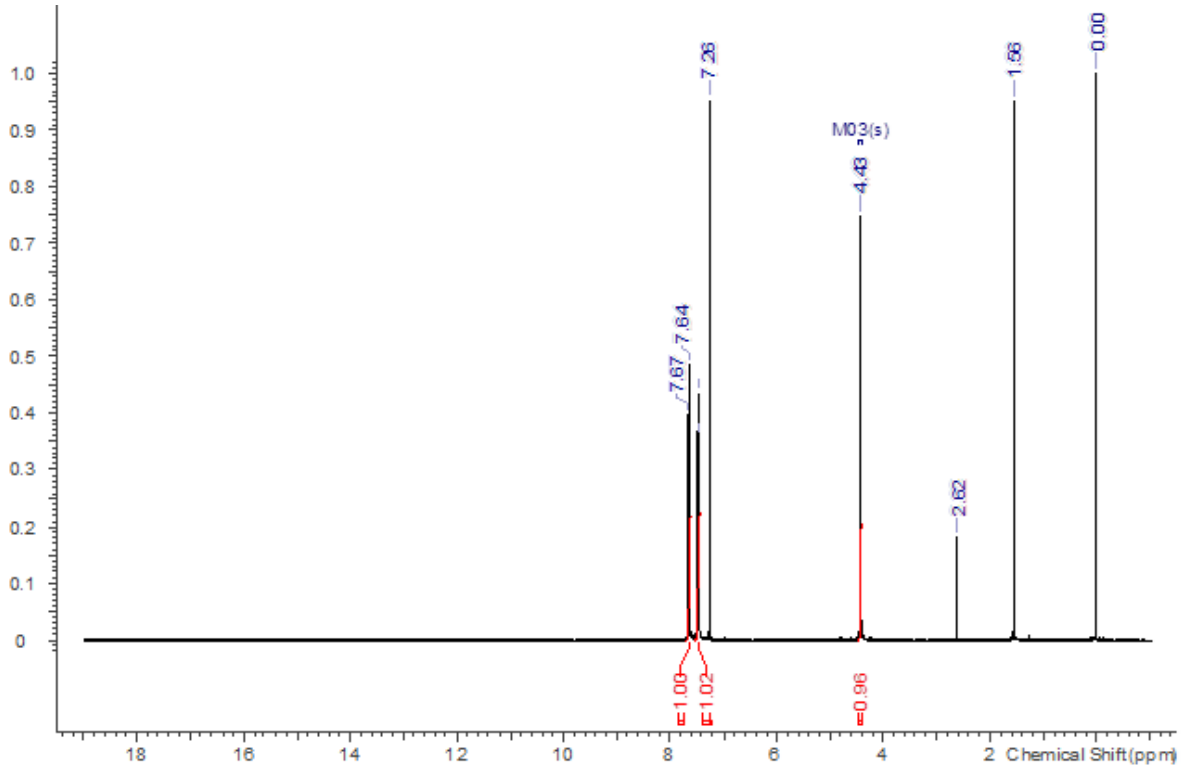
7.67
7.64
7.26
M03(s)
4.43
2.62
1.66
0.00
1.00
1.02
0.96
Chemical Shift (ppm)

APPENDIX 2

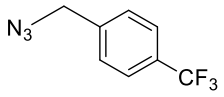
N3
CF3

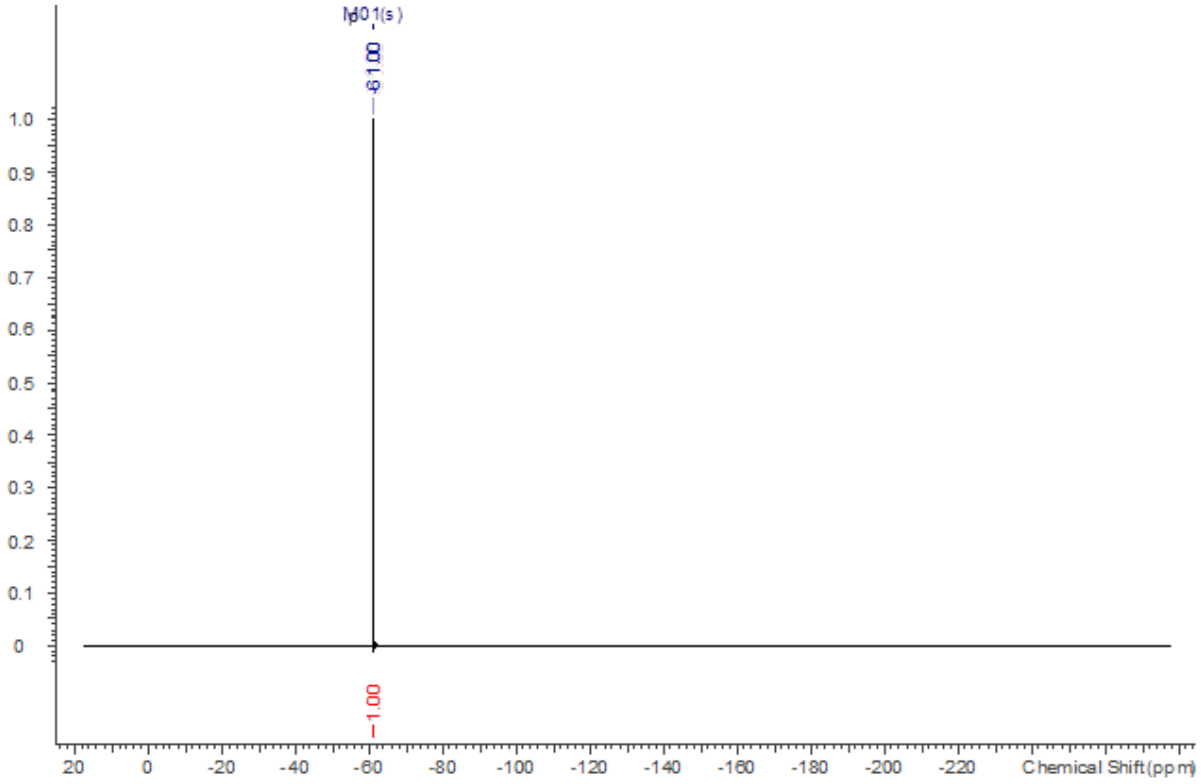
1.00
1.0
0.9
0.8
0.7
0.6
0.5
0.4
0.3
0.2
0.1
0
-1.00
20
0
-20
-40
-60
-80
-100
-120
-140
-160
-180
-200
-220
Chemical Shift (ppm)

APPENDIX 3

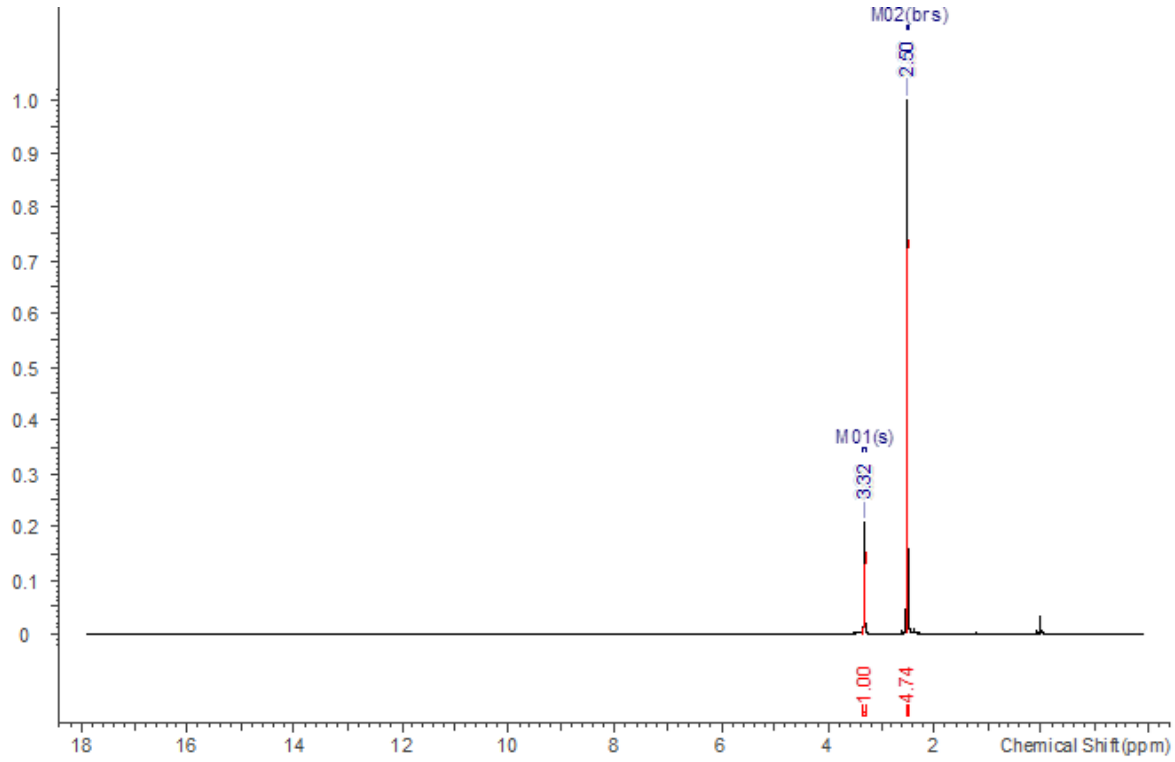
M02(brs)
2.50
M01(s)
3.32
1.00
4.74
1.0
0.9
0.8
0.7
0.6
0.5
0.4
0.3
0.2
0.1
0
18
16
14
12
10
8
6
4
2
Chemical Shift(ppm)

APPENDIX 4

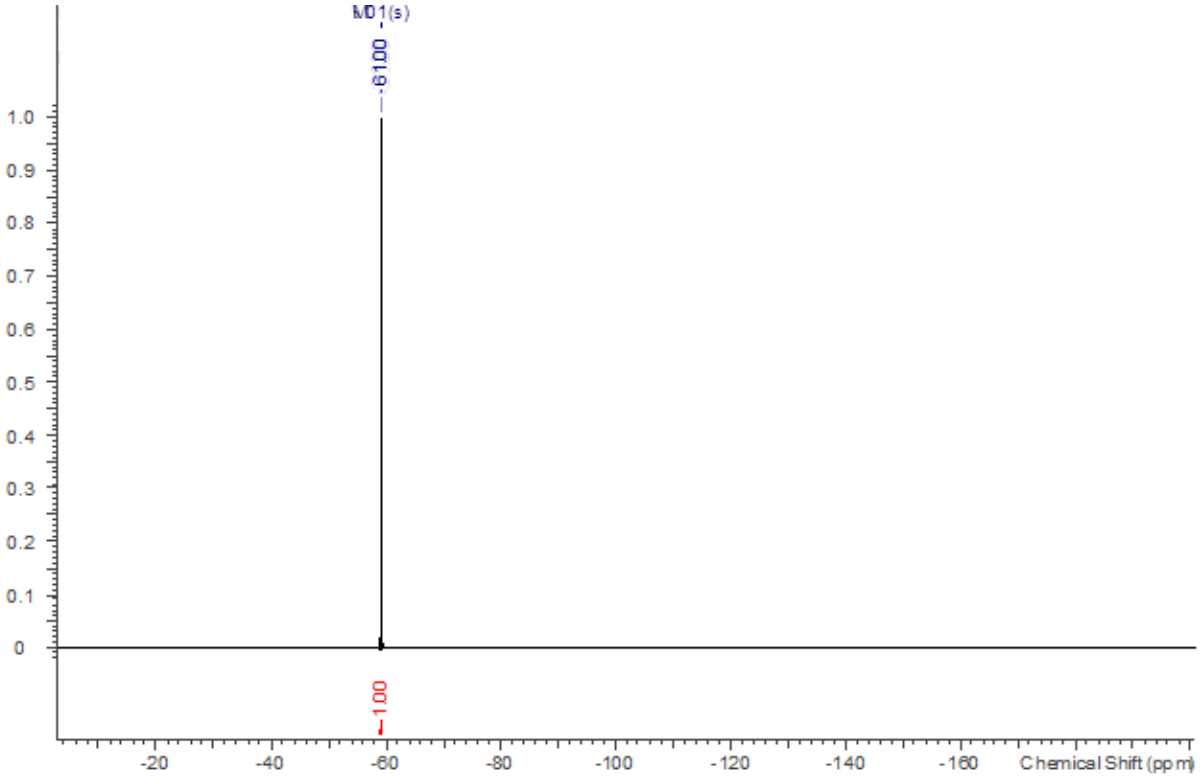
MD1(s)
6100
1.00
1.0
0.9
0.8
0.7
0.6
0.5
0.4
0.3
0.2
0.1
0
-20
-40
-60
-80
-100
-120
-140
-160
Chemical Shift (ppm)